18

Calle, Amanda Z., Brian K. Horton, Rodrigo Limachi, Daniel F. Stockli, Geila V. Uzeda-Orellana, Ryan B. Anderson, and Sean P. Long, 2018, Cenozoic provenance and depositional record of the sub-Andean foreland basin during growth of the central Andean fold-thrust belt, southern Bolivia, *in* G. Zamora, K. R. McClay, and V. A. Ramos, eds., Petroleum basins and hydrocarbon potential of the Andes of Peru and Bolivia: AAPG Memoir 117, p. 483–530.

Cenozoic Provenance and Depositional Record of the Sub-Andean Foreland Basin during Growth of the Central Andean Fold-Thrust Belt, Southern Bolivia

Amanda Z. Calle and Brian K. Horton

Department of Geological Sciences and Institute for Geophysics, Jackson School of Geosciences, University of Texas at Austin, 2275 Speedway Stop C9000, Austin, Texas 78712, U.S.A. (e-mails: azcallep@utexas.edu; horton@jsg.utexas.edu)

Rodrigo Limachi

Repsol E&P Bolivia S.A., Av. Las Ramblas No. 100, Barrio Equipetrol, Santa Cruz de la Sierra, Bolivia (e-mail: jlimachim@repsol.com)

Daniel F. Stockli

Department of Geological Sciences, Jackson School of Geosciences, University of Texas at Austin, 2275 Speedway Stop C9000, Austin, Texas 78712, U.S.A. (e-mail: stockli@jsg.utexas.edu)

Geila V. Uzeda-Orellana

Instituto de Investigaciones Geológicas y Medio Ambiente, Universidad Mayor de San Andrés, Calle 27 Cota Cota, La Paz, Bolivia (e-mail: geilauo@hotmail.com)

Ryan B. Anderson and Sean P. Long

School of the Environment, Washington State University, PO Box 642812, Pullman, Washington 99164, U.S.A. (e-mails: ryan.b.anderson@wsu.edu; sean.p.long@wsu.edu)

ABSTRACT

The sub-Andean foreland basin of southern Bolivia chronicles erosional unroofing of the central Andean fold-thrust belt during Cenozoic shortening. Analyses of five stratigraphic sections document regional paleosol development in forebulge to distal foredeep depozones, followed by proximal accumulation of a greater than 4 km (2.5 mi) thick upward coarsening and thickening succession of mixed fluvial to megafan deposits. New timing constraints from zircon U-Pb ages for sandstones and interbedded volcanic horizons indicate Oligocene to late Miocene facies migration and eastward progradation from growing structures and

DOI:10.1306/13622132M1173777

point sources of sediment. Detrital zircon U-Pb results, sandstone/conglomerate compositions, and paleocurrent data reveal subarkosic and sublitharenitic sand derived from Andean sources to the west, with (1) contributions from upper Paleozoic strata (420–570 Ma zircon age components) of the inter-Andean Zone; (2) variable input from the Eastern Cordillera, including lower Paleozoic strata (650–800 Ma zircon ages), Mesozoic strata (66–360 Ma zircon ages), and recycled Paleogene basin fill; and (3) later arrival of a cosmopolitan age assemblage from upper Paleozoic to Cenozoic strata of the incipient sub-Andean Zone. Eastward advance of the fold-thrust belt corresponds to an increase in sediment accumulation from 3 m (10 ft)/m.y. to 90–2000 m (295–6562 ft)/m.y. The integrated results suggest a progressive early–middle Miocene transition from foredeep to wedge-top deposition within the eastern inter-Andean Zone to western sub-Andean Zone, with a generally post–12 Ma age for most sub-Andean structures. We propose that either (1) pre-Cenozoic stratigraphic and structural heterogeneities promoted nonsystematic activation and shortening advance, with an unsteady eastward migration of flexural foreland subsidence, or (2) the fold-thrust belt and foreland basin advanced systematically eastward, with a marked southward reduction in the magnitude of shortening along the inter-Andean-sub-Andean Zone. Surface uplift associated with advancing deformation guided the creation of topographic barriers in the fold-thrust belt and proximal foreland, inducing variable unroofing patterns, drainage network evolution, and deposition of fluvial megafans.

INTRODUCTION

Foreland basins are excellent recorders of the growth and erosion of contractional orogenic belts (Jordan, 1981, 1995; DeCelles and Giles, 1996; DeCelles, 2012). However, inherited pre-orogenic conditions and complex shortening patterns may lead to nonsystematic behavior in fold-thrust belts and foreland basin systems. In the central Andes (Figure 1), the retro-arc foreland basin spans along-strike (north–south) and across-strike (east–west) heterogeneities that may induce spatial and temporal variations in depositional, deformational, and exhumational histories (e.g., Masek et al., 1994; Kley, 1996; Jordan et al., 1997; Horton, 1999; Montgomery et al., 2001; Barnes and Pelletier, 2006; McGroder et al., 2015). Although differences in structural style exist between Bolivia and Argentina (e.g., transition zone of Figure 1), the foreland basin record and the timing of exhumation and deformation remain relatively consistent along strike (Allmendinger and Gubbels, 1996; Kley et al., 1999; McQuarrie, 2002a; Carrapa et al., 2011; DeCelles et al., 2011; Anderson et al., 2017). Synorogenic sediments preserved in Andean outcrop belts and foreland regions provide key records to unravel the patterns of deformation and basin evolution.

Despite a similar Eocene–Oligocene history of exhumation and deformation in southern Bolivia to northern Argentina, thermochronologic, structural, and basin fill records highlight Miocene and younger discrepancies across these regions (Marshall and Sempere, 1991; Hernández et al., 1996; Horton, 1998, 2005, 2012; Coutand et al., 2001; Horton et al., 2001, 2002; Reynolds et al., 2001; Gillis et al., 2006; Ege et al., 2007; Barnes and Ehlers, 2009; Carrapa et al., 2011; Mosolf et al., 2011; Siks and Horton, 2011; Del Papa et al., 2013; Galli et al., 2016). For example, the ~10 Ma cessation of exhumation in the Eastern Cordillera of Bolivia conflicts with observations in northern Argentina, where active faulting characterizes the Eastern Cordillera and may be coupled with increasing accumulation rates in the sub-Andean Zone (e.g., Echavarría et al., 2003; Uba et al., 2009; Pingel et al., 2013; Streit et al., 2015). Further contrasts involve the variable influence of large basement-involved thrusts, pre-Cenozoic heterogeneities, the timing and magnitude of flexural subsidence, and the role of climate-related surface processes (Kley et al., 1997, 1999; Horton and DeCelles, 2001; McQuarrie, 2002b; Sobel et al., 2003; Leier et al., 2005; Strecker et al., 2007, 2009; Barnes and Heins, 2009; Barnes et al., 2012; Anderson et al., 2014, 2017). Remaining uncertainties include (1) the timing of initial shortening in the frontal thrust belt, where estimates range from ~20 to 5 Ma (e.g., Kley, 1996; DeCelles and Horton, 2003; McQuarrie et al., 2005; Uba et al., 2005, 2009; Lease et al., 2016); (2) the mode of deformation advance, either by steady eastward propagation or punctuated out-of-sequence thrusting (Dunn et al., 1995; Moretti et al., 1996; Brusset et al., 2002; Echavarría et al., 2003; Uba et al., 2009); and (3) the linkages between sub-Andean shortening and surface uplift of the Altiplano and Puna plateaus (Allmendinger et al., 1997; Garzione et al., 2006, 2008; Lamb, 2011, 2016; Canavan et al., 2014; Carrapa and DeCelles, 2015; Quade et al., 2015).

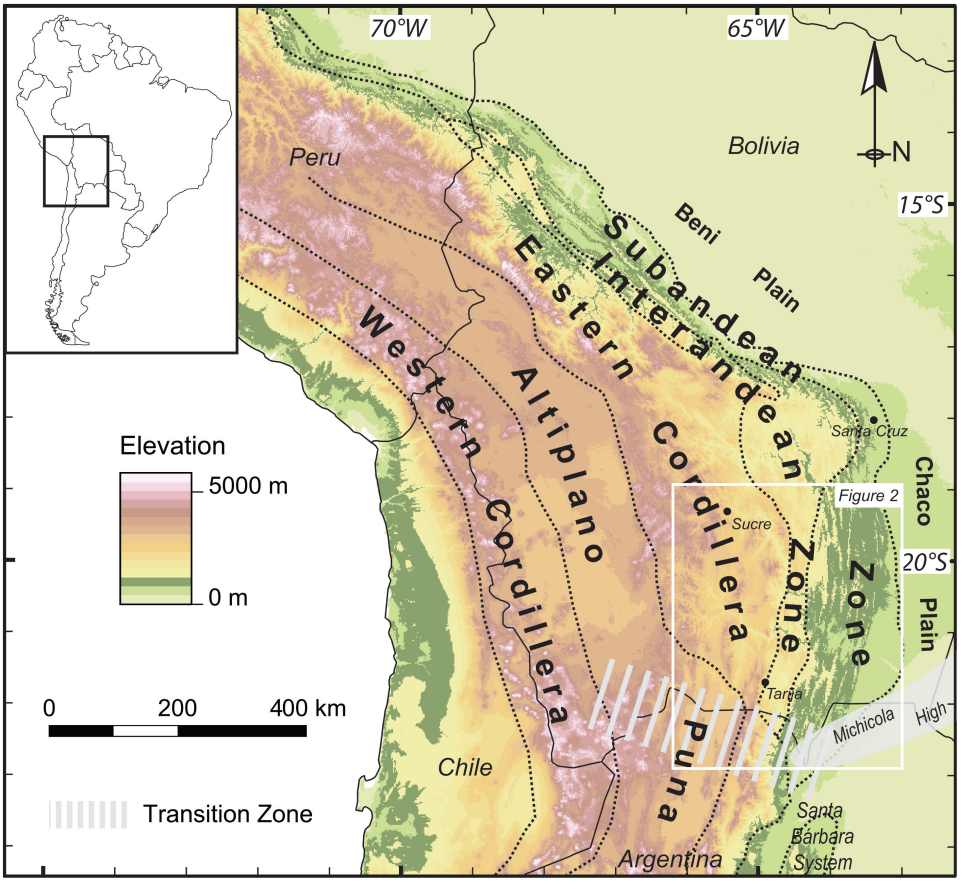

Figure 1. Shaded topographic map of the central Andes within South America (inset map) showing major tectonomorphic zones, the modern foreland basin (Chaco and Beni Plains), and a roughly east–west-trending structural-stratigraphic transition zone near the Bolivia–Argentina border, as defined in the fold-thrust belt (dashed gray line) and in the foreland by a Cretaceous-age basement high (Michicola High, light gray shading; Viramonte et al., 1999).

In Bolivia, sub-Andean foreland basin deposits provide a record of sustained (>20 m.y.) and substantial (>4 km [2.5 mi]) sediment accumulation. This thick clastic fill provides a depositional and provenance record of the onset and spatiotemporal distribution of shortening along the zone of maximum crustal thickening, which contains the highest and widest mean topography in the Andes. Comparison of the depo-systems, provenance, and accumulation histories of the sub-Andean Zone of Bolivia with its counterparts in northern Argentina can help address the timing and sequence of foreland deposition, fold-thrust deformation, and erosional input from growing local and regional Andean topography. This study explores the spatial and temporal variations of foreland sedimentation in the western sub-Andean Zone to eastern inter-Andean Zone of southern Bolivia at 19.5–22.5°S (Figure 1). Integrated analyses of the sedimentologic, stratigraphic, and detrital zircon U-Pb geochronologic and provenance constraints from five Cenozoic sections (Figure 2) are employed to define the interactions of the advancing central Andean fold-thrust belt and adjacent sub-Andean foreland basin and their regional context relative to northern Argentina. The results highlight the Oligocene–Miocene history of synorogenic sedimentation and reveal the apparent time-transgressive development of flexural accommodation and sediment routing systems from the growing thrust belt.

GEOLOGIC AND STRATIGRAPHIC FRAMEWORK

Subduction of the oceanic Nazca plate beneath South America drove Cenozoic shortening and growth of the central Andes (Isacks, 1988; Gubbels et al., 1993; Baby et al., 1997; Oncken et al., 2006). In southern Bolivia (Figures 1, 2), distinct tectonomorphic zones of the retro-arc fold-thrust belt exhibit characteristic topography and structural-stratigraphic configurations related to basement-involved deformation, including crustal-scale footwall ramps concealed at depth (e.g., Kley, 1993, 1996; McQuarrie, 2002b; Eichelberger et al., 2013; Anderson et al., 2017). The Eastern Cordillera (~3–4 km [~2–2.5 mi] elevation) is composed of bivergent east- and west-directed thrust systems, with the deepest structural levels (Neoproterozoic–Ordovician rocks) exposed in a broad anticlinorium along its eastern margin. To the east, the inter-Andean Zone (~2–3 km [~1.2–2 mi] elevation) involves a narrow, thin-skinned thrust system developed atop a

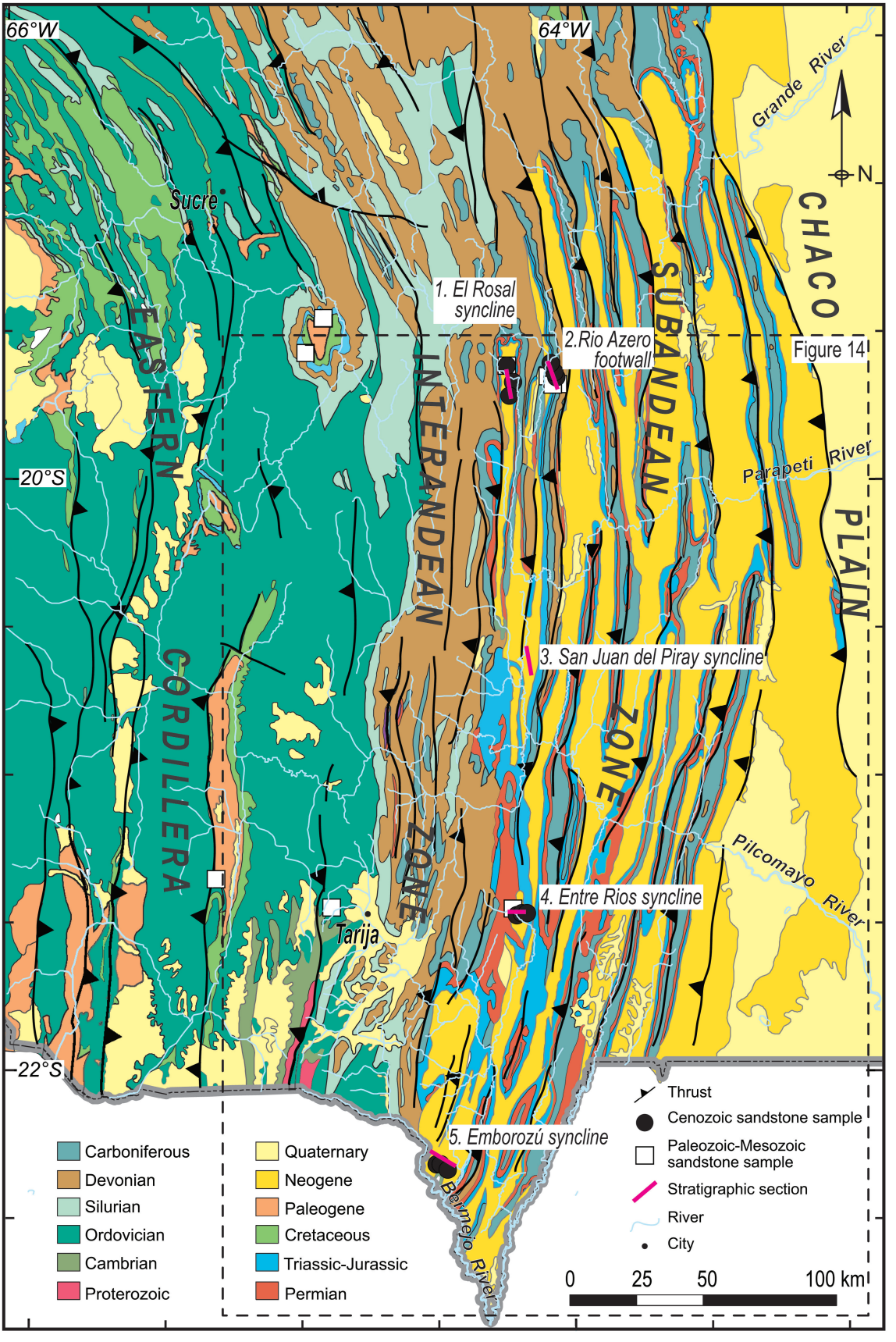

Figure 2. Regional geologic map of the central Andean fold-thrust belt and proximal foreland basin of southern Bolivia (Choque and Almendras, 2012) displaying tectonomorphic zones, major faults, measured stratigraphic sections, and the locations of detrital zircon U-Pb samples from potential source regions (Paleozoic and Mesozoic) and from Cenozoic fill in the sub-Andean Zone and eastern inter-Andean Zone.

basement-involved thrust, the inter-Andean thrust. Farther east, a second basement-involved thrust, the sub-Andean thrust, transfers shortening to the sub-Andean Zone (~1–2 km [~0.6–1.2 mi] elevation), an east-vergent, thin-skinned thrust system with multiple fault-propagation folds and imbricate splay faults. The lower (sub-Andean) structure passively elevated and translated the Eastern Cordillera and inter-Andean Zone as basement slip was fed eastward into the basal décollement (Silurian shale) beneath the sub-Andean Zone (e.g., Baby et al., 1992; Dunn et al., 1995; Anderson et al., 2017). Along the eastern mountain front, the Chaco plain (< 0.5 km [< 0.3 mi] elevation) defines the modern foreland basin (Horton and DeCelles, 1997; Mascle and Zubieta-Rossetti, 2005).

A significant tectonic boundary near the Bolivia–Argentina border is expressed in the overall southward plunge and transition from the thin-skinned sub-Andean Zone to the thick-skinned Santa Bárbara System, with an accompanying decrease in shortening from ~100 to ~21 km (~62 to 13 mi) (Figure 1; Kley et al., 1996, 1999; Allmendinger et al., 1997; Kley and Monaldi, 2002; Pearson et al., 2013). This change in structural style may be related to the pronounced southward thinning of the Paleozoic sedimentary prism (Allmendinger et al., 1983, 1997; Kley and Monaldi, 1998; McQuarrie, 2002a; McGroder et al., 2015) and inherited pre-Andean basement fabrics (e.g., Hongn et al., 2010; Insel et al., 2012). In addition, the Cretaceous Salta rift in northern Argentina generated basement-high rift shoulders that may have impeded deformation advance (e.g., Michicola High on the northern flank of the Lomas de Olmedo subbasin; Figure 1; Viramonte et al., 1999) and basement-involved normal faults that may have been selectively reactivated, focusing Cenozoic shortening in parts of the Puna, Eastern Cordillera, and Santa Bárbara System (Grier et al., 1991; Coutand et al., 2001; Kley et al., 2005; Siks and Horton, 2011; Del Papa et al., 2013; Pearson et al., 2013; Carrapa et al., 2014). The structural contrasts between Bolivia and Argentina may also influence the linkages between topographic barriers and regional climate, which played an important role in Neogene intermontane and foreland basin development (Horton, 1998, 1999, 2005, 2012; Sobel et al., 2003; Strecker et al., 2007, 2009; Pingel et al., 2013; Amidon et al., 2015; Streit et al., 2015).

The timing of shortening has been estimated from thermochronologic data, stratigraphic studies, cross-cutting structural relationships, and geomorphic surface dating. At 19–21.5°S, shortening-related exhumation in the Eastern Cordillera took place from the middle Eocene to Miocene (~45–15 Ma; Horton, 1998; Müller et al., 2002; McQuarrie et al., 2005; Ege et al., 2007; Barnes et al., 2008), prior to development of the San Juan del Oro geomorphic surface at ~10 Ma (Gubbels et al., 1993; Kennan et al., 1995). During the Miocene (~20–5 Ma), exhumation advanced eastward into the inter-Andean Zone and sub-Andean Zone, although the exact timing remains debated (e.g., Erikson and Kelley, 1995; Kley, 1996; Jordan et al., 1997; Brusset et al., 2002; DeCelles and Horton, 2003; Hernández and Echavarría, 2009). South of 22.5°S, the geologic record is consistent with slow protracted shortening from Eocene to early Miocene time, followed by high exhumation rates thereafter (Echavarría et al., 2003; Carrapa et al., 2011; DeCelles et al., 2011; Siks and Horton, 2011; Carrapa and DeCelles, 2015; Quade et al., 2015; Reiners et al., 2015).

The greater than 4 km (2.5 mi) thick foreland succession in the sub-Andean Zone to eastern inter-Andean Zone is composed of Oligocene to Quaternary clastic deposits that disconformably overlie Jurassic–Cretaceous Ichoa Formation eolian sandstones. Previous studies of the eastern sub-Andean Zone (Uba et al., 2005, 2009) recognized the following lithostratigraphic units (Figure 3), although the exact age assignments and regional distributions are anticipated

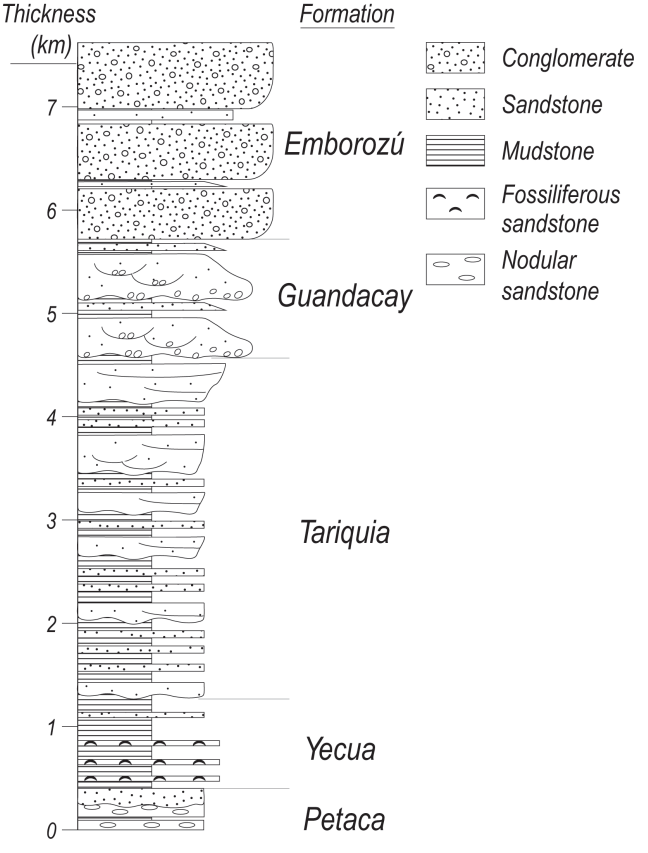

Figure 3. Schematic stratigraphic profile of the Cenozoic clastic succession of the sub-Andean–Chaco foreland basin of southern Bolivia (modified from Uba et al., 2005).

to vary within the basin due to diachronous fold-thrust deformation and flexural subsidence. At the base, the Oligocene–lower Miocene Petaca Formation represents pedogenically altered sandstones and minor conglomerates of a low-sinuosity fluvial system (Figure 3). The middle Miocene Yecua Formation, which is restricted to the eastern sub-Andean Zone and Chaco foreland, consists of bundled mudstones, marls, and fossiliferous sandstones deposited in tidally influenced marine settings (Marshall and Sempere, 1991; Marshall et al., 1993; Hernández et al., 2005; Hulka et al., 2006; Uba et al., 2007). The main body of the foreland succession is defined by upper Miocene sandstones and mudstones of the Tariquia Formation (Figure 3), which represent mixed anastomosing and braided fluvial systems. In upper stratigraphic levels, the uppermost Miocene–lower Pliocene conglomeratic Guandacay Formation and Pliocene–Quaternary Emborozú Formation represent deposition in braided fluvial, fluvial megafan, and localized alluvial fan environments (Ayaviri, 1964; Dunn et al., 1995; Moretti et al., 1996; Echavarría et al., 2003; Uba et al., 2005; Calle, 2013).

In northern Argentina, a broadly similar foreland succession consisting of the ~7 km (~4.3 mi) thick Orán Group records comparable deposystems and lithostratigraphic relationships but a contrasting accumulation history. A basal unit, the Tranquitas Formation, represents a probable Oligocene to middle Miocene condensed interval correlative with the Petaca Formation, the basal unit in Bolivia (DeCelles et al., 2011). The disconformably overlying upper Miocene "Terciario Subandino" and Pliocene–Pleistocene El Simbolar Formation, dated by magnetostratigraphy and tuff geochronology at less than 12 Ma, recorded braided and ephemeral fluvial systems followed by alluvial fan sedimentation (Hernández et al., 1996; Reynolds et al., 2001; Constantini et al., 2002a; Echavarría et al., 2003; Amidon et al., 2015).

SEDIMENTOLOGY

Five stratigraphic sections were measured and lithofacies analyses were performed along a north–south transect spanning the greater than 4 km (2.5 mi) thick nonmarine foreland basin succession (Figures 2, 4; Ayaviri, 1964, 1971; Uba et al., 2006). The El Rosal and Entre Rios sections correspond to the eastern inter-Andean Zone, whereas the Rio Azero, San Juan del Piray, and Emborozú sections define the western sub-Andean Zone. Major facies trends include basal Petaca Formation paleosols overlain by an upward coarsening and thickening succession of meandering fluvial deposits (lower Tariquia Formation), sheetflood and braided fluvial deposits (upper Tariquia and Guandacay Formations), and alluvial fan conglomerates (Emborozú Formation). Lateral and vertical facies variations accompanied by an upsection increase in channel amalgamation suggest progradation of fluvial megafans (Horton and DeCelles, 2001; Uba et al., 2005; Hartley et al., 2010). The following section describes the characteristic lithofacies associations with their corresponding facies codes (e.g., P1, S1) affiliated with different stratigraphic units and depositional environments (Table 1; Figure 5).

Petaca Formation: Pedogenically Altered Fluvial Deposits

The Petaca Formation overlies Jurassic–Cretaceous eolian quartzose sandstones and is characterized by a 2–20 m (7–66 ft) thick basal silcrete accumulation (Figure 4). These basal pedogenic deposits are overlain by 2–10 m (7–33 ft) thick upward-fining sandstone packages lacking internal sedimentary structures with variable degrees of nodule formation. The Petaca Formation tapers southward from 100 m (328 ft) at the El Rosal and Rio Azero sections to 20 m (66 ft) at the Entre Rios section (Figures 2, 4).

Paleosols (P1) Fine- to medium-grained sandstones with irregular texture, isolated pebbles, and silica (chalcedony) and calcite cement characterize the Petaca Formation (Figure 5a.). The 0.2–2 m (0.7–7 ft) thick beds are laterally continuous for tens of meters. A basal, 2–20 m (7–66 ft) thick nodular silcrete displays a disorganized pebble conglomerate/breccia appearance surrounded by a fine-grained sandstone matrix. Intense physical and chemical weathering has obliterated primary sedimentary structures and precipitated abundant chert and calcite nodules with irregular morphologies ranging from moderately elongate to vertical rhizocretions (2–3 cm [0.8–1.2 in.] wide, 20–60 cm [8–24 in.] long) and semispherical forms (Figure 5a.). At the El Rosal section, an isolated, basal tabular calcareous mudstone (0.05–0.60 m [0.16–2 ft] thick) that persists laterally for tens of meters is capped by mottled calcareous massive sandstones with blocky peds (Figure 5b.).

We interpret the basal silcrete as intensely weathered bedrock regolith material derived locally from eolian quartzose sandstones of the underlying Jurassic–Cretaceous formations. In contrast, the nodular sandstones with silica and calcite cement forming the main body of the Petaca Formation likely represent braided fluvial channels variably overprinted

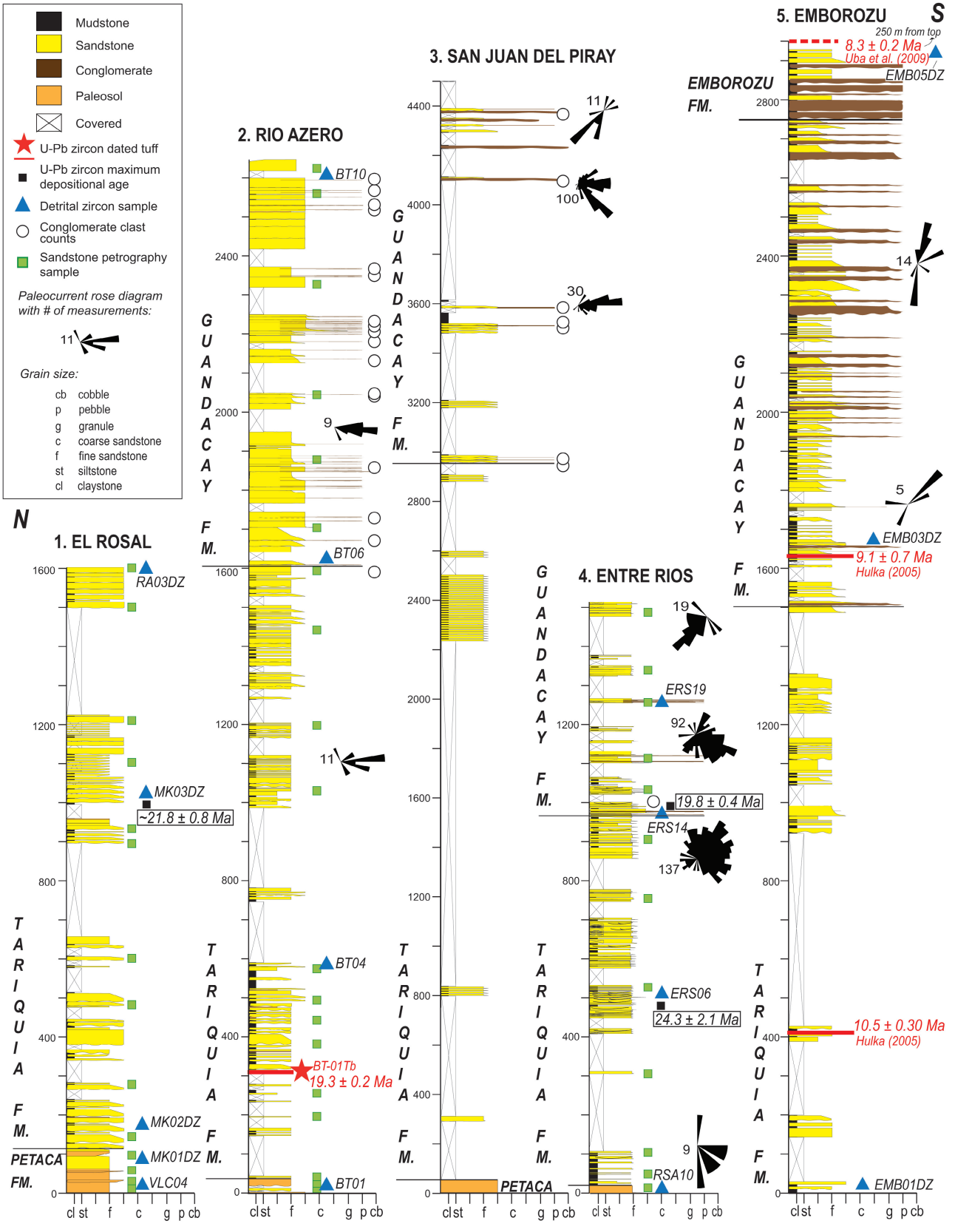

Figure 4. Cenozoic measured stratigraphic sections of the sub-Andean foreland basin (see Figure 2 for locations) showing formations (Fm.), lithofacies, paleocurrent rose diagrams, and locations of samples for sandstone petrographic, clast compositional, and U-Pb detrital zircon and tuff analyses. U-Pb tuff and detrital zircon maximum depositional ages are highlighted. Notice the change in vertical scale for the San Juan del Piray section.

Table 1. Facies associations and interpretations for the Petaca, Tariquia, Guandacay, and Emborozú Formations using categories modified from Miall (1992, 2010).

	Facies Association	Lithofacies	Description	Interpretation
P1	Paleosol	P, Sm, C	Massive, structureless sandstones with irregular calcite nodules, rhizocretions, and chert nodules, floating granules, irregular contacts. Chalcedony and calcite cement. Interbedded calcareous mudstones	Subaerially exposed braided channels altered by pedogenesis; calcisols
S1	Upward-fining, cross-stratified sandstones capped by mudstones	Sp, St, Sl, Fm, Fl,	Large-scale epsilon cross-stratified (< 2.5 m thick bedset), trough cross-stratified, and cross-laminated sandstones capped by structureless, massive and minor laminated mudstones (1–3 m thick) with calcareous nodules at the top	Meandering point bars overlain by floodplain deposits with incipient paleosols
S2	Tabular, thick-stratified sandstones	Sm, Sp, Fl, Fm	Tabular to irregular, structureless, planar laminated sandstones with mud rip-clasts at the base, and minor dessication cracks, current ripples. and bioturbation. Multistory sandstones (> 50 m thick) with internal scouring less than 0.6 m deep filled with low-angle inclined sandstones and mudstones. Associated up-section with S3.	Unconfined sheetfloods to confined braided channels
S3	Thinly interstratified sandstones and mudstones	Sm, Sp, St, Sl, Fl	Tabular to lenticular, cross-laminated, planar laminated, and minor bioturbated sandstones laterally interfingering with laminated and nodular mudstones less than 0.5 m thick.	Crevasse splay systems on ephemeral streams
S4	Lenticular, tabular cross-stratified, thick-stratified sandstones	St, Sp, Gh, Sm	Wavy, large-scale inclined, trough cross-stratified sandstones; less than 5 m thick cycle. Up to 2 m thick basal intraformational conglomerates. Tabular to lenticular conglomerates with faint imbricated clasts at the base less than 5 m thick, light yellow, green nodular sandstones at top of cycles; occasional bioturbation.	Downstream accretion of compound braided bars, and conglomerate lags in braided channels
G1	Upward-fining, cross-stratified conglomerates and sandstones	Gp, Gh, Gt, St, Sp	Well-organized, large-scale, low-angle cross-stratified conglomerates grading to sandstones in 10–20 cm thick cycles; clast imbrication; eroded by moderately organized, faintly graded conglomerates with erosional surfaces less than 1 m deep.	Compound braided channels fills with lateral and downstream accretion of bars
G2	Matrix-supported conglomerates and sandstones	Gm, Sh	Irregular to tabular, disorganized, matrix-supported conglomerates (<5 m thick), with subtle reverse grading; capped by structureless and massive sandstones, less than 5 m thick.	Debris flows and sheetfloods on alluvial fans

by paleosols, here interpreted as composite calcisols (e.g., Thiry and Maréchal, 2001; Nash et al., 2004). Prolonged calcisol formation involved the coalescence of calcareous nodules and local development of resistant horizons of pedogenic carbonate or calcrete (e.g., Retallack, 1988; Kraus, 1999).

Tariquia and Guandacay Formations: Fluvial Channel and Floodplain Deposits

The variably preserved 1000–4500 m (3281–14,764 ft) thick Tariquia–Guandacay Formations exhibit a conspicuous upward coarsening and thickening trend

Figure 5. Photos of Cenozoic sedimentary facies, including the Petaca, Tariquia, Guandacay, and Emborozú Formations. A. Nodular paleosols with rhyzocretions in the Petaca Formation (see hammer for scale). B. Calcareous mudstones attributed to protracted pedogenesis, including coalescence of calcareous nodules in the Petaca Formation. C. Wedge sandstones capped by mudstones, interpreted as meandering point bars and floodplain deposits in the Tariquia Formation. D. Tabular, thick-bedded, multistory sandstones alternating with thin mudstones, interpreted as sheetflood deposits of the Tariquia Formation (see vehicle in the lower right for scale). E. Tabular sandstones with low-angle internal scours filled with mudstones and sandstones interpreted as sheetflood deposits. F. Thinly bedded sandstones and mudstones representing crevasse splay deposits typical of the Tariquia Formation. G. Wavy, trough cross-stratified sandstones formed by dune migration in less than 2 m (7 ft) deep braided channels of the Guandacay Formation. H. Large-scale cross-bedded pebble conglomerates and sandstones representing compound bars eroded by braided channels of the Guandacay Formation. I. Lenticular cobble-conglomerates and sandstones interpreted as downstream accretion of braided bars of the Guandacay Formation. J. Matrix-supported, disorganized cobble-boulder conglomerates and structureless sandstones attributed to debris flows and sheetfloods in alluvial fans of the Emborozú Formation (see hammer for scale).

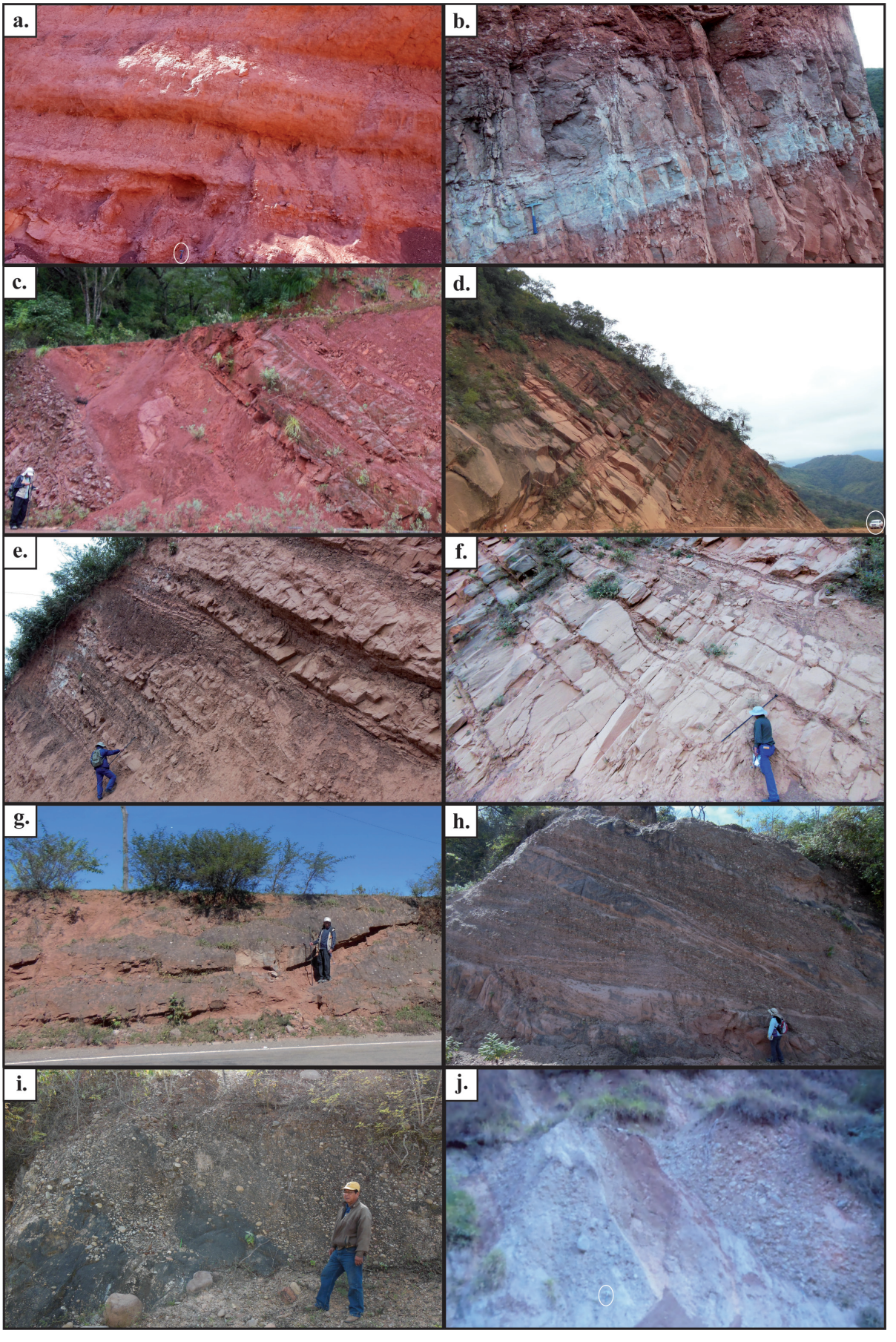
a.
b.
c.
d.
e.
f.
g.
h.
i.
j.

(Figure 4). Sandstones of the Tariquia Formation are wedge shaped and cross-bedded at the base of the succession, but in upper levels, they are tabular, typically structureless, with common rip-up clasts. Bedsets persist along strike for 30 m (98 ft) or more. The basal upward-fining packages include epsilon cross-stratification overlain by thick mudstones, consistent with deposition in meandering fluvial systems. In middle and upper levels, multistoried sandstone bodies represent the amalgamation of braided channels alternating with tabular sheetflood deposits. The basal erosive and undulatory sandy- and pebble-cobble–dominated conglomerates of the Guandacay Formation are laterally persistent for more than 15 m (49 ft). This upper segment is interpreted as braided channels typical of medial and proximal fluvial megafans.

Upward-Fining, Cross-Stratified Sandstones Capped by Mudstones (S1) In the lower Tariquia Formation, 0.5–5 m (1.6–16 ft) thick, upward-fining, fine-grained sandstones to mudstones with associated gypsum veins are laterally extensive for greater than 30 m (98 ft) (Figure 5c.). The sandstones include large-scale epsilon cross-stratification (<2.5 m [<8 ft] thick bedset) and current ripple cross-stratification, which are capped by 1–3 m (3–10 ft) thick structureless to horizontal laminated mudstones with scattered calcite nodules at the top. The upward-fining packages and lateral accretion surfaces perpendicular to the flow direction suggest deposition on meandering point bars followed by well-developed floodplain deposition with incipient paleosol development (Miall, 2010; Nardin et al., 2013).

Tabular, Thick-Stratified Sandstones (S2) The middle-upper Tariquia Formation consists of sheet-like to irregular, 1–22 m (3–72 ft) thick, fine-grained sandstones intercalated with 5–10 cm (2–4 in.) thick laminated mudstones that persist laterally for hundreds of meters (Figure 5d., e.). Individual beds of structureless to horizontally stratified sandstones contain basal mudstone rip-up clasts and discrete desiccation cracks, asymmetric ripples, and moderate bioturbation in upper levels. Most sandstone beds alternate with thin, lensoid, low-angle inclined mudstones. In the upper Tariquia Formation, however, isolated sandy packages are replaced by multistory sandstone bodies greater than 50 m (164 ft) in thickness with lateral continuity up to 400 m (1312 ft) (Figure 5d.). The thick, sharp-basal sandstones define three or more discontinuous, slightly concave-up erosional surfaces with 2–3 m (7–10 ft) of relief incised into underlying mudstones. The uppermost Tariquia Formation contains more laterally extensive sandstone bodies with erosive basal surfaces and minor trough cross-bedding.

Amalgamation of sandstone bodies suggests multiple avulsion events accompanied by waxing of currents and incorporation of rip-up clasts from previous floodplain deposits. We interpret these deposits as unconfined sheetflows to confined braided channels encased in thin floodplains deposited during episodic water discharge or monsoonal activity (Leier et al., 2005; Hampton and Horton, 2007; Plink-Björklund, 2015).

Thinly Interstratified Sandstones and Mudstones (S3) The Tariquia Formation also consists of tabular to lenticular, less than 8 m (26 ft) thick fine to medium-grained sandstones and mudstones overlying facies assemblage S2 (Figure 5f.). Sheet and lensoid less than 0.5 m (1.6 ft) thick sandstones encased in less than 2 m (7 ft) thick mudstones are laterally extensive for more than 50 m (164 ft). The sandstones with current ripples, horizontal lamination, and bioturbation pinch out or pass laterally over ~50–70 m (~164–230 ft) into laminated and concretion-bearing mudstones.

This facies assemblage represents overbank deposition of crevasse splays in proximity to major avulsed channel systems, with repeated injection of suspended sand during high-flood events (Galloway and Hobday, 1996; McCarthy and Martini, 1997). The lateral continuity, and in some cases the pronounced cycle thickness, can be attributed to deposition in a low-relief, rapidly aggrading and sporadically exposed floodplain.

Lenticular, Tabular Cross-Stratified, Thick-Stratified Sandstones (S4) In the Guandacay Formation, wavy, 1–5 m (3–16 ft) thick tabular cross-bedded fine- to medium-grained sandstones are laterally continuous for more than 100 m (328 ft) (Figure 5g.). Large-scale tabular cross-bedded sandstones with individual trough cross-bed units, foreset drapes of mudstone rip-up clasts, and floating pebble clasts overlie less than 2 m (7 ft) deep erosional surfaces. In every section, 5–30 cm (2–12 in.) thick lenses of pebble-cobble conglomerates define the basal contact, whereas the upper levels consist of less than 0.5 m (2 ft) thick light yellow and green nodular sandstones, with occasional vertical bioturbation and plant fragments.

We interpret that the large-tabular cross-strata with internal trough cross-bedded sandstones resulted from episodic water fluctuations during downstream accretion of compound braided bars, with sandy bedload transport of 3-D dunes (e.g., Collinson, 1996;

Plink-Björklund, 2015). Deposition of flat to gently inclined thin-bedded conglomerate lags supports rapid transport conditions (Miall, 1996). In turn, the paucity of overbank facies, limited pedogenesis, and bioturbation suggests that the sand bars were subaerially exposed for short terms in perhaps an arid region (Miall, 1992).

Upward-Fining, Cross-Stratified Conglomerates and Sandstones (G1) The upper Guandacay Formation comprises irregular, less than 3 m (10 ft) thick, normal- to un-graded pebble-cobble conglomerates and medium- to fine-grained sandstones (Figure 5h., i.). Low-angle, large-scale cross-strata of multiple 10–20 cm (4–8 in.) thick, upward-fining sets persist laterally for ~40 m (~131 ft) along and across depositional slope. The conglomerate presents pebble-support fabric and imbrication, whereas the sandstones contain occasional imbricated clasts. The clasts are moderately sorted with exceptions in tabular and isolated lenses. Poorly sorted conglomerates with concave-up erosional basal surfaces and subtle cross-bedding cut underlying cross bedded and graded sets.

This assemblage is interpreted as braided fluvial channel fills with lateral and downstream accretion of compound bars. Fluctuating water discharge and bedload delivery over flood cycles are demonstrated by channelization followed by development of multidirectional braided bars and 3-D dunes (e.g., Steel and Thompson, 1983; Bridge and Lunt, 2006).

Emborozú Formation: Matrix-Supported Conglomerates and Sandstones (G2)

Irregular to tabular, 0.6–5 m (2–16 ft) thick sheet conglomerates overlain by ~3–5 m (~10–16 ft) thick fine-grained sandstones are typical of the Emborozú Formation (Figure 5j). Poorly sorted, matrix-supported cobble-boulder conglomerates capped by sharp based, structureless and massive sandstones are laterally continuous for greater than 20 m (66 ft). The clasts are subangular to subrounded and display subtle reverse grading. Sporadic 10–30 cm (4–12 in.) thick lensoids of sandstones and siltstones are encased in the disorganized conglomerates. The matrix-supported texture and lack of internal structure suggest deposition of debris flows on alluvial fans, including the effect of dispersive pressure for the development of reverse grading. Upward grading of conglomerates to sandy and mudstone facies suggests hyperconcentrated sheet-flow deposition in alluvial fans (e.g., Nemec and Steel, 1984; Uba et al., 2005).

U-PB GEOCHRONOLOGY

U-Pb geochronologic results for 26 sandstones (16 Cenozoic samples from the sub-Andean foreland basin and 10 Paleozoic to Cenozoic samples from the Eastern Cordillera and inter-Andean Zone), and an ashfall tuff provides insights into sediment provenance and depositional ages (Figures 2, 4). Zircons were isolated following traditional separation techniques, including crushing, grinding, water table, and heavy liquid and magnetic separation. Analyses were conducted at the University of Texas at Austin using laser ablation inductively coupled plasma mass spectrometry (LA-ICP-MS), following methods outlined by Horton et al. (2016). For each sample, we analyzed ~120 randomly selected, tape-mounted, unpolished detrital zircons, avoiding cracks, inclusions, and grain edges. For volcanic samples, ~30 analyses were carried out on euhedral, inclusion- and fracture-free grains that were individually picked and mounted (e.g., Levina et al., 2014). Corrections for depth-dependent, interelemental fractionation were calculated using zircon standards GJ1 (600.4 ± 0.1 Ma) and Plesovice (PL-1; 337.2 ± 0.4 Ma). Further methods are outlined in Appendix 1.

U-Pb ages and 2σ errors (Figures 6–8; Appendix 2) are reported for analyses with less than 10% $^{206}Pb/^{238}U$ uncertainties, less than 30% discordance, and less than 5% reverse discordance. Reported ages represent $^{206}Pb/^{238}U$ ages for grains younger than 950 Ma and $^{207}Pb/^{206}Pb$ ages for older grains. Where appropriate, estimates of maximum depositional age (Figure 6) are derived from the calculated weighted mean age of the youngest concordant grains (three samples) or youngest single grain (one sample), following the approach of Dickinson and Gehrels (2009). Results are displayed as probability density functions and organized in stratigraphic order (Figures 7, 8). The plotted age spectra show ages less than 2000 Ma, as older grains encompass less than 5% of grains and are not diagnostic for regional provenance.

For statistical comparison of U-Pb spectra (Figures 7, 8), we employ a nonmetric multidimensional scaling (MDS) plot, which portrays the D values of the Kolmogorov-Smirnov test (K-S test; Vermeesch, 2013). This two-dimensional plot identifies greater similarity for samples that cluster together and less similarity for those plotting farther apart. To evaluate if the MDS plot accurately represents dissimilarity between samples (goodness of fit), a Shepard plot is presented, with a stress factor of zero for a perfect goodness of fit and greater than 0.2 for a poor goodness of fit. From a catalog of U-Pb results for potential sediment sources (Calle, 2013), we delimited

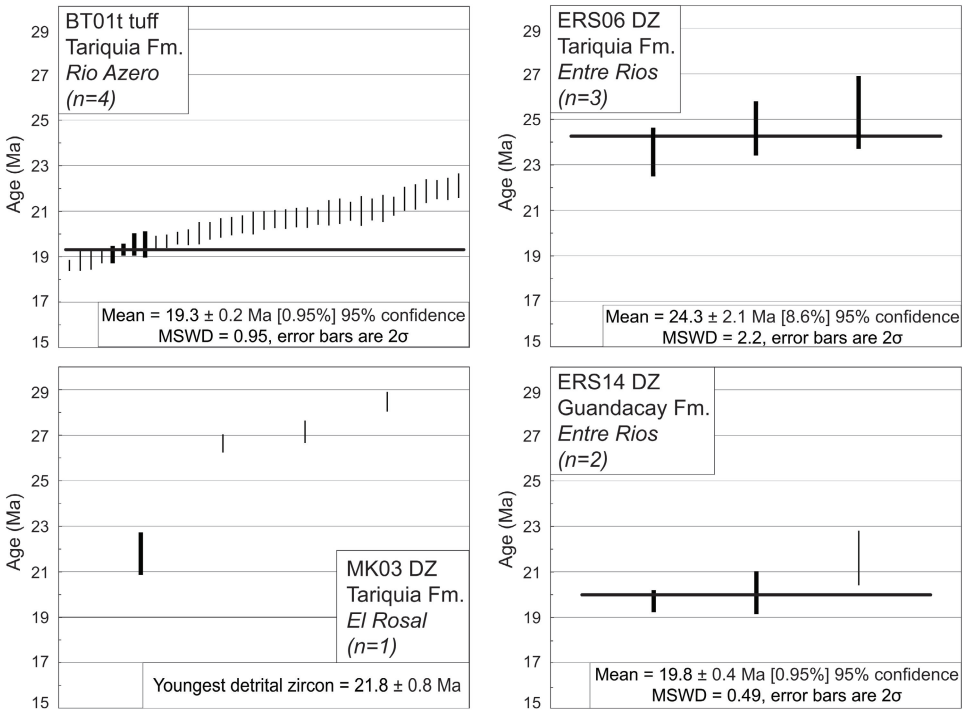

Figure 6. Mean U-Pb ages for a tuff from the Rio Azero section and detrital zircon (DZ) estimates of maximum depositional ages for the El Rosal and Entre Rios sections. Mean ages were calculated from the youngest concordant zircon grains. Mean ages include systematic and random errors. Thicker bars represent grains used for calculation (n = number of grains).

different domains in the MDS plot representing the principal sources (Appendix 3) and obtained a fair goodness of fit (stress) equal to 0.111 (Figure 9). A second statistical test evaluating the similarity of Cenozoic samples to source regions was followed by calculation of cross-correlation coefficients of probability density functions (Appendix 4) using guidelines of Saylor and Sundell (2016). Cross-correlation coefficients take into account the shape, magnitude, and presence of age peaks. The R^2 value range from 0 to 1, with $R^2 \sim 1$ when two samples show higher similarity.

Depositional Age Constraints

A refined history of sub-Andean foreland sedimentation is provided by maximum age constraints from U-Pb results for one tuff and three detrital samples (Figures 4, 6). The new age estimates are integrated with past results and reported from north to south.

The Tariquia Formation shows conflicting ages from north to south (Figures 4, 6). A detrital sample at El Rosal (1010 m [3314 ft] level, sample MK03DZ) yields a youngest zircon age of 21.8 ± 0.8 Ma. A ~30 cm (~12 in.) tuff at Rio Azero (300 m [984 ft] level, sample BT01t) dated at ~19.3 ± 0.2 Ma (n = 4 youngest concordant grains out of 37 grains); this age refines the 24.4 ± 2.6 Ma zircon fission track age reported by Erikson and Kelley (1995) for the same horizon. Similarly, at Entre Rios (495 m [1624 ft] level, sample ERS06), the Tariquia cannot be older than 24.3 ± 2.1 Ma (n = 3). At Emborozú, however, deposits attributed to the Tariquia contain an interbedded tuff dated at 10.5 ± 0.30 Ma (Hulka, 2005).

Depositional ages for the upper Tariquia and lower Guandacay Formations are less well constrained. In the north, at the San Juan del Piray and Rio Azero sections, the best age estimates for the top of Tariquia derive from linear interpolation of an 11.7 Ma apatite fission track age (Lease et al., 2016) and the aforementioned basal Tariquia tuff of ~19.3 ± 0.2 Ma. Assuming the 11.7 Ma age delimits the top of the Guandacay at San Juan del Piray section (~4500 m [~14,764 ft] level) and steady accumulation rates (553 m/m.y., see next section), the top of Tariquia at San Juan del Piray and Rio Azero would be roughly at 14.5 Ma and 17.0 Ma, respectively. The most robust age for the lower Guandacay is defined at Emborozú by a tuff dated by Hulka (2005) at ~9.1 ± 0.7 Ma. At Entre Rios (972 m [3189 ft] level, sample ERS14), the maximum depositional age for the top of Tariquia cannot be older than 19.8 Ma ± 0.4 Ma (n = 2). Therefore, from regional extrapolation, Tariquia deposition at Entre Rios should be between 24.3 ± 2.1 and ~9.1 ± 0.7 Ma. Finally, upsection, a tuff from the basal Emborozú Formation at the Emborozú section yields an age of 8.3 ± 0.2 Ma (Uba et al., 2009; Figure 4).

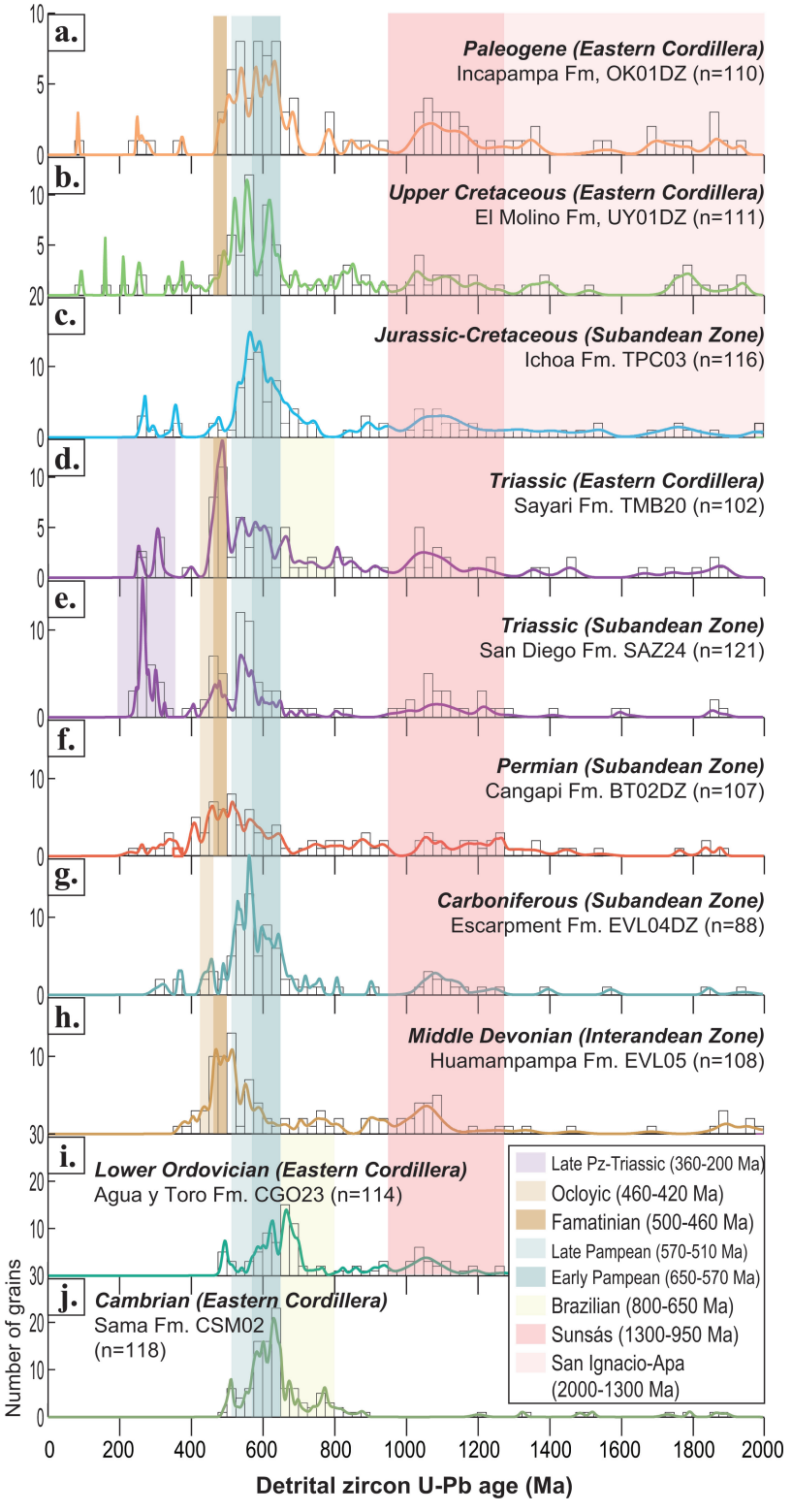

Figure 7. U-Pb age distributions for 10 potential Paleozoic–Cenozoic sources from the Eastern Cordillera, inter-Andean Zone, and sub-Andean Zone of southern Bolivia. Age spectra are shown as probability density functions, color-coded according to bedrock (Figure 2), and age histograms (open rectangles with bin size spanning 25 m.y.) arranged in stratigraphic order (*n* = number of analyzed grains). Diagnostic age components are depicted as color-shaded boxes in order to track Cenozoic sediment sources. Note the Brazilian components of lower Paleozoic strata of the Eastern Cordillera, Famatinian–Ocloyic zircons characteristic of the inter-Andean Zone and sub-Andean Zone, and late Paleozoic–Triassic ages typical of Triassic formations. Cretaceous and Paleogene samples of the Eastern Cordillera depict first-cycle Cretaceous grains and cosmopolitan components.

Therefore, from north to south, available geochronologic results indicate an Oligocene–earliest Miocene (~32–24 Ma) age for the Petaca Formation and most of the correlative Tranquitas Formation of northern Argentina (Marshall and Sempere, 1991; DeCelles et al., 2011; Poire et al., 2013). In contrast, an apparent time-transgressive southward-younging trend of lithostratigraphic units is revealed by an early–middle Miocene U-Pb component for the Tariquia and Guandacay Formations at 19.5–21.5°S, yet late Miocene (<10 Ma) ages for the Tariquia, Guandacay, and Emborozú Formations south of 22°S, including equivalent formations in northern Argentina (Hernández et al., 1996; Reynolds et al., 2001; Echavarría et al., 2003; Hulka, 2005; Uba et al., 2009; Amidon et al., 2015). This along-strike (north–south) age variation is matched by a cross-strike (east–west) diachroneity developed during eastward advance of the orogenic wedge. For example, U-Pb tuff ages delimit an upper Miocene Tariquia Formation (7.9–5.9 Ma), uppermost to Pliocene Guandacay Formation (5.9–2.1 Ma), and Pleistocene Emborozú Formation (<2.1 Ma) in the eastern Angosto del Pilcomayo section (Moretti et al., 1996; Hulka, 2005; Uba et al., 2005, 2006, 2007, 2009).

Sediment Accumulation Rates

Average sub-Andean accumulation rates are estimated on the basis of youngest U-Pb age components and

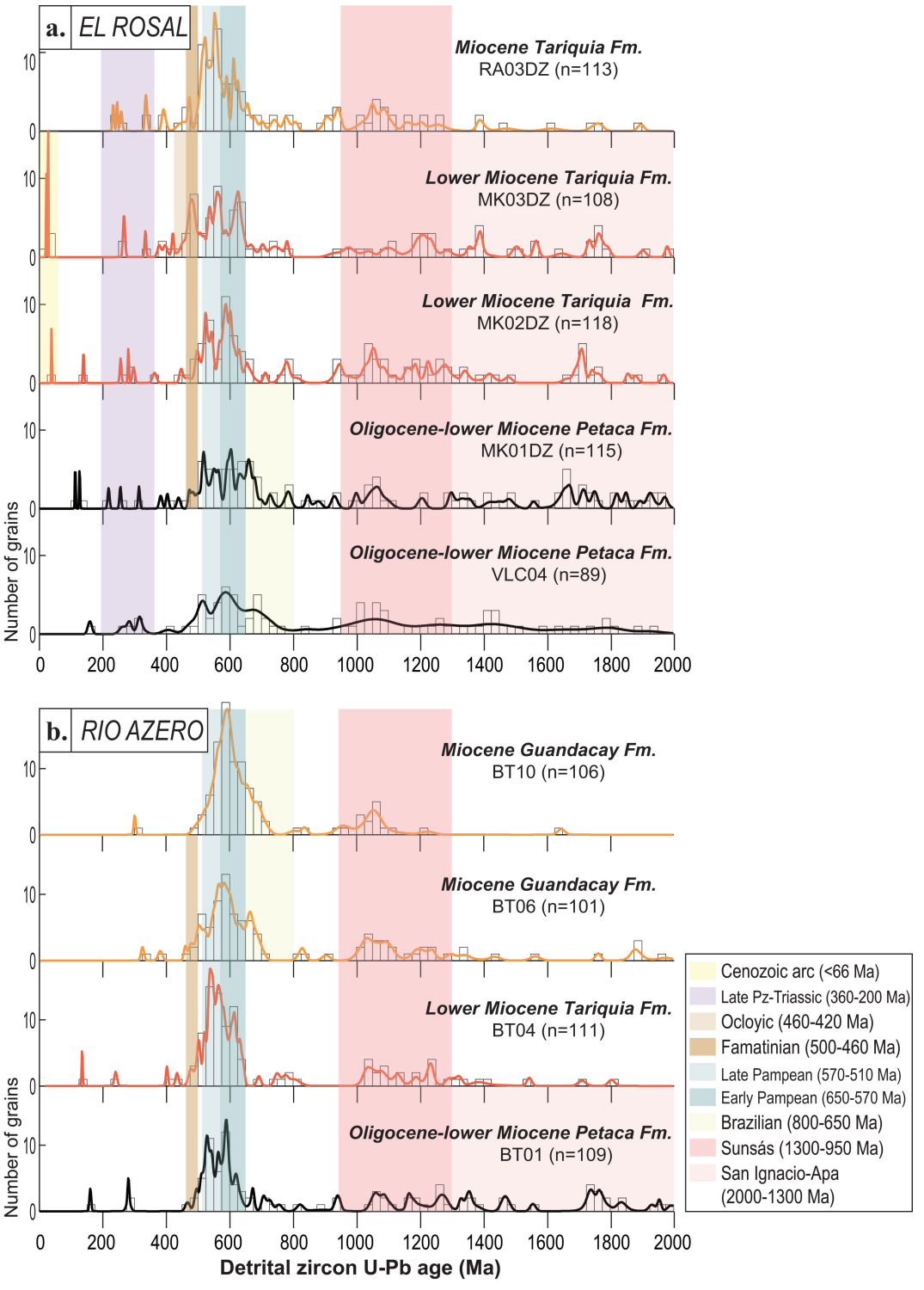

Figure 8. Comparative plots of U-Pb detrital distributions for 16 Cenozoic samples from (A.) El Rosal, (B.) Rio Azero, (C.) Entre Rios, and (D.) Emborozú sections of the sub-Andean foreland basin (see Figure 2 for locations). Age distributions are color-coded according to formation (Fm.): Petaca (black), Tariquia (red), Guandacay (orange), and Emborozú (yellow) Formation samples. Shaded boxes are color-coded as in Figure 7. Notice the variable U-Pb contributions from the inter-Andean Zone (Famatinian–Ocloyic and late Pampean grains) and Eastern Cordillera (early Pampean, Brazilian, and Cretaceous grains) and variable introduction of Cenozoic grains likely corresponding to synmagmatic deposition.

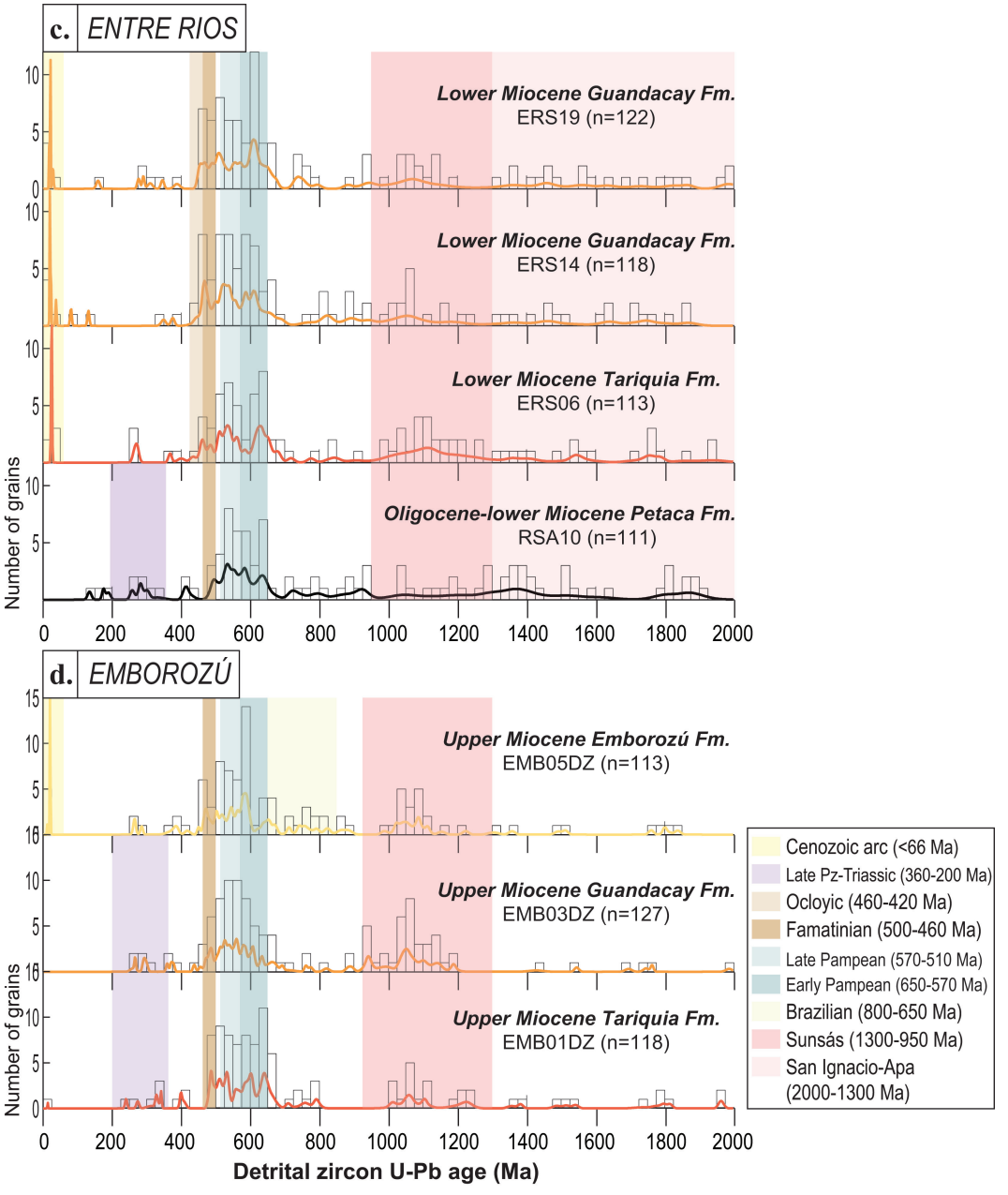

Figure 8. (Continued)

measured stratigraphic thicknesses. We did not correct for compaction given the limited overburden and preservation of primary porosity in sandstone petrographic analyses. At Entre Rios, the Petaca Formation (25 m [82 ft]) yields an Oligocene accumulation rate of only 3 m (10 ft)/m.y. (32.0–24.3 Ma). For the overlying Tariquia Formation (956 m [3136 ft]), bounding ages of 19.3 ± 0.2 Ma (Rio Azero tuff) and 9.1 ± 0.7 Ma (Emborozú tuff; Hulka, 2005) define Miocene accumulation of 93 m (305 ft)/m.y. (88–97 m [289–318 ft]/m.y. within analytical error). For the San Juan del Piray section, along-strike stratigraphic tuff correlation of the 19.3 ± 0.2 Ma tuff and an 11.7 Ma apatite fission track age for the top of the section (Lease et al., 2016) yield a Miocene accumulation rate for the composite Tariquia and Guandacay Formations of ~553 m (~1814 ft)/m.y. (539–568 m [1768–1864 ft]/m.y. within analytical error). At Emborozú, reported tuff ages of 10.5 and

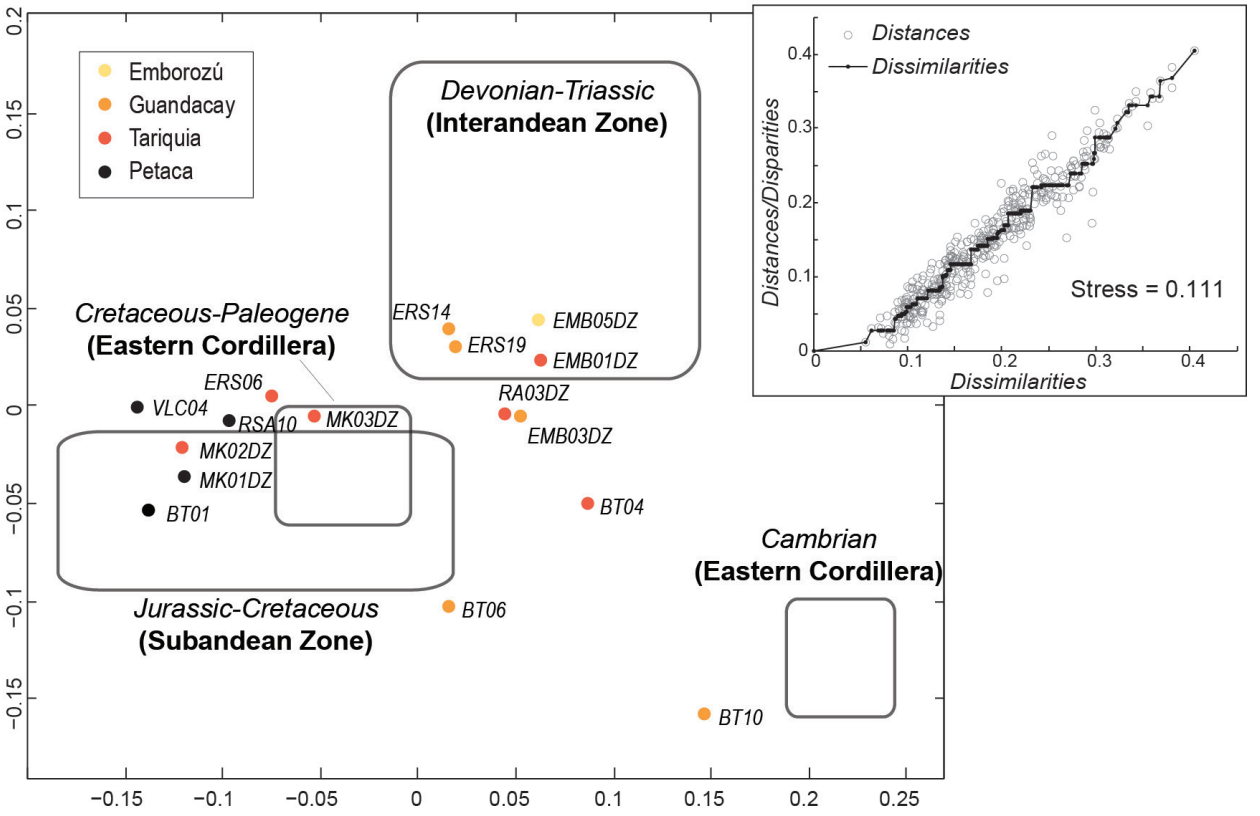

Figure 9. Nonmetric multidimensional scaling (MDS) plot of 16 Cenozoic samples from the sub-Andean foreland basin (color-coded dots as in Figure 8) and Shepard plot (Stress = 0.111). For comparison, sediment source domains including bedrock age are plotted as rectangular fields (Eastern Cordillera, inter-Andean Zone, and sub-Andean Zone). Source domains derived from regional Paleozoic–Cenozoic U-Pb detrital zircon databases (Calle, 2013; this study). Note the clustering of Petaca Formation samples in the sub-Andean Zone source domain and in proximity to the Cretaceous–Paleogene Eastern Cordillera domain. The Tariquia, Guandacay, and Emborozú Formation samples show higher similarity to inter-Andean Zone and Eastern Cordillera domains.

9.1 Ma for the Tariquia and lowermost Guandacay Formations (1230 m [4035 ft]; Hulka, 2005; Uba et al., 2009) reveal a late Miocene accumulation rate of 879 m (2884 ft)/m.y. (684–1230 m [2244–4035 ft]/m.y. within error). The Guandacay and Emborozú Formations (1650 m [5413 ft]) at Emborozú display a latest Miocene accumulation rate of 2062 m (6765 ft)/m.y. (1239–5500 m [4065–18,045 ft]/m.y. within error), in agreement with faster accumulation rates after ~8 Ma in northernmost Argentina (Echavarría et al., 2003).

The clear pattern of accelerated accumulation over a greater than 20–25 m.y. time frame (from Oligocene to latest Miocene) is typical of advancing foreland depozones. However, an additional along-strike pattern is revealed by a post–10 Ma increase in accumulation rates south of 22°S, from 878 m (2881 ft)/m.y. to 2062 m (6765 ft)/m.y. Supporting a coupled eastern progression of foreland histories, at ~8–6 Ma sediment, accumulation rates beneath the sub-Andean thrust front increased from 130 m (427 ft)/m.y. to 630 m (2067 ft)/m.y. (Uba et al., 2007).

Detrital Zircon U-Pb Geochronology

Potential Sediment Sources Detrital zircon U-Pb age spectra for 10 bedrock samples (Figure 2; Calle, 2013) help discriminate contributions from Cambrian, lower Ordovician, middle Devonian, Carboniferous, Permian, Triassic, Jurassic, Cretaceous, and Paleogene stratigraphic units. Although recycling may hinder unambiguous determination of some central Andean domains (e.g., Augustsson et al., 2015), integrated analyses allow characterization of key bedrock sources affiliated to distinct source domains in the MDS plot (Figure 9).

Diagnostic U-Pb age components (Figure 7) include San Ignacio–Apa (2000–1300 Ma); Sunsás (1300–950 Ma); Brazilian (800–650 Ma); Pampean (650–510 Ma); Famatinian (500–460 Ma); Ocloyic (460–420 Ma); and late Paleozoic–Triassic (360–200 Ma). San Ignacio–Apa ages are indicative of sub-Andean Jurassic–Cretaceous (Figure 7c.) and Eastern Cordillera Upper Cretaceous–Paleogene samples (Figure 7a., b.). The Grenville-age equivalent Sunsás age component is present in all samples. In turn, Brazilian age components are limited to lower Ordovician (Figure 7i.) and Cambrian (Figure 7j.) samples of the Eastern Cordillera. Older Pampean (650–570 Ma) components are typical of lower Paleozoic samples (Figure 7i., j.), whereas younger Pampean (570–510 Ma) components characterize Carboniferous (Figure 7g.) and variable Jurassic–Paleogene (Figure 7a.–c.) samples from the sub-Andean Zone and Eastern Cordillera. In turn, Famatinian (500–460 Ma) grains constitute the dominant mode of Devonian successions and were later recycled into Permian–Paleogene samples, except in the sub-Andean Jurassic–Cretaceous sample (Figure 7c.). The Ocloyic (460–420 Ma) signature is recognized in middle Devonian to Triassic (Figure 7d.–h.) samples from the Eastern Cordillera to the sub-Andean Zone. Conspicuous late Paleozoic–Triassic signatures are ascribed solely to Triassic samples (Figure 7d., e.), but sparse Jurassic–Cretaceous zircon grains are present throughout Mesozoic samples from the Eastern Cordillera and sub-Andean Zone.

Cenozoic Basin Fill Spatial and temporal variations in provenance are revealed through U-Pb age distributions from four outcrop belts (Figure 8). Results for 16 sandstone samples from the northern (19.5°S, El Rosal syncline and Rio Azero footwall), central (21.5°S, Entre Rios syncline), and southern (~22.5°S, Emborozú syncline) segments of the sub-Andean foreland basin (Figure 2) are presented sequentially for Oligocene to upper Miocene units. Acknowledging the diachroneity of lithostratigraphic units, the stratigraphic age of samples is included for description and interpretation purposes.

Four samples of the Oligocene–lowermost Miocene Petaca Formation (Figure 8) are dominated by Sunsás–San Ignacio–Apa (2000–950 Ma) and Pampean (650–510 Ma) age components, with minor Famatinian (500–460 Ma) and late Paleozoic–Mesozoic zircon grains. The two dominant signatures are well expressed in the MDS plot (Figure 9) and unambiguously correlated with eolian sediments of the Jurassic–Cretaceous Botucatu-Ichoa Formation (Scherer and Goldberg, 2007; Canile et al., 2016; Peri et al., 2016) and/or Cretaceous–Paleogene fill of the Eastern Cordillera (DeCelles and Horton, 2003; Horton, 2005).

Nine samples from the lower to middle Miocene Tariquia and Guandacay Formations show complex age distributions representing shifts in source regions (Figures 8, 9). In the north at El Rosal (19.5°S), Tariquia age spectra show minor Sunsás–San Ignacio (2000–1300 Ma) and persistent Pampean (650–510 Ma) components linked to gradual input of Famatinian, Ocloyic, and synvolcanic Cenozoic grains (Figure 8a.). Cosmopolitan age distributions coupled with a systematic upsection shift from early Pampean (570–650 Ma) to late Pampean (510–570 Ma) ages suggest diminished input from Cretaceous–Paleogene sources of the Eastern Cordillera accompanied by initial Devonian–Triassic contributions from the inter-Andean Zone. East of El Rosal, at Rio Azero, the most distinctive pattern is the upsection shift from late Pampean (570–510 Ma) to early Pampean (650–570 Ma) components (Figure 8b.). In conjunction, the gradual emergence of Brazilian (800–650 Ma) and decline of Famatinian (500–460 Ma) ages suggest initial input of Devonian–Permian detritus from the inter-Andean Zone and lower Paleozoic detritus from the Eastern Cordillera, with an upsection transition to dominant Eastern Cordillera sources. This shift in source regions is clearly depicted in trends between source domains of the MDS plot (Figure 9).

In contrast, in the south at Entre Rios (21.5°S), a composite age distribution is represented by substantial Sunsás–Apa (2000–950 Ma) and Pampean (650–510 Ma) signatures, subordinate Famatinian (500–460 Ma) and Ocloyic (460–420 Ma) components, and limited Cretaceous and Cenozoic ages (Figure 8c.). The Sunsás–Apa signature together with cosmopolitan ages, particularly the Cretaceous grains, require the continuous input of Mesozoic (and/or reworked Paleogene) along with minor early Paleozoic detritus from the Eastern Cordillera. In contrast, Famatinian and Ocloyic signatures argue for Devonian–Carboniferous contributions from the inter-Andean Zone. Both Eastern Cordillera and inter-Andean components are well expressed in a MDS plot for lower Miocene Entre Rios samples (Figure 9). Therefore, in contrast to the northern sections, a drainage system linking the foreland basin with older segments of the thrust belt, both the Eastern Cordillera and inter-Andean Zone, along with possible downstream fertility variations, may be interpreted from Entre Rios zircon components.

Three samples of the upper Miocene Tariquia, Guandacay, and Emborozú Formations from the Emborozú section reveal upsection fluctuations in

Pampean (650–510 Ma) and Sunsás (1300–950 Ma) age distributions, along with sustained minor components of Famatinian (500–460 Ma), late Paleozoic–Triassic (360–200 Ma), and Cenozoic age (Figure 8d.). An upsection shift is observed from broadly distributed Pampean ages (650–510 Ma) to major late Pampean (570–510 Ma) and Sunsás (1300–950 Ma) contributions. These patterns are consistent with initial mixing of dominantly early Paleozoic and minor late Paleozoic sources from the Eastern Cordillera and inter-Andean Zone, respectively, as represented specifically within the inter-Andean Zone domain, and trending to the Eastern Cordillera domain of the MDS plot (Figure 9). The upsection increase in Pampean and Sunsás grains suggests the introduction of granitic (Escayola et al., 2011) and late Paleozoic sedimentary detritus from the inter-Andean Zone, with selective input of Brazilian (800–650 Ma) grains highlighting variable contributions from the Eastern Cordillera.

SEDIMENT PROVENANCE

Paleocurrents

We measured 439 paleocurrents at 34 stations to assess sediment routing systems. Paleocurrents were obtained from axes of trough cross-bedding, large-scale epsilon cross-strata, rippled sandstones, pebble-cobble clast imbrications, and limited scour axes and flute casts. Mean vector orientations were corrected for bedding dip (Figure 4; Appendix 5).

For the Rio Azero section, dominantly east-directed sediment transport reveals dispersal transverse to growing sub-Andean structures (Figure 4). At the San Juan del Piray section, an east–northeast to southeast transverse routing system is defined for the middle Guandacay Formation, but the uppermost Guandacay records a switch to oblique southwest-directed transport that may signal drainage reorganization related to growth of a frontal sub-Andean structure to the east (Figure 4). At the Entre Rios section, eastward paleoflow patterns for the Tariquia and lower Guandacay Formations suggest a broad range of flow directions, spanning from south to north, along a point-source fluvial megafan (e.g., Horton and DeCelles, 2001). At the top of the Guandacay Formation, however, oblique sediment transport to the southwest likely reflects a drainage shift due to eastward propagation of the deformation front (Figure 4). For the Emborozú section, paleocurrent vectors are variable but are consistent with a temporal shift to more axial (north–south) flow, potentially due to the greater influence of growing fold-thrust structures and isolation of wedge-top sub-basins in the western sub-Andean Zone.

Sandstone Composition

Sandstone compositional point counting was performed according to the Gazzi-Dickinson method for 45 samples, to assess upsection framework grain variability and sediment provenance (Dickinson and Suczek, 1979; Dickinson, 1985). Thin sections were stained for calcium- and potassium-feldspars, and 350 framework grains were counted per thin section. Modal sandstone parameters and recalculated framework grains are presented (Appendices 6, 7), with data plotted in ternary diagrams (Figure 10).

Regionally, sandstone compositions from Petaca to Guandacay vary from subarkoses to sublitharenites and litharenites (Figure 10). The Petaca sandstones exhibit modal variability from subarkoses to sublitharenites, with average $Q_{86}F_9L_5$. The well-rounded monocrystalline quartz grains of the Jurassic–Cretaceous Ichoa Formation are the dominant grains, followed by potassium feldspar and plagioclase, and minor low-grade metasiltstone fragments. Such modal patterns are consistent with dual derivation from the underlying Mesozoic successions and/or Precambrian cratons located eastward the fold-thrust belt (Hulka and Heubeck, 2010) and the westward Andean recycled orogen. The Tariquia modal framework ($Q_{82}F_5L_{13}$) corresponds to sublitharenites and litharenites (Figure 10). The sustained input of foliated metasiltstones, siltstones, and mudstones and limited microlitic and felsitic volcanic grains, coupled with a decrease of feldspars, highlights major provenance from fold-thrust belts rather than from the magmatic arc. Correspondingly, limited influence of the magmatic arc is supported by the lack of young (<40 Ma) zircons. The Guandacay sandstones ($Q_{78}F_7L_{15}$) consist of sublitharenites and litharenites (Figure 10). Input of metasiltstones, mudstones, siltstones, and chert fragments is noticeably higher compared to the underlying Tariquia sandstones and still supports a recycled orogen provenance. Local, upsection influx of feldspars and chert fragments documents erosion of Mesozoic igneous and upper Paleozoic chert successions from the inter-Andean Zone (e.g., Sempere, 1994; Grader et al., 2007). Persistent distribution of durable metasiltstone fragments in all samples argues for sustained erosion from the lower Paleozoic and/or perhaps recycling of the lower Mesozoic and Cenozoic successions of the Eastern Cordillera (DeCelles and Horton, 2003; Horton, 2005).

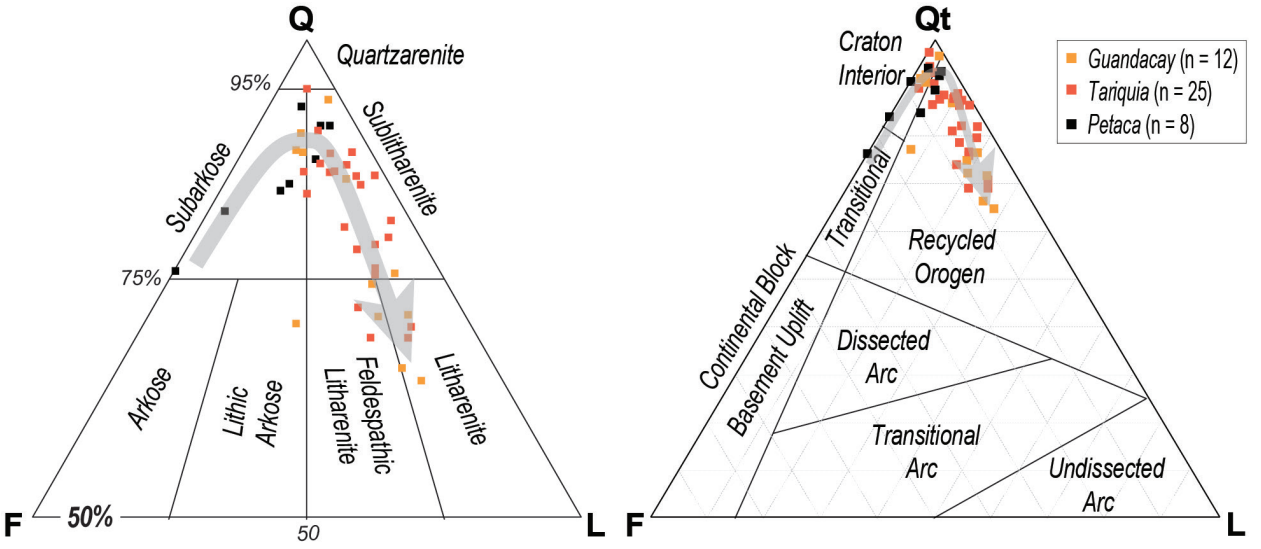

Figure 10. Standard ternary diagrams displaying modal framework grain compositions (Folk, 1980) and provenance regions (Dickinson and Suczek, 1979) from 45 Cenozoic samples of the sub-Andean foreland basin (*n* = number of samples). Samples are color coded as in Figure 8. Gray arrows show an upsection provenance trend from craton-interior Petaca Formation quartzofeldesphatic sandstones toward Tariquia and Guandacay Formation quartzolithic sandstones from recycled orogen sources.

Conglomerate Clast Composition

Clast composition counts were performed at 24 stations from the Rio Azero, San Juan del Piray, and Entre Rios sections (Figure 11). The criteria utilized to assign clast compositions to particular stratigraphic units are presented in Appendix 8. At Rio Azero, conglomeratic lags of the lower Guandacay Formation record the progressive introduction of Silurian–Devonian clasts, requiring erosion from intermediate to deep levels of the inter-Andean Zone (Figure 11; Choque and Almendras, 2012). Therefore, upsection input of Carboniferous–Permian clasts may indicate drainage reorganization and/or unroofing of frontal structures in the inter-Andean Zone. Sequential input from Jurassic, then Triassic, upper Paleozoic, and finally lower Paleozoic rocks in the lower-middle San Juan del Piray section (Figure 11) suggests progressive unroofing of shallow to intermediate levels of the inter-Andean Zone. In the upper-middle section, significant input of lower Paleozoic clasts derived from sources farther west in the Eastern Cordillera (Choque and Almendras, 2012) may indicate (1) efficient sediment pathways with limited input from late Paleozoic and Mesozoic sources of the inter-Andean Zone and/or (2) exhumation of a rejuvenated Eastern Cordillera passively uplifted along deeper structures (e.g., Steidtmann and Schmitt, 1988). In the uppermost section, higher proportions of Mesozoic and Paleozoic clasts may indicate initial unroofing of sub-Andean stratigraphic panels in growing fold-thrust structures and/or recycling of older foreland basin fill. For the Entre Rios section, the prevailing Devonian clasts indicate erosion of intermediate levels of the inter-Andean Zone during initial deposition of the Guandacay Formation.

DEFORMATION TIMING

Cross-cutting relationships in the easternmost inter-Andean Zone reveal growth strata in footwall synclines of the El Rosal (19.5°S) and Entre Rios (21.5°S) sections (Figure 12). Upsection fanning of stratal dip, changes in bed thickness, and internal angular unconformities within the Tariquia and Guandacay Formations indicate synorogenic deposition during early–middle Miocene shortening.

Synorogenic deposition in the footwall syncline at Entre Rios is associated with slip on the Santa Lucia fault (Figure 12a.). This east–southeast-verging fault places Carboniferous strata on Mesozoic strata for at least 10 km (6 mi) along strike (Figure 12b.). Pregrowth strata defined by 70–55°E-dipping Triassic to lower Miocene Tariquia strata are overlain by upper Tariquia-lower Guandacay growth strata displaying a systematic change in dip from upright 55° to 21°E, in less than 200 m (656 ft) across the syncline

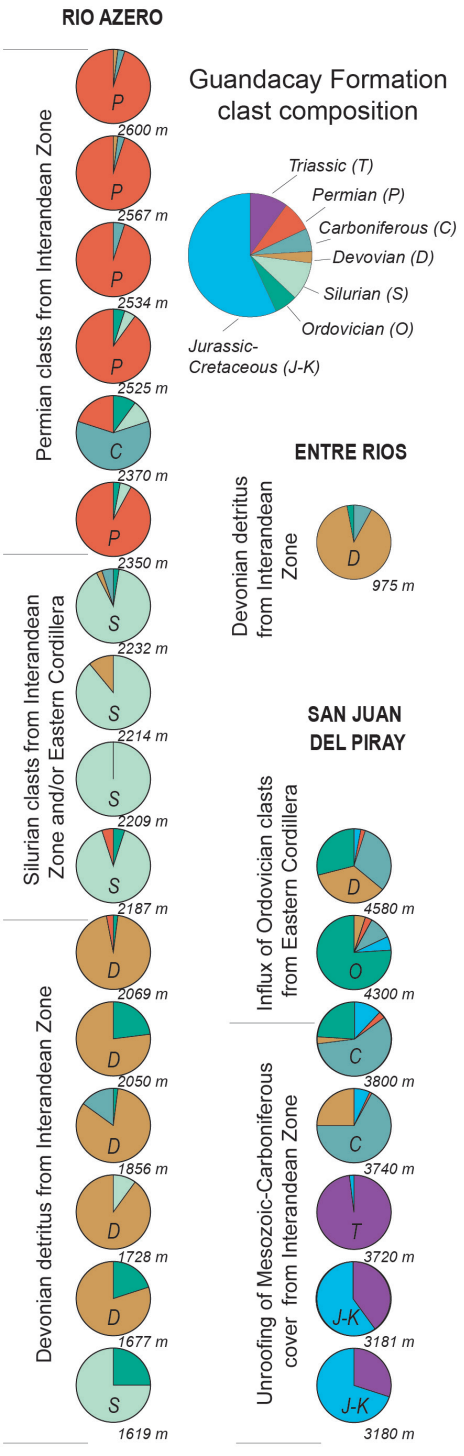

Figure 11. Guandacay Formation clast compositional data for the Rio Azero, San Juan del Piray, and Entre Rios sections. Pie charts are organized by stratigraphic level and color-coded according to bedrock units in Figure 3, with a single letter indicating the dominant composition (e.g., T = Triassic). Notice the progressive upsection introduction of older clast compositions derived from the inter-Andean Zone, with the conspicuous input of Ordovician clasts from the Eastern Cordillera at the top of the San Juan del Piray section.

axis (Figure 12a.). Abrupt lateral thickness changes including wedging of bedsets, stratal thinning toward the fault trace, and multiple updip onlap relationships are indicative of progressive unconformities (e.g., Riba, 1976). Moreover, a shift in depositional geometries is observed from pregrowth tabular sandstones to syngrowth wavy, lensoid, and wedging sandstones that scour greater than 2.5 m (8 ft) into underlying strata.

In the footwall syncline of the El Rosal section, lower Miocene Tariquia growth strata resulted from motion along the El Potrero fault (Figure 12c.). This fault juxtaposed middle Devonian strata against Carboniferous strata for at least 25 km (16 mi) along strike (Figure 12d.). A flat-on-flat fault cutoff relationship exposes an overturned (86°W) to steeply (~78°E) dipping Carboniferous to Oligocene pregrowth panel, and lower Miocene Tariquia growth strata defining an upsection fanning of dip from ~40° to 15°E (Figure 12c.). This ~90° of tilting along the west flank of El Rosal syncline is accompanied by a thickness change from 1.5 km (1 mi) near the northern plunge of the syncline to greater than 2.5 km (2 mi) along the syncline axis near the Azero River (La Revuelta locality) (Cabrera-Vildoso, 1965). Minor lateral changes include eastward thickening of resistant sandstone packages away from the fault, with multiple onlap terminations subtly observed in some resistant Tariquia sandstone packages.

These growth strata relationships reveal that the deformation front of the central Andean fold-thrust belt may have reached the easternmost inter-Andean Zone no earlier than early Miocene time (<24 Ma). When combined with past results from the Eastern Cordillera (e.g., Gubbels et al., 1993; Kley et al., 1997; Horton, 1998, 2005; Müller et al., 2002), it appears that deformation from broadly 20–10 Ma involved synchronous motion along multiple fold-thrust structures of the Eastern Cordillera to inter-Andean Zone, including structures kinematically linked to the upper (inter-Andean) basement thrust sheet.

DISCUSSION

Cenozoic advance of the fold-thrust belt and coupled foreland basin is well established for the central Andes (Kley, 1996; Moretti et al., 1996; Baby et al., 1997; Horton and DeCelles, 1997; Horton et al., 2001, 2002; DeCelles and Horton, 2003; Echavarría et al., 2003; Uba et al., 2005, 2009). However, contrasting interpretations remain regarding the timing of upper-crustal shortening in the sub-Andean segment of

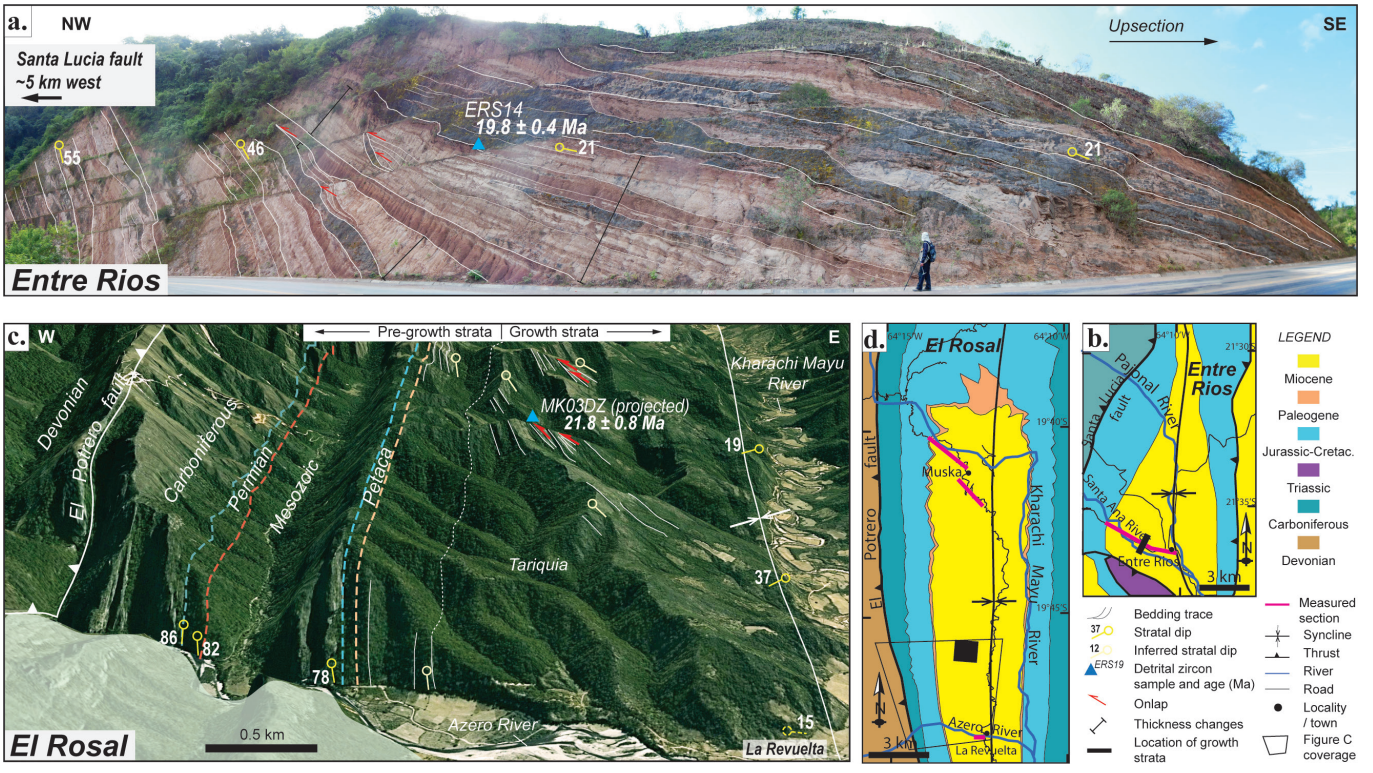

Figure 12. Photograph, maps (after Choque and Almendras, 2012), and 3-D imagery (Google Earth) of synclinal footwall growth strata at (A., D.) Entre Rios and (C., D.) El Rosal sections. Tracing of individual beds highlights fanning dip and stratal thinning relationships. Blue triangles denote detrital zircon sample horizons for which the youngest U-Pb age components constrain the timing of thrust motion.

the thrust belt, along- and across-strike variations in deformation and exhumation, and their influence on the evolution of the foreland basin. These issues are relevant for the debate over potential linkages between shortening in the sub-Andean Zone and surface uplift of the Altiplano plateau (Lamb and Hoke, 1997; Garzione et al., 2006, 2008; Lamb, 2011, 2016; Lease et al., 2016).

Our findings bear on the sub-Andean foreland depositional record and its linkage to advancing fold-thrust deformation in the Eastern Cordillera and inter-Andean Zone (Figure 13). New results concerning deposystems, U-Pb geochronology, provenance, and sediment routing for five Cenozoic outcrop belts help delineate Oligocene–Miocene advance of flexural subsidence in southern Bolivia (19.5–21.5°S) and rapid late Miocene accumulation across the sub-Andean Zone of southern Bolivia and northern Argentina (Figure 14). To highlight north–south and east–west differences in thrust belt development and foreland basin response, a reconstruction of sub-Andean basin evolution is presented along several segments, affording insights into the patterns of deformation and accumulation in both cross-section (Figure 13) and map view (Figure 14).

Oligocene-Middle Miocene Limited Accommodation and Distal Foreland Deposition

At 19.5–21.5°S, the Oligocene–lowermost Miocene Petaca Formation was deposited by low-accommodation braided fluvial systems overprinted by significant pedogenesis, with derivation from both cratonal and Andean sources. U-Pb ages and sandstone compositional data for the El Rosal and Rio Azero sections are consistent with complex sediment routing from cratonal sources as well as sub-Andean Jurassic–Cretaceous units (e.g., Hulka and Heubeck, 2010) and Eastern Cordillera Mesozoic–Lower Cenozoic rocks. These provenance results, along with regionally distributed paleosols documenting severely limited accumulation (3 m (10 ft)/m.y.), lead us to attribute Petaca deposition to a low-accommodation forebulge and the adjacent flanks of the backbulge and/or foredeep depozones (Figure 13a.).

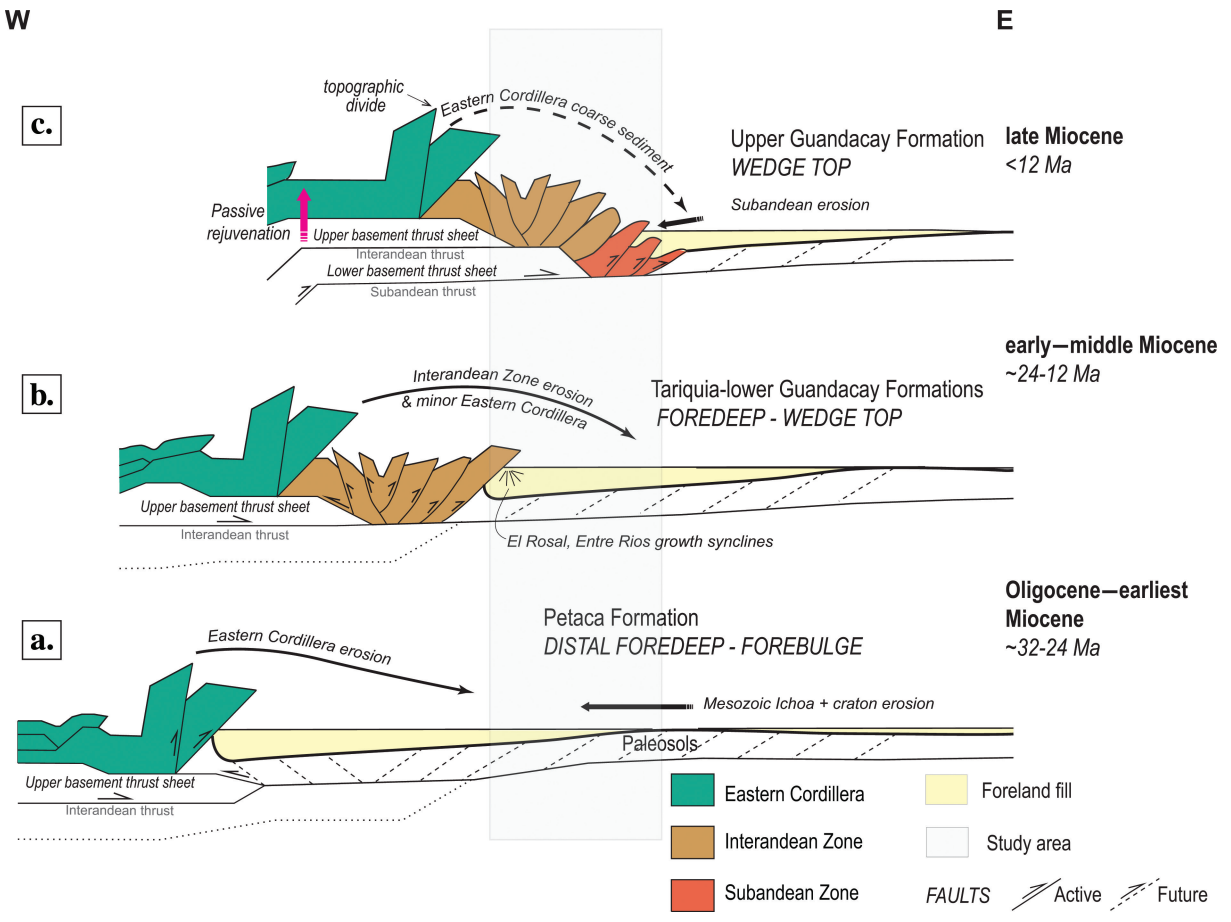

Figure 13. Schematic model of sub-Andean foreland basin evolution in Bolivia at 19.5–21.5°S with structural details from Anderson et al. (2017). Black arrows (solid and dashed) show sediment dispersal pathways, and vertical pink arrow shows possible passive rejuvenation of the Eastern Cordillera. The two basement thrust sheets (Anderson et al., 2017) responsible for growth of the inter-Andean and sub-Andean segments of the fold-thrust belt are shown diagrammatically. A. Oligocene–earliest Miocene (~32–24 Ma) accumulation of pedogenically altered fluvial deposits (derived from the Eastern Cordillera and/or eastern Mesozoic Ichoa Formation) in forebulge to distal foredeep depozones. B. Early–middle Miocene (~24–12 Ma) propagation of the inter-Andean Zone and Eastern Cordillera above the upper (inter-Andean) basement thrust sheet, inducing eastward advance of flexural subsidence and influx of Andean sediments to fluvial systems in foredeep and wedge-top depozones. C. Post–12 Ma activation of the lower (sub-Andean) basement thrust sheet along a footwall ramp, guiding passive rejuvenation of the Eastern Cordillera and long-distance transport of coarse braided fluvial deposits to foredeep locations, followed by and continued sub-Andean shortening with more proximal sources feeding and compartmentalized wedge-top sub-basins.

South of 22°S, protracted deposition of the correlative Oligocene–middle Miocene Tranquitas Formation reveals a broadly similar depositional history (Ayaviri, 1964; Hernández et al., 1996; Reynolds et al., 2001; Constantini et al., 2002a, b; Echavarría et al., 2003; DeCelles et al., 2011; Amidon et al., 2015). In northern Argentina, however, the basal paleosol zone (30–70 m [98–230 ft] thick) sits unconformably on upper Paleozoic strata of the Michicola High (the northern rift shoulder of the Lomas de Olmedo sub-basin of the Cretaceous Salta rift) and is capped by a much thicker succession (370–700 m [1214–2297 ft]) of braided fluvial, lacustrine, and eolian deposits (Figure 14a.; Hernández et al., 1996; Constantini et al., 2002a, b; Starck, 2011). Therefore, we suggest that derivation of the lithic-rich Tranquitas succession from the Eastern Cordillera (Constantini et al., 2002a; DeCelles et al., 2011; Amidon et al., 2015) recorded the Oligocene to

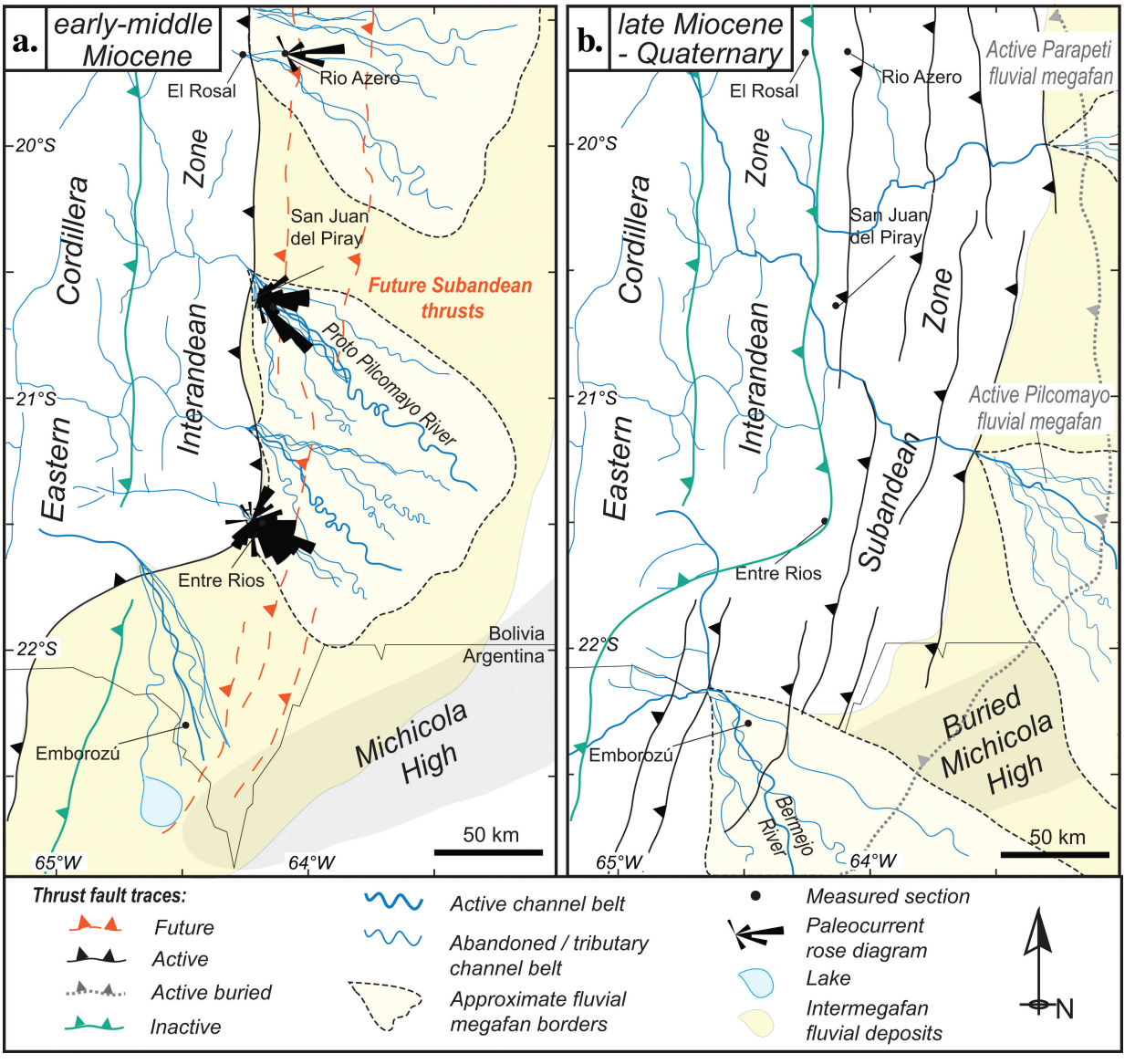

Figure 14. Proposed early Miocene to Quaternary map-view tectonic reconstruction showing eastward advance of the fold-thrust belt and evolution of fluvial megafans in southern Bolivia and northern Argentina. a. Early–middle Miocene shortening in the Eastern Cordillera and inter-Andean Zone fed point-source fluvial megafans such as the proto-Pilcomayo at 19.5–21.5°S, with ephemeral fluvial and lacustrine systems south of 22°S. Potential displacement transfer from the lower to upper basement thrust sheet at ~21.5–22°S produced out-of-sequence deformation, likely guided by inherited stratigraphic thickness trends of the Paleozoic sedimentary prism and pre-Cenozoic structural fabrics such as the Michicola High. Alternatively, diminished shortening in the south may have led to a stalled Eastern Cordillera south of 22°S. b. Late Miocene–Quaternary eastward propagation of the thrust front drove sub-Andean flexural subsidence and time-transgressive accumulation of fluvial megafans, as expressed in the modern Parapeti, Pilcomayo, and Bermejo Rivers.

middle Miocene transition from an erosional forebulge to a foredeep depozone dominated by Andean sources.

Along the eastern sub-Andean basin, a slightly younger late Oligocene–middle Miocene Petaca Formation derived from eastern sediment sources recorded the eastward-younging migration of the backbulge-forebulge depozones (McQuarrie et al., 2005; Uba et al., 2005, 2007, 2009; Hulka and Heubeck, 2010). This advance of flexural subsidence was likely coeval with Andean shortening concentrated in the Eastern Cordillera and inter-Andean Zone (e.g., Brusset et al., 2002; Ege et al., 2007; Lease et al., 2016).

Early–Middle Miocene Proximal Foreland Deposition: 19.5–21.5°S

At 19.5–20.5°S, the Tariquia and Guandacay Formations recorded early to middle Miocene growth of fluvial megafans dominated by lithic-rich Andean sediments (Figure 14a.). Complex paleoflow patterns are consistent with drainage reorganization in response to growing topographic barriers in the west, including (1) initial sediment input from lower Paleozoic strata of the Eastern Cordillera with variable Mesozoic–Cenozoic contributions; (2) unroofing of Devonian–Mesozoic strata of the inter-Andean Zone; (3) renewed influx of lower Paleozoic sources in the Eastern Cordillera; and (4) local upper Paleozoic sources exhumed during incipient thrusting in the western sub-Andean Zone (Figure 13b., c.). Upsection provenance variations track eastward unroofing of source regions, in accordance with cross-cutting relationships and published cooling ages (Barnes et al., 2008). From these results, we infer exhumation at 19.5°S induced by distributed shortening in the Eastern Cordillera (~30–23 Ma), in-sequence thrusting in the inter-Andean Zone (~22–13 Ma; Barnes et al., 2008; Lease et al., 2016), and east-directed routing systems in a foredeep depozone that was incorporated by ~20 Ma into growing inter-Andean structures of a wedge-top depozone (Figure 13b.). At ~20.5°S, a likely point source in the form of the proto-Pilcomayo fluvial megafan (Figure 14a.) distributed detritus across a rapidly subsiding foredeep. After ~19 Ma, advance of thrust-induced exhumation in the inter-Andean Zone signified emplacement of the upper basement thrust sheet (inter-Andean thrust; e.g. Horton, 2005; Anderson et al., 2017). Continued middle Miocene and younger shortening (<12 Ma; Lease et al., 2016) documents the in-sequence activation of the lower basement thrust sheet (sub-Andean thrust) that fed slip forward and promoted exhumation across the sub-Andean Zone (Figure 13c.). Advance of the lower basement thrust sheet triggered passive rejuvenation of the Eastern Cordillera and establishment of a topographic divide, with incorporation of fluvial megafan deposits into the migrating wedge-top depozone (Figures 13c., 14a.).

At 21.5°S, the Entre Rios section contains a comparable record of foreland basin sedimentation. U-Pb maximum depositional ages suggest that fluvial megafan development was underway no earlier than ~24 Ma, with accumulation rates estimated at 93 m (305 ft)/m.y. Syncline growth likely in the ~24.3–9.1 Ma age range recorded a depositional change from sheetflood to sandy braided fluvial systems carrying inter-Andean Devonian–Carboniferous clasts and cosmopolitan U-Pb age components indicative of a shift to sediment sources in the inter-Andean Zone. This provenance shift may correspond with thrust-induced exhumation of the western inter-Andean Zone, with the earliest possible growth of the Entre Rios syncline at ~16.4 ± 1.4 Ma, but potentially as young as 9.2 ± 1.2 Ma (apatite fission track ages; Ege, 2004; Ege et al., 2007). Persistent Cretaceous–Cenozoic magmatic grains suggest continued transverse fluvial connectivity to the Eastern Cordillera, consistent with a larger drainage system in the west. When integrated with data from farther north, the age and location of growth strata successions suggest early–middle Miocene deformation advance into the easternmost inter-Andean Zone at ~19.5–21.5°S, followed by deformation advance into the sub-Andean Zone after 12 Ma (Figures 13, 14).

Late Miocene Accelerated Deposition

Upper Miocene foreland basin fill of the sub-Andean Zone recorded eastward migration of the Andean orogenic wedge (e.g., Gubbels et al., 1993; Moretti et al., 1996; Uba et al., 2005, 2007, 2009; Lease et al., 2016). At 19.5–20.5°S (San Juan del Piray and Rio Azero), accelerated late Miocene sedimentation rates (~553 m [~1814 ft]/m.y.) coincided with a provenance shift from the Eastern Cordillera–inter-Andean Zone to the incipient sub-Andean Zone, coeval with ~12 Ma activation of wedge-top deposition (Figure 13c.). At 22°S (Emborozú), facies trends and detrital zircon provenance within a less than 10 Ma upward coarsening succession recorded fluvial-megafan progradation during unroofing of the inter-Andean Zone and easternmost Eastern Cordillera (Ege et al., 2007; Figure 14b.). Clast compositional data reveal the sequential input of orthoquarzite clasts and sedimentary clasts, defining a ~9 Ma shift from lower Paleozoic sources of the easternmost Eastern Cordillera to major Devonian–Carboniferous input from the inter-Andean Zone. This record agrees with evidence for rapid post–15 Ma exhumation in the Eastern Cordillera of Bolivia and northern Argentina (e.g., DeCelles et al., 2011). Stratal thickness changes and high rates of accommodation (>900 m [>2953 ft]/m.y.) in equivalent units of northern Argentina (Terciario Subandino and El Simbolar Formations) argue for pre–8 Ma deposition in a rapidly subsiding foredeep. In turn, alluvial fan deposition after 8 Ma (Echavarría et al., 2003; Amidon et al., 2015) coupled with the complex U-Pb age distributions suggests isolated wedge-top deposition from the late Miocene onward (Figure 14b.).

By comparison, the less than 4.5 km (2.8 mi) thick eastern sub-Andean stratigraphic succession documents high subsidence rates after 12 Ma attributed to sub-Andean shortening linked to foredeep and less

than 6 Ma wedge-top deposition (e.g., Horton and DeCelles, 1997; Brusset et al., 2002; Ege et al., 2007; Uba et al., 2007, 2009). Coupling interactions between the Altiplano–Eastern Cordillera surface uplift and generation of greater than 3 km (2 mi) topographic relief may have driven increased sediment accumulation rates (from 130 to 630 m [427 to 2067 ft]/m.y.) linked to facies shifts from lacustrine and/or shallow marine facies transitioning to climatically modulated fluvial megafans (e.g., Garzione et al., 2006, 2008; Hulka et al., 2006; Uba et al., 2006, 2009; Prezzi et al., 2009; Mulch et al., 2010). Eastward migration of foreland depozones occupied by fluvial and interfluvial megafans suggests a progressive in-sequence advance of the sub-Andean thrust belt, in agreement with data on exhumation timing (Brusset et al., 2002; Lease et al., 2016; Figure 14b.).

Foreland Basin Summary

Cenozoic fill of the eastern inter-Andean Zone to sub-Andean Zone documents the migration of foreland depocenters and an apparent early–middle Miocene north–south discrepancy in foreland and thrust-belt evolution (Figure 14). At 19.5–21.5°S, Oligocene–earliest Miocene deposition in a distal foredeep to forebulge depozone was followed by early to middle Miocene deformation advance in the Eastern Cordillera–inter-Andean Zone, recording flexural subsidence and sediment dispersal into the migrating foredeep (Figure 13a.). Growth strata preserved at 19.5°S (~22 Ma) and 21.5°S (<16 Ma) indicate eastward advance of the orogenic wedge with associated unroofing of the inter-Andean Zone (Figure 13b.), followed by less than 12 Ma earliest thrusting in the western sub-Andean Zone, partitioning of local subsidence and sediment flux to a proximal wedge-top depozone (Figure 13c.). Detrital input from Eastern Cordillera sources, commonly as point-source fluvial megafans, suggests middle to early late Miocene (<12 Ma) construction of high topography in the Eastern Cordillera through passive rejuvenation and/or focused erosion driven by a climate-induced increase in erosion and transport efficiency (Figure 13c.). In contrast, south of 22°S, near a major tectonic transition, Oligocene to middle Miocene (~32–10 Ma) forebulge and distal foredeep conditions prevailed, even with active deformation (but potentially limited exhumation) in the Eastern Cordillera–inter-Andean Zone (Figure 14a.). The rapid generation of accommodation typical of a foredeep depozone is reflected by high accumulation rates after ~10 Ma, with variable Eastern Cordillera and inter-Andean Zone sources. In turn, after 8 Ma, proximal thrust-induced subsidence governed accumulation in a wedge-top depozone. In contrast to the north–south discrepancy in early–middle Miocene foreland histories, a broadly synchronous late Miocene (<12 Ma) record of rapid accumulation across the proximal foreland signaled the arrival of the sub-Andean deformation front and eastward migration of the foreland basin system (Figure 14b.).

Along-Strike Variations

Our results point to late Miocene eastward orogenic growth preceded by an along-strike discrepancy in the advance of the foreland basin system and associated Andean fold-thrust belt in the transition zone near the Bolivia–Argentina border. Provenance results from 19.5 to 21.5°S support Oligocene–middle Miocene eastward advance of the upper basement thrust sheet with translation over its footwall ramp promoting erosional unroofing of lower Paleozoic–Cenozoic strata of the Eastern Cordillera and middle Paleozoic–Mesozoic rocks of the inter-Andean Zone (Figure 13b.). Subsequent late Miocene (<12 Ma) activation of the lower basement thrust sheet fed slip into nascent sub-Andean Zone structures with an associated reduction in Eastern Cordillera–inter-Andean Zone deformation, consistent with an overall eastward shift in cooling ages (Figure 13c.; Anderson et al., 2014, 2017; Carrapa and DeCelles, 2015; Reiners et al., 2015; Lease et al., 2016). Compared to northern regions, an apparent Oligocene to middle Miocene delay in the advance of the coupled thrust-belt and foreland basin system at southern than 22°S is defined by the regional late Miocene onset of rapid sub-Andean accumulation (<12 Ma; e.g., Barnes et al., 2008; Mosolf et al., 2011; Eichelberger et al., 2013; Lease et al., 2016).

South of 22°S, middle to late Miocene displacement transfer from the lower to upper basement thrust sheet (Kley, 1996; Figure 14a) potentially induced slower growth of orogenic wedge taper and reduced flexural subsidence, compatible with protracted sediment recycling in the Eastern Cordillera–inter-Andean Zone (Hernández et al., 1996; Kley, 1996; Starck and Schulz, 1996; DeCelles et al., 2011). North–south variability in thrust belt dynamics from Bolivia to northern Argentina may point to pre-orogenic inheritance or be an artefact of an along-strike shortening gradient. The first option argues for pre-orogenic inheritance defined by a southward-thinning Paleozoic stratigraphic wedge with fewer detachment horizons and the locus of pre-Andean basement fabrics such as the east-northeast–west-southwest Cretaceous Michicola High that may be responsible for displacement transfer during shortening along an oblique ramp

(Allmendinger et al., 1983; Allmendinger and Gubbels, 1996; Viramonte et al., 1999; Jacques, 2003; Hongn et al., 2010). In contrast, the second option suggests that roughly two-fold greater shortening within the inter-Andean Zone in the north (19.5°S) translated early Miocene foreland deposits farther eastward relative to their upper Miocene counterparts in the south (22.5°S) (Figure 15; McQuarrie, 2002; Anderson et al., 2017). In this scenario, the fold-thrust belt in the north sustained considerable shortening and advanced systematically eastward relative to southern localities, prior to the main phase of shortening in the sub-Andean Zone. Although these elements may have temporarily influenced along-strike variations in thrust belt and foreland basin evolution, relatively uniform spatiotemporal patterns from the late Miocene onward appear to define orogenic growth in the central Andes and associated construction of the Altiplano and Puna plateaus.

Linkages between Foreland Shortening and Hinterland Uplift

Multiple studies suggest that rapid late Miocene surface uplift of the Altiplano and Eastern Cordillera was linked with the onset of sub-Andean shortening (e.g., Garzione et al., 2006, 2008; Uba et al., 2009; Lease et al., 2016). We propose two scenarios. First, our observed rapid provenance shift from inter-Andean to sub-Andean sources is consistent with a late Miocene (roughly 12 Ma) onset of significant exhumation in the sub-Andean Zone. This timing corresponds with diminished exhumation and the abrupt cessation of shortening in the Eastern Cordillera hinterland, as denoted by genesis of the San Juan del Oro geomorphic surface (Gubbels et al., 1993; Horton, 1998, 1999, 2005; Ege et al., 2007). In this scenario, a rapid eastward jump in the orogenic wedge at ~12 Ma partitioned the once-extensive sub-Andean foreland depozone and triggered pronounced sub-Andean shortening, accelerated sediment accumulation, and a rapid change to proximal source regions (Brusset et al., 2002; Echavarría et al., 2003; Uba et al., 2005, 2009; DeCelles et al., 2011; Lease et al., 2016). This history would support a rapid surface uplift in the Altiplano and Eastern Cordillera, depending on the subsurface structural linkages between the sub-Andean and hinterland regions.

Alternatively, a steadily advancing locus of shortening may have progressed systematically from the eastern inter-Andean Zone into the sub-Andean Zone, promoting gradual hinterland surface uplift. In this scenario, our observed ~14 Ma provenance change from the inter-Andean Zone to Eastern Cordillera would reflect headward drainage expansion associated with the creation of a topographic divide capable of modulating erosion and taper of the eastern orogenic slope (e.g., Bookhagen and Strecker, 2008; Barnes et al., 2012). Given the timing constraints

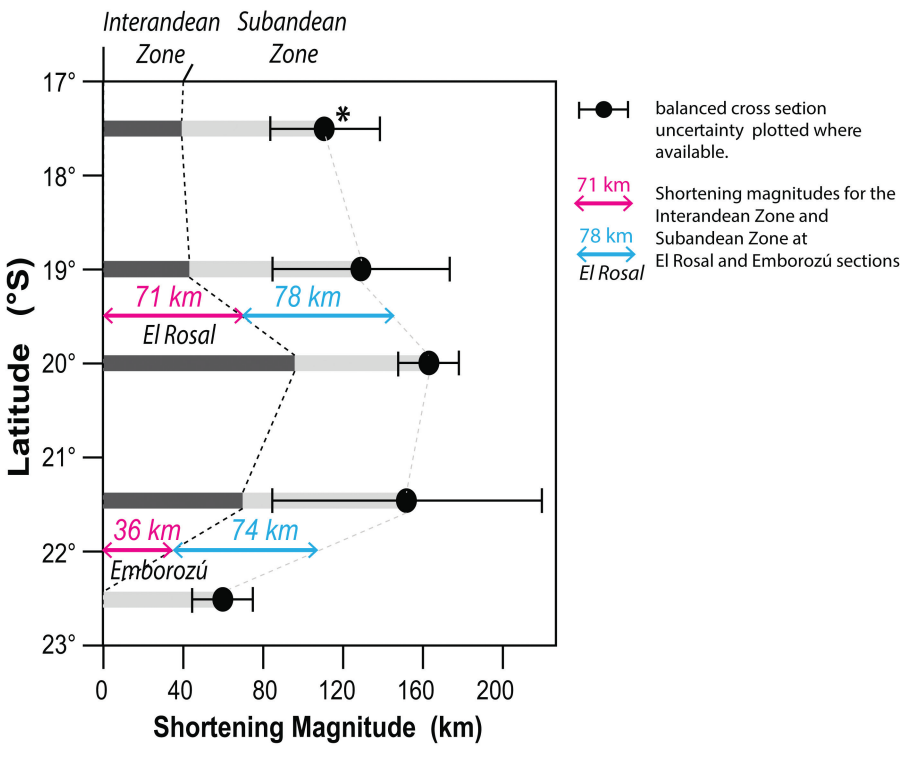

Figure 15. Comparative plot showing along-strike (north–south) variations in shortening for the inter-Andean Zone and sub-Andean Zone of southern Bolivia and northern Argentina (modified from Anderson et al., 2017). Enhanced shortening sustained by basin fill of the El Rosal section (~19.5°S) relative to the Emborozú section (~22.5°S) may explain apparent north–south differences in foreland deposition within the western sub-Andean basin.

from available growth structures, consistent sediment source areas may indicate a rough balance between shortening and rock uplift in the inter-Andean Zone (e.g., Uba et al., 2005, 2007; Barnes et al., 2012). Gradual thickening and attainment of sufficient orogenic taper, as assisted by west-directed thrusting in the inter-Andean Zone, may have promoted steady surface uplift in the erosion-protected hinterland until 10 Ma (including development of the San Juan del Oro surface), followed by eastward deformation advance along a more efficient sub-Andean décollement (Gubbels et al., 1993). In addition to pre-Cenozoic heterogeneities conditioning growth of orogenic taper, structural alternatives within this model include either a single basement involved thrust sheet (Anderson et al., 2017) or basement-involved imbricate fans (Kley, 1996; Ege et al., 2007). Ultimately, although our study clarifies critical issues of timing and along-strike variability, resolution of the debate over rapid versus gradual hinterland uplift requires further testing involving temporal constraints in shortening-related exhumation.

CONCLUSIONS

1. Sedimentologic, provenance, U-Pb geochronological, and accumulation results for sub-Andean foreland basin fill in southern Bolivia reveal temporal and spatial variations in central Andean orogenesis. Although flexural subsidence during high-magnitude east–west shortening has governed clastic sedimentation since Oligocene time, accelerated accumulation commenced in early to middle Miocene time. Eastward propagation of thin-skinned thrusting across the sub-Andean Zone occurred relatively uniformly from 12 Ma to present.
2. Facies analyses of greater than 4 km (2.5 mi) thick clastic succession reveal a basal paleosol zone (Petaca Formation) capped by an upward coarsening and thickening succession that represents mixed meandering and braided fluvial systems (Tariquia and Guandacay Formations) followed by alluvial fan systems (Emborozú Formation). This progradational history is consistent with an advancing foreland basin characterized by enhanced deposition by point-source fluvial megafans (e.g., proto-Pilcomayo River).
3. Early–middle Miocene propagation of fold-thrust deformation from the Eastern Cordillera into the eastern inter-Andean Zone at 19.5–21.5°S is signaled by thrust-generated growth strata preserved in the El Rosal and Entre Rios synclines. Available timing constraints suggest late inter-Andean deformation at ~21.8 ± 0.8 Ma at 19.5°S and no earlier than ~16.4 ± 1.4 Ma at 21.5°S. We attribute this phase of shortening to activation and eastward advance of the upper basement thrust sheet (inter-Andean thrust) prior to large-scale motion of the lower basement thrust sheet (sub-Andean thrust).
4. An Oligocene–early Miocene onset of flexural subsidence was marked by limited accumulation (3 m [10 ft]/m.y.; Petaca Formation, and correlative Tranquitas Formation) of Andean and cratonal detritus in forebulge and distal foredeep depozones. Thereafter, increased accommodation (from ~90–550 m [~295–1804 ft]/m.y. to ~600–2000 m [~1969–6562 ft]/m.y.); Yecua, Tariquia, Guandacay, and Emborozú Formations) recorded the transition to proximal foredeep and wedge-top deposition during Miocene advance of shortening. Out-of-sequence deformation above an oblique ramp at ~21.5–22°S (Kley, 1996) associated with pre-Cenozoic stratigraphic and structural heterogeneities or along-strike shortening variations may explain a north–south contrast in the timing of thrust-belt advance and sub-Andean subsidence. Such along-strike variability underscores the complex transition from southern Bolivia to northern Argentina and should be considered in models of Altiplano–Puna plateau uplift.

ACKNOWLEDGMENTS

This research was funded by a U.S. National Science Foundation grant (EAR-0908518) awarded to B. K. Horton and S. P. Long, and research support awarded to A. Z. Calle from AAPG, Repsol E&P Bolivia, the Geological Society of America, the Society for Sedimentary Geology, and the Jackson School of Geosciences at the University of Texas at Austin. Edgar Requena, Gerardo Villacorta, and Victor Ramirez offered critical insights on the regional geology. Field and logistical assistance was provided by Ramiro Matos, Orlando Quenta, Christina Andry, Hernan Orellana, Alcides Buchizo, and Paul Muñoz. Special thanks to the inhabitants of Puente Azero, Muskha, La Revuelta, Añimbo, and Entre Rios for their hospitality. We benefited from fruitful discussions with Daniel Starck, Nicholas Perez, Victor Ramos, Jonas Kley, Leslie Wood, Kitty Milliken, Gonzalo Astorga, Oscar Arispe, Raúl García, Peter Flaig, Antonio Teixell, and Randy Marrett. We thank Lily Jackson and Sarah George for comments on earlier drafts and Joel Saylor, Barbara Carrapa, and editor Gonzalo Zamora for helpful reviews that improved the manuscript.

Appendix 1

Zircon U-Pb LA-ICP-MS methodology

All detrital and volcanic zircon grains dated for this study were depth-profiled using a Photon Machines Analyte G2 ATLex 300si ArF 193 nm Excimer Laser with the following energy settings (4 mJ attenuated to 24%; Fluence − 1.45J/cm^2; Rep rate – 10 Hz; Spot size- 30 or 40 µm), laser settings (6 preablation shots, 25 sec of baseline data collection, 300 ablation shots [30 sec equaling an approximate depth of 15 to 17 µm], and 35 sec washout), and two-volume Helex ablation cell settings (total of 1 L/min He carrier gas flow). The ablation aerosols (dry plasma) were transported using He carrier gas to, and analyzed with, a ThermoFisher Element2 double-focusing magnetic sector SC-ICP-MS with the following settings: 1100–1250 W RF power; 16 L/min Ar cooling gas; 0.9 L/min Ar auxiliary gas; and 0.9–1.2 L/min Ar sample gas flow. For the U-Pb analyses, the following masses were measures using secondary analog and electron multiplier: ^{202}Hg, ^{204}Pb/Hg, ^{206}Pb, ^{207}Pb, ^{208}Pb, ^{232}Th, ^{235}U, and ^{238}U.

ICP-MS U-Pb data were processed using the Iolite™ plug-in (Paton et al., 2011) on the Wavemetrics Igor Pro™ platform and the VizualAge™ data reduction scheme (Petrus and Kamber, 2012). For U-Pb data reduction, GJ1 zircon was used as the primary reference material (^{206}Pb/^{238}U 601.7 ± 1.3 Ma, ^{207}Pb/^{206}Pb 607 ± 4 Ma; Jackson et al., 2004) and Pak1 (in-house ^{206}Pb/^{238}U 43.03 ± 0.01 [unpublished TIMS data]) and Plesovice zircon (337.13 ± 0.37; Slama et al., 2008). Secondary standard data were used to monitor data quality. No common Pb correction applied. Uncertainty level and propagation ages are quoted at 2-sigma absolute error, propagation is by quadratic addition, and reproducibility and age uncertainty of reference material are not propagated.

Concordia plots generated by the VizualAge™ live concordia function (Petrus and Kamber, 2012) were visually inspected during data reduction for age mixing or disturbance to a closed isotopic system.

REFERENCES

Jackson, S. E., N. J. Pearson, W. L. Griffin, and E. A. Belousova, 2004, The application of laserablation-inductively coupled plasma-mass spectrometry to in situ U-Pb zircon geochronology: Chemical Geology, v. 211, p. 47–69, doi: 10.1016/j.chemgeo.2004.06.017.

Paton, C., J. Hellstrom, B. Paul, J. Woodhead, and J. Hergt, 2011, Iolite: Freeware for the visualization and processing of mass spectrometric data: Journal of Analytical Atomic Spectrometry, v. 26, p. 2508–2518, doi: 10.1039/c1ja10172b.

Petrus, J. A., and B. S. Kamber, 2012, VizualAge: A novel approach to laser ablation ICPMS U-Pb geochronology data reduction: Geostandards and Geoanalytical Research, v. 36, p. 247–270, doi: 10.1111/j.1751-908X.2012.00158.x.

Slama, J., et al., 2008, Plesovice zircon—A new natural reference material for U-Pb and Hf isotopic microanalysis: Chemical Geology, v. 249, no. 1–2, p. 1–35, doi: 10.1016/j.chemgeo.2007.11.005.

Appendix 2

Laser ablation, high-resolution, inductively coupled plasma mass spectrometry (LA-HR-ICP-MS) analyses for detrital zircon U-Pb geochronology

The oversized Appendix 2 can be found online on AAPG Datashare at: https://www.aapg.org/publications/journals/bulletin/datashare.

Appendix 3

Nonmetric multidimensional scaling plot (MDS) of source regions

Nonmetric multidimensional scaling plot (MDS) of Paleozoic to Cenozoic U-Pb detrital zircon databases (Calle, 2013; this study) from the Eastern Cordillera, inter-Andean Zone, and sub-Andean Zone (color-coded dots as in Figure 7). Rectangular fields ascribed to source domains are used to track Cenozoic provenance areas as shown in Figure 9.

Appendix 3

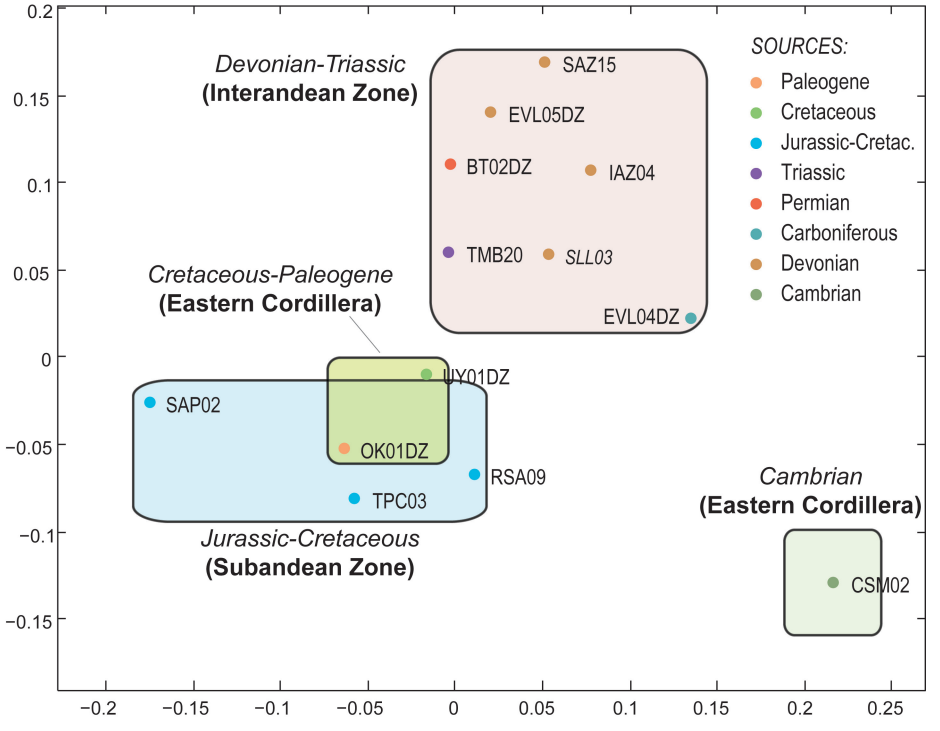

Appendix 4

Cross-correlation coefficients from probability density plots testing similarity of Cenozoic sub-Andean foreland samples to source domains

Source domain		Eastern Cordillera		Inter-Andean Zone								Sub-Andean Zone			Eastern Cordillera	
Source age / Cenozoic Fm.		Cambrian	Ordovician	Devonian				Carboniferous	Permian	Triassic		Jurassic–Cretaceous			Cretaceous	Paleogene
Sample		CSM02	CGO23	SLL03	IAZ04	EVL05DZ	SAZ15	EVL04DZ	BT02DZ	SAZ24	TMB20	TPC03	RSA09	SAP02	UY01DZ	OK02DZ
Eastern Cordillera	CSM02	**1.00**	0.36	0.05	0.20	0.04	0.06	0.31	0.10	0.03	0.09	0.41	0.51	0.23	0.20	0.20
	CGO23	0.36	***1.00***	0.14	0.17	0.07	0.09	0.12	0.05	0.01	0.16	0.20	0.13	0.11	0.11	0.10
Inter-Andean Zone	SLL03	0.05	0.14	**1.00**	0.46	0.31	0.34	0.16	0.20	0.10	0.42	0.16	0.18	0.20	0.19	0.10
	IAZ04	0.20	0.17	0.46	**1.00**	0.53	0.63	0.28	0.43	0.10	0.49	0.23	0.23	0.16	0.28	0.15
	EVL05DZ	0.04	0.07	0.31	0.53	**1.00**	0.58	0.17	0.45	0.08	0.46	0.09	0.13	0.07	0.21	0.03
	SAZ15	0.06	0.09	0.34	0.63	0.58	**1.00**	0.20	0.40	0.08	0.47	0.12	0.09	0.14	0.18	0.11
	EVL04DZ	0.31	0.12	0.16	0.28	0.17	0.20	**1.00**	0.30	0.18	0.23	0.58	0.42	0.37	0.49	0.31
	BT02DZ	0.10	0.05	0.20	0.43	0.45	0.40	0.30	**1.00**	0.13	0.33	0.19	0.17	0.14	0.22	0.12
	SAZ24	0.03	0.01	0.10	0.10	0.08	0.08	0.18	0.13	**1.00**	0.19	0.20	0.12	0.11	0.07	0.08
	TMB20	0.09	0.16	0.42	0.49	0.46	0.47	0.23	0.33	0.19	**1.00**	0.16	0.13	0.13	0.17	0.12
Sub-Andean Zone	TPC03	0.41	0.20	0.16	0.23	0.09	0.12	0.58	0.19	0.20	0.16	**1.00**	0.38	0.33	0.35	0.35
	RSA09	0.51	0.13	0.18	0.23	0.13	0.09	0.42	0.17	0.12	0.13	0.38	**1.00**	0.23	0.28	0.23
	SAP02	0.23	0.11	0.20	0.16	0.07	0.14	0.37	0.14	0.11	0.13	0.33	0.23	**1.00**	0.23	0.40
Eastern Cordillera	UY01DZ	0.20	0.11	0.19	0.28	0.21	0.18	0.49	0.22	0.07	0.17	0.35	0.28	0.23	**1.00**	0.08
	OK02DZ	0.20	0.10	0.10	0.15	0.03	0.11	0.31	0.12	0.08	0.12	0.35	0.23	0.40	0.08	**1.00**
Petaca	VLC04	0.35	0.38	0.17	0.28	0.20	0.22	0.35	0.18	0.07	0.19	0.47	0.26	0.27	0.27	0.24
	MK01DZ	0.19	0.21	0.14	0.20	0.13	0.12	0.22	0.09	0.02	0.12	0.21	0.22	0.18	0.17	0.11
	BT01	0.21	0.11	0.19	0.22	0.14	0.21	0.36	0.21	0.08	0.12	0.46	0.21	0.39	0.26	0.28
	RSA10	0.32	0.09	0.16	0.20	0.13	0.17	0.37	0.23	0.15	0.16	0.34	0.37	0.32	0.26	0.28
Tariquia	MK02DZ	0.22	0.16	0.19	0.20	0.13	0.16	0.23	0.15	0.07	0.13	0.30	0.21	0.38	0.15	0.27
	MK03DZ	0.22	0.13	0.21	0.28	0.20	0.21	0.33	0.22	0.20	0.27	0.31	0.20	0.25	0.32	0.16
	RA03DZ	0.17	0.08	0.22	0.30	0.30	0.21	0.48	0.30	0.13	0.14	0.36	0.36	0.25	0.46	0.17
	BT04	0.24	0.08	0.27	0.21	0.15	0.17	0.58	0.21	0.20	0.21	0.45	0.39	0.49	0.35	0.31
	ERS06	0.26	0.15	0.20	0.32	0.19	0.19	0.45	0.26	0.20	0.18	0.36	0.37	0.29	0.34	0.18
	EMB01DZ	0.41	0.19	0.17	0.33	0.23	0.29	0.39	0.34	0.09	0.28	0.36	0.37	0.31	0.25	0.24
Guandacay	BT06	0.45	0.38	0.27	0.28	0.19	0.20	0.51	0.21	0.10	0.27	0.61	0.46	0.38	0.30	0.39
	BT10	0.59	0.36	0.17	0.24	0.09	0.11	0.55	0.15	0.10	0.20	0.75	0.40	0.36	0.31	0.36
	ERS14	0.19	0.13	0.37	0.51	0.46	0.41	0.38	0.36	0.11	0.36	0.32	0.24	0.29	0.33	0.22
	ERS19	0.39	0.24	0.23	0.46	0.36	0.31	0.47	0.39	0.11	0.40	0.36	0.37	0.27	0.39	0.18
	EMB03DZ	0.15	0.14	0.30	0.36	0.34	0.36	0.43	0.32	0.18	0.32	0.39	0.29	0.28	0.29	0.24
Emborozú	EMB05DZ	0.23	0.10	0.34	0.33	0.34	0.29	0.29	0.28	0.16	0.32	0.39	0.31	0.20	0.17	0.23

The interval of interest is between 66 and 2000 Ma, given that Cenozoic grains are ascribed to the sub-Andean foreland basin, and 95% of the detrital zircons ages are less than 2000 Ma. The cutoff used to highlight Cenozoic samples to identical source regions is $R^2 > 0.4$ (bolded and italicized values). Such cutoff derives from high similarity of samples throughout Phanerozoic source domains.

Notice that (1) the Petaca samples show similarity with Jurassic–Cretaceous samples from the sub-Andean Zone; (2) Tariquia samples are similar to age distributions from the inter-Andean Zone, Jurassic–Cretaceous samples from the sub-Andean Zone, and Cretaceous–Paleogene samples from the Eastern Cordillera; (3) the Guandacay samples show a mixing of sources from the inter-Andean Zone, the Jurassic–Cretaceous sub-Andean Zone, and the Eastern Cordillera samples; and (4) the Emborozú sample shows similarity with Guandacay sample EMB03DZ recording higher similarity with inter-Andean Zone provenance.

Sub-Andean Foreland Basin															
Petaca Formation				Tariquia Formation						Guandacay Formation					Emborozú Fm.
VLC04	MK01DZ	BT01	RSA10	MK02DZ	MK03DZ	RA03DZ	BT04	ERS06	EMB01DZ	BT06	BT10	ERS14	ERS19	EMB03DZ	EMB05DZ
0.35	0.19	0.21	0.32	0.22	0.22	0.17	0.24	0.26	***0.41***	***0.45***	***0.59***	0.19	0.39	0.15	0.23
0.38	0.21	0.11	0.09	0.16	0.13	0.08	0.08	0.15	0.19	0.38	0.36	0.13	0.24	0.14	0.10
0.17	0.14	0.19	0.16	0.19	0.21	0.22	0.27	0.20	0.17	0.27	0.17	0.37	0.23	0.30	0.34
0.28	0.20	0.22	0.20	0.20	0.28	0.30	0.21	0.32	0.33	0.28	0.24	***0.51***	***0.46***	0.36	0.33
0.20	0.13	0.14	0.13	0.13	0.20	0.30	0.15	0.19	0.23	0.19	0.09	***0.46***	0.36	0.34	0.34
0.22	0.12	0.21	0.17	0.16	0.21	0.21	0.17	0.19	0.29	0.20	0.11	***0.41***	0.31	0.36	0.29
0.35	0.22	0.36	0.37	0.23	0.33	***0.48***	***0.58***	***0.45***	0.39	***0.51***	***0.55***	0.38	***0.47***	***0.43***	0.29
0.18	0.09	0.21	0.23	0.15	0.22	0.30	0.21	0.26	0.34	0.21	0.15	0.36	0.39	0.32	0.28
0.07	0.02	0.08	0.15	0.07	0.20	0.13	0.20	0.20	0.09	0.10	0.10	0.11	0.11	0.18	0.16
0.19	0.12	0.12	0.16	0.13	0.27	0.14	0.21	0.18	0.28	0.27	0.20	0.36	***0.40***	0.32	0.32
0.47	0.21	***0.46***	0.34	0.30	0.31	0.36	***0.45***	0.36	0.36	***0.61***	***0.75***	0.32	0.36	0.39	0.39
0.26	0.22	0.21	0.37	0.21	0.20	0.36	0.39	0.37	0.37	***0.46***	***0.40***	0.24	0.37	0.29	0.31
0.27	0.18	0.39	0.32	0.38	0.25	0.25	***0.49***	0.29	0.31	0.38	0.36	0.29	0.27	0.28	0.20
0.27	0.17	0.26	0.26	0.15	0.32	***0.46***	0.35	0.34	0.25	0.30	0.31	0.33	0.39	0.29	0.17
0.24	0.11	0.28	0.28	0.27	0.16	0.17	0.31	0.18	0.24	0.39	0.36	0.22	0.18	0.24	0.23
1.00	0.29	0.38	0.23	0.31	0.21	0.33	0.31	0.23	0.37	***0.63***	***0.61***	0.36	***0.44***	0.36	0.37
0.29	**1.00**	0.14	0.11	0.20	0.10	0.20	0.17	0.13	0.25	0.30	0.30	0.23	0.24	0.19	0.14
0.38	0.14	**1.00**	0.37	***0.46***	0.20	0.34	0.37	0.26	0.28	0.37	***0.43***	0.38	0.31	0.32	0.36
0.23	0.11	0.37	**1.00**	0.27	0.26	0.30	***0.43***	0.27	***0.41***	0.33	0.35	0.24	0.27	0.28	0.27
0.31	0.20	0.46	0.27	**1.00**	0.13	0.21	0.37	0.16	0.26	0.37	***0.40***	0.34	0.25	0.31	0.28
0.21	0.10	0.20	0.26	0.13	**1.00**	0.31	0.37	0.36	0.28	0.29	0.26	0.28	0.36	0.25	0.21
0.33	0.20	0.34	0.30	0.21	0.31	**1.00**	***0.44***	0.33	0.26	0.35	0.34	***0.43***	0.39	***0.43***	0.28
0.31	0.17	0.37	0.43	0.37	0.37	0.44	**1.00**	0.32	0.30	***0.50***	***0.47***	***0.41***	0.40	***0.40***	0.36
0.23	0.13	0.26	0.27	0.16	0.36	0.33	0.32	**1.00**	0.38	0.31	0.25	0.34	0.39	0.34	0.22
0.37	0.25	0.28	0.41	0.26	0.28	0.26	0.30	0.38	**1.00**	0.41	0.42	0.32	***0.44***	0.37	0.29
0.63	0.30	0.37	0.33	0.37	0.29	0.35	0.50	0.31	0.41	**1.00**	0.77	0.40	***0.44***	***0.44***	***0.48***
0.61	0.30	0.43	0.35	0.40	0.26	0.34	0.47	0.25	0.42	0.77	**1.00**	0.37	***0.44***	0.39	***0.40***
0.36	0.23	0.38	0.24	0.34	0.28	0.43	0.41	0.34	0.32	0.40	0.37	**1.00**	***0.55***	***0.45***	***0.43***
0.44	0.24	0.31	0.27	0.25	0.36	0.39	0.40	0.39	0.44	0.44	0.44	0.55	**1.00**	***0.41***	0.32
0.36	0.19	0.32	0.28	0.31	0.25	0.43	0.40	0.34	0.37	0.44	0.39	0.45	0.41	**1.00**	***0.44***
0.37	0.14	0.36	0.27	0.28	0.21	0.28	0.36	0.22	0.29	0.48	0.40	0.43	0.32	0.44	**1.00**

Appendix 5

Paleocurrent data from the western sub-Andean foreland basin

Section	Latitude (°S)	Longitude (°W)	Formation	Stratigraphic Position (mabs)[1]	Trend (°, already rotated for bedding dip)	Sedimentary Structure
Rio Azero	19.66	64.04	Tariquia	513.5	159	Axis trough cross-stratification
			Tariquia	1119.0	142	Scour Axis
			Tariquia	1124.0	104	Axis trough cross-stratification
			Tariquia	1124.0	80	Axis trough cross-stratification
			Tariquia	1124.0	92	Flute marks
			Tariquia	1124.0	108	Axis trough cross-stratification
			Tariquia	1171.0	53	Scour Axis
			Tariquia	1171.0	66	Scour Axis
			Tariquia	1171.0	84	Scour Axis
			Tariquia	1171.0	81	Scour Axis
			Guandacay	1706.0	330	Clast imbrication
			Guandacay	1727.2	117	Clast imbrication
			Guandacay	1813.0	91	Clast imbrication
			Guandacay	1824.0	100	Low angle cross-stratification
			Guandacay	1824.0	90	Scour Axis
			Guandacay	1841.0	85	Clast imbrication
			Guandacay	1856.0	90	Scour Axis
			Guandacay	2214.0	82	Clast imbrication
			Guandacay	2234.0	155	Clast imbrication
			Guandacay	2238.0	109	Clast imbrication
San Juan del Piray	20.63	64.14	Guandacay	2957.3	88	Clast imbrication
			Guandacay	3520.0	60	Clast imbrication
			Guandacay	3520.0	71	Clast imbrication
			Guandacay	3520.0	97	Clast imbrication
			Guandacay	3520.0	93	Clast imbrication
			Guandacay	3520.0	121	Clast imbrication
			Guandacay	3520.0	82	Clast imbrication
			Guandacay	3520.0	87	Clast imbrication
			Guandacay	3520.0	70	Clast imbrication
			Guandacay	3520.0	67	Clast imbrication
			Guandacay	3520.0	31	Clast imbrication
			Guandacay	3520.0	36	Clast imbrication
			Guandacay	3520.0	80	Clast imbrication
			Guandacay	3520.0	78	Clast imbrication
			Guandacay	3520.0	73	Clast imbrication
			Guandacay	3520.0	107	Clast imbrication
			Guandacay	3520.0	80	Clast imbrication
			Guandacay	3520.0	89	Clast imbrication
			Guandacay	3520.0	82	Clast imbrication
			Guandacay	3520.0	102	Clast imbrication
			Guandacay	3520.0	92	Clast imbrication
			Guandacay	3520.0	178	Clast imbrication
			Guandacay	3615.0	85	Clast imbrication
			Guandacay	3615.0	108	Clast imbrication
			Guandacay	3615.0	134	Clast imbrication

Section	Latitude (°S)	Longitude (°W)	Formation	Stratigraphic Position (mabs)[1]	Trend (°, already rotated for bedding dip)	Sedimentary Structure
			Guandacay	3615.0	116	Clast imbrication
			Guandacay	3615.0	135	Clast imbrication
			Guandacay	3615.0	148	Clast imbrication
			Guandacay	3615.0	227	Clast imbrication
			Guandacay	3615.0	110	Tabular cross-stratification
			Guandacay	4100.0	150	Clast imbrication
			Guandacay	4100.0	160	Clast imbrication
			Guandacay	4100.0	135	Clast imbrication
			Guandacay	4100.0	181	Clast imbrication
			Guandacay	4100.0	175	Clast imbrication
			Guandacay	4100.0	131	Clast imbrication
			Guandacay	4100.0	155	Clast imbrication
			Guandacay	4100.0	132	Clast imbrication
			Guandacay	4100.0	135	Clast imbrication
			Guandacay	4100.0	147	Clast imbrication
			Guandacay	4100.0	148	Clast imbrication
			Guandacay	4100.0	133	Clast imbrication
			Guandacay	4100.0	146	Clast imbrication
			Guandacay	4100.0	137	Clast imbrication
			Guandacay	4100.0	140	Clast imbrication
			Guandacay	4100.0	169	Clast imbrication
			Guandacay	4100.0	144	Clast imbrication
			Guandacay	4100.0	142	Clast imbrication
			Guandacay	4100.0	133	Clast imbrication
			Guandacay	4100.0	106	Clast imbrication
			Guandacay	4100.0	96	Clast imbrication
			Guandacay	4100.0	109	Clast imbrication
			Guandacay	4100.0	144	Clast imbrication
			Guandacay	4100.0	162	Clast imbrication
			Guandacay	4100.0	162	Clast imbrication
			Guandacay	4100.0	147	Clast imbrication
			Guandacay	4100.0	139	Clast imbrication
			Guandacay	4100.0	138	Clast imbrication
			Guandacay	4100.0	107	Clast imbrication
			Guandacay	4100.0	113	Clast imbrication
			Guandacay	4235.0	82	Clast imbrication
			Guandacay	4235.0	96	Clast imbrication
			Guandacay	4235.0	130	Clast imbrication
			Guandacay	4235.0	57	Clast imbrication
			Guandacay	4235.0	95	Clast imbrication
			Guandacay	4235.0	88	Clast imbrication
			Guandacay	4235.0	47	Clast imbrication
			Guandacay	4235.0	84	Clast imbrication
			Guandacay	4235.0	98	Clast imbrication
			Guandacay	4235.0	81	Clast imbrication
			Guandacay	4235.0	70	Clast imbrication
			Guandacay	4235.0	95	Clast imbrication
			Guandacay	4235.0	109	Clast imbrication
			Guandacay	4235.0	23	Clast imbrication
			Guandacay	4235.0	80	Clast imbrication
			Guandacay	4235.0	76	Clast imbrication
			Guandacay	4235.0	115	Clast imbrication
			Guandacay	4235.0	123	Clast imbrication
			Guandacay	4235.0	124	Clast imbrication

Section	Latitude (°S)	Longitude (°W)	Formation	Stratigraphic Position (mabs)[1]	Trend (°, already rotated for bedding dip)	Sedimentary Structure
			Guandacay	4235.0	104	Clast imbrication
			Guandacay	4235.0	134	Clast imbrication
			Guandacay	4235.0	103	Clast imbrication
			Guandacay	4235.0	92	Clast imbrication
			Guandacay	4235.0	87	Clast imbrication
			Guandacay	4235.0	93	Clast imbrication
			Guandacay	4235.0	90	Clast imbrication
			Guandacay	4235.0	95	Clast imbrication
			Guandacay	4235.0	99	Clast imbrication
			Guandacay	4235.0	105	Clast imbrication
			Guandacay	4235.0	81	Clast imbrication
			Guandacay	4235.0	77	Clast imbrication
			Guandacay	4340.0	73	Clast imbrication
			Guandacay	4340.0	73	Clast imbrication
			Guandacay	4340.0	51	Clast imbrication
			Guandacay	4340.0	121	Clast imbrication
			Guandacay	4340.0	123	Clast imbrication
			Guandacay	4340.0	59	Clast imbrication
			Guandacay	4340.0	50	Clast imbrication
			Guandacay	4340.0	31	Clast imbrication
			Guandacay	4340.0	28	Clast imbrication
			Guandacay	4340.0	30	Clast imbrication
			Guandacay	4340.0	69	Clast imbrication
			Guandacay	4340.0	39	Clast imbrication
			Guandacay	4340.0	56	Clast imbrication
			Guandacay	4340.0	55	Clast imbrication
			Guandacay	4340.0	10	Clast imbrication
			Guandacay	4340.0	57	Clast imbrication
			Guandacay	4340.0	49	Clast imbrication
			Guandacay	4340.0	44	Clast imbrication
			Guandacay	4340.0	15	Clast imbrication
			Guandacay	4340.0	237	Tangential cross-stratification
			Guandacay	4340.0	6	Tangential cross-stratification
			Guandacay	4340.0	125	Clast imbrication
			Guandacay	4340.0	198	Tabular cross-stratification
			Guandacay	4340.0	177	Tabular cross-stratification
			Guandacay	4340.0	81	Clast imbrication
			Guandacay	4340.0	142	Clast imbrication
			Guandacay	4340.0	133	Clast imbrication
			Guandacay	4340.0	135	Clast imbrication
			Guandacay	4340.0	132	Clast imbrication
			Guandacay	4340.0	169	Clast imbrication
			Guandacay	4340.0	141	Clast imbrication
			Guandacay	4340.0	100	Tabular cross-stratification
			Guandacay	4340.0	66	Clast imbrication
			Guandacay	4340.0	111	Clast imbrication
			Guandacay	4340.0	82	Clast imbrication
			Guandacay	4340.0	48	Clast imbrication
			Guandacay	4340.0	61	Clast imbrication
			Guandacay	4340.0	193	Clast imbrication
			Guandacay	4340.0	80	Clast imbrication
			Guandacay	4375.0	225	Clast imbrication
			Guandacay	4375.0	226	Clast imbrication
			Guandacay	4375.0	73	Clast imbrication

Section	Latitude (°S)	Longitude (°W)	Formation	Stratigraphic Position (mabs)[1]	Trend (°, already rotated for bedding dip)	Sedimentary Structure
			Guandacay	4375.0	208	Clast imbrication
			Guandacay	4375.0	213	Clast imbrication
			Guandacay	4375.0	250	Clast imbrication
			Guandacay	4375.0	226	Clast imbrication
			Guandacay	4375.0	13	Tabular cross-stratification
			Guandacay	4380.0	197	Tabular cross-stratification
			Guandacay	4380.0	42	Tabular cross-stratification
			Guandacay	4380.0	194	Axis trough cross-stratification
Entre Rios	21.51°	64.21°	Tariquia	27.1	0	Axis trough cross-stratification
			Tariquia	67.6	173	Current ripple
			Tariquia	82.3	106	Current ripple
			Tariquia	82.3	114	Current ripple
			Tariquia	82.3	98	Current ripple
			Tariquia	82.3	148	Current ripple
			Tariquia	82.3	131	Current ripple
			Tariquia	82.3	173	Current ripple
			Tariquia	82.3	155	Current ripple
			Tariquia	704.9	137	Epsilon cross-stratification*
			Tariquia	704.9	136	Epsilon cross-stratification*
			Tariquia	704.9	288	Epsilon cross-stratification*
			Tariquia	704.9	193	Epsilon cross-stratification*
			Tariquia	704.9	342	Epsilon cross-stratification*
			Tariquia	704.9	235	Epsilon cross-stratification*
			Tariquia	704.9	116	Epsilon cross-stratification*
			Tariquia	704.9	264	Epsilon cross-stratification*
			Tariquia	704.9	134	Epsilon cross-stratification*
			Tariquia	704.9	84	Epsilon cross-stratification*
			Tariquia	704.9	147	Epsilon cross-stratification*
			Tariquia	704.9	231	Epsilon cross-stratification*
			Tariquia	704.9	281	Epsilon cross-stratification*
			Tariquia	704.9	39	Epsilon cross-stratification*
			Tariquia	704.9	128	Epsilon cross-stratification*
			Tariquia	704.9	128	Epsilon cross-stratification*
			Tariquia	704.9	136	Epsilon cross-stratification*
			Tariquia	704.9	122	Epsilon cross-stratification*
			Tariquia	704.9	135	Epsilon cross-stratification*
			Tariquia	866.0	142	Epsilon cross-stratification*
			Tariquia	866.0	113	Epsilon cross-stratification*
			Tariquia	866.0	153	Epsilon cross-stratification*
			Tariquia	866.0	35	Epsilon cross-stratification*
			Tariquia	866.0	340	Epsilon cross-stratification*
			Tariquia	866.0	35	Epsilon cross-stratification*
			Tariquia	866.0	25	Epsilon cross-stratification*
			Tariquia	866.0	96	Epsilon cross-stratification*
			Tariquia	866.0	324	Epsilon cross-stratification*
			Tariquia	866.0	158	Epsilon cross-stratification*
			Tariquia	866.0	29	Epsilon cross-stratification*
			Tariquia	866.0	36	Epsilon cross-stratification*
			Tariquia	866.0	342	Epsilon cross-stratification*
			Tariquia	866.0	40	Epsilon cross-stratification*
			Tariquia	869.3	24	Epsilon cross-stratification*
			Tariquia	869.3	360	Epsilon cross-stratification*
			Tariquia	869.3	91	Epsilon cross-stratification*
			Tariquia	869.3	22	Epsilon cross-stratification*

Section	Latitude (°S)	Longitude (°W)	Formation	Stratigraphic Position (mabs)[1]	Trend (°, already rotated for bedding dip)	Sedimentary Structure
			Tariquia	869.3	73	Epsilon cross-stratification*
			Tariquia	869.3	19	Epsilon cross-stratification*
			Tariquia	869.3	3	Epsilon cross-stratification*
			Tariquia	869.3	7	Epsilon cross-stratification*
			Tariquia	869.3	259	Epsilon cross-stratification*
			Tariquia	869.3	64	Epsilon cross-stratification*
			Tariquia	869.3	300	Epsilon cross-stratification*
			Tariquia	874.6	230	Epsilon cross-stratification*
			Tariquia	874.6	101	Epsilon cross-stratification*
			Tariquia	874.6	93	Epsilon cross-stratification*
			Tariquia	874.6	48	Epsilon cross-stratification*
			Tariquia	874.6	101	Epsilon cross-stratification*
			Tariquia	874.6	23	Epsilon cross-stratification*
			Tariquia	874.6	49	Epsilon cross-stratification*
			Tariquia	874.6	131	Epsilon cross-stratification*
			Tariquia	874.6	83	Epsilon cross-stratification*
			Tariquia	874.6	45	Epsilon cross-stratification*
			Tariquia	874.6	33	Epsilon cross-stratification*
			Tariquia	874.6	111	Epsilon cross-stratification*
			Tariquia	876.4	40	Epsilon cross-stratification*
			Tariquia	876.4	47	Epsilon cross-stratification*
			Tariquia	876.4	52	Epsilon cross-stratification*
			Tariquia	879.7	104	Epsilon cross-stratification*
			Tariquia	883.0	104	Epsilon cross-stratification*
			Tariquia	883.0	140	Epsilon cross-stratification*
			Tariquia	883.0	80	Epsilon cross-stratification*
			Tariquia	883.0	329	Epsilon cross-stratification*
			Tariquia	883.0	337	Epsilon cross-stratification*
			Tariquia	883.0	64	Epsilon cross-stratification*
			Tariquia	883.0	351	Epsilon cross-stratification*
			Tariquia	883.0	68	Epsilon cross-stratification*
			Tariquia	883.0	109	Epsilon cross-stratification*
			Tariquia	883.0	71	Epsilon cross-stratification*
			Tariquia	883.0	45	Epsilon cross-stratification*
			Tariquia	888.8	39	Epsilon cross-stratification*
			Tariquia	888.8	355	Epsilon cross-stratification*
			Tariquia	888.8	75	Epsilon cross-stratification*
			Tariquia	888.8	17	Epsilon cross-stratification*
			Tariquia	888.8	14	Epsilon cross-stratification*
			Tariquia	888.8	77	Epsilon cross-stratification*
			Tariquia	888.8	101	Epsilon cross-stratification*
			Tariquia	888.8	81	Epsilon cross-stratification*
			Tariquia	895.4	318	Epsilon cross-stratification*
			Tariquia	895.4	99	Epsilon cross-stratification*
			Tariquia	895.4	61	Epsilon cross-stratification*
			Tariquia	895.4	180	Epsilon cross-stratification*
			Tariquia	895.4	104	Epsilon cross-stratification*
			Tariquia	895.4	76	Epsilon cross-stratification*
			Tariquia	895.4	119	Epsilon cross-stratification*
			Tariquia	895.4	40	Epsilon cross-stratification*
			Tariquia	895.4	70	Epsilon cross-stratification*
			Tariquia	895.4	32	Epsilon cross-stratification*
			Tariquia	895.4	109	Epsilon cross-stratification*
			Tariquia	897.5	38	Epsilon cross-stratification*

Section	Latitude (°S)	Longitude (°W)	Formation	Stratigraphic Position (mabs)[1]	Trend (°, already rotated for bedding dip)	Sedimentary Structure
			Tariquia	897.5	82	Epsilon cross-stratification*
			Tariquia	897.5	55	Epsilon cross-stratification*
			Tariquia	897.5	49	Epsilon cross-stratification*
			Tariquia	908.5	7	Epsilon cross-stratification*
			Tariquia	908.5	15	Epsilon cross-stratification*
			Tariquia	908.5	46	Epsilon cross-stratification*
			Tariquia	911.0	344	Epsilon cross-stratification*
			Tariquia	911.0	359	Epsilon cross-stratification*
			Tariquia	911.0	32	Epsilon cross-stratification*
			Tariquia	911.0	357	Epsilon cross-stratification*
			Tariquia	915.3	58	Epsilon cross-stratification*
			Tariquia	915.3	11	Epsilon cross-stratification*
			Tariquia	915.3	69	Epsilon cross-stratification*
			Tariquia	915.3	43	Epsilon cross-stratification*
			Tariquia	915.3	80	Epsilon cross-stratification*
			Tariquia	915.3	37	Epsilon cross-stratification*
			Tariquia	916.8	243	Axis trough cross-stratification
			Tariquia	916.8	266	Axis trough cross-stratification
			Tariquia	916.8	118	Axis trough cross-stratification
			Tariquia	919.2	27	Epsilon cross-stratification*
			Tariquia	919.2	356	Epsilon cross-stratification*
			Tariquia	920.6	83	Epsilon cross-stratification*
			Tariquia	920.6	32	Epsilon cross-stratification*
			Tariquia	920.6	62	Epsilon cross-stratification*
			Tariquia	922.4	327	Epsilon cross-stratification*
			Tariquia	922.4	340	Epsilon cross-stratification*
			Tariquia	922.4	124	Epsilon cross-stratification*
			Tariquia	922.4	45	Epsilon cross-stratification*
			Tariquia	922.4	93	Epsilon cross-stratification*
			Tariquia	922.4	70	Epsilon cross-stratification*
			Tariquia	936.7	57	Epsilon cross-stratification*
			Tariquia	936.7	52	Epsilon cross-stratification*
			Tariquia	936.7	86	Epsilon cross-stratification*
			Tariquia	936.7	42	Epsilon cross-stratification*
			Tariquia	936.7	55	Epsilon cross-stratification*
			Tariquia	942.9	350	Epsilon cross-stratification*
			Tariquia	942.9	14	Epsilon cross-stratification*
			Tariquia	942.9	6	Epsilon cross-stratification*
			Tariquia	942.9	68	Epsilon cross-stratification*
			Tariquia	942.9	119	Epsilon cross-stratification*
			Tariquia	942.9	112	Epsilon cross-stratification*
			Tariquia	943.0	79	Epsilon cross-stratification*
			Tariquia	957.1	19	Epsilon cross-stratification*
			Tariquia	957.1	340	Epsilon cross-stratification*
			Tariquia	957.1	68	Epsilon cross-stratification*
			Tariquia	957.1	63	Epsilon cross-stratification*
			Guandacay	957.1	159	Clast imbrication
			Guandacay	958.7	74	Axis trough cross-stratification
			Guandacay	960.1	102	Axis trough cross-stratification
			Guandacay	961.6	129	Clast imbrication
			Guandacay	961.6	111	Clast imbrication
			Guandacay	961.6	149	Clast imbrication
			Guandacay	961.6	112	Clast imbrication
			Guandacay	963.0	157	Axis trough cross-stratification

Section	Latitude (°S)	Longitude (°W)	Formation	Stratigraphic Position (mabs)[1]	Trend (°, already rotated for bedding dip)	Sedimentary Structure
			Guandacay	1005.0	220	Tabular cross-stratification
			Guandacay	1005.0	176	Tabular cross-stratification
			Guandacay	1005.0	155	Tabular cross-stratification
			Guandacay	1005.0	181	Tabular cross-stratification
			Guandacay	1005.0	114	Tabular cross-stratification
			Guandacay	1005.0	167	Axis trough cross-stratification
			Guandacay	1008.0	222	Tabular cross-stratification
			Guandacay	1008.0	131	Tabular cross-stratification
			Guandacay	1008.0	150	Tabular cross-stratification
			Guandacay	1008.0	159	Tabular cross-stratification
			Guandacay	1008.0	93	Tabular cross-stratification
			Guandacay	1018.8	145	Tabular cross-stratification
			Guandacay	1018.8	34	Tabular cross-stratification
			Guandacay	1018.8	123	Tabular cross-stratification
			Guandacay	1021.6	113	Tabular cross-stratification
			Guandacay	1021.6	75	Tabular cross-stratification
			Guandacay	1044.4	329	Tabular cross-stratification
			Guandacay	1044.4	356	Tabular cross-stratification
			Guandacay	1044.4	212	Tabular cross-stratification
			Guandacay	1044.4	20	Tabular cross-stratification
			Guandacay	1082.7	178	Tabular cross-stratification
			Guandacay	1082.7	20	Tabular cross-stratification
			Guandacay	1082.7	266	Axis trough cross-stratification
			Guandacay	1083.5	198	Axis trough cross-stratification
			Guandacay	1084.0	36	Axis trough cross-stratification
			Guandacay	1086.2	23	Tabular cross-stratification
			Guandacay	1086.2	45	Tabular cross-stratification
			Guandacay	1086.2	35	Tabular cross-stratification
			Guandacay	1086.2	53	Tabular cross-stratification
			Guandacay	1086.2	147	Tabular cross-stratification
			Guandacay	1086.2	132	Tabular cross-stratification
			Guandacay	1087.9	209	Axis trough cross-stratification
			Guandacay	1087.9	174	Axis trough cross-stratification
			Guandacay	1087.9	215	Axis trough cross-stratification
			Guandacay	1089.9	194	Axis trough cross-stratification
			Guandacay	1089.9	32	Axis trough cross-stratification
			Guandacay	1089.9	171	Axis trough cross-stratification
			Guandacay	1089.9	229	Axis trough cross-stratification
			Guandacay	1089.9	209	Axis trough cross-stratification
			Guandacay	1092.6	148	Tabular cross-stratification
			Guandacay	1092.6	143	Tabular cross-stratification
			Guandacay	1092.6	90	Tabular cross-stratification
			Guandacay	1092.6	110	Tabular cross-stratification
			Guandacay	1092.6	87	Tabular cross-stratification
			Guandacay	1092.6	99	Tabular cross-stratification
			Guandacay	1099.7	145	Tabular cross-stratification
			Guandacay	1099.7	92	Tabular cross-stratification
			Guandacay	1099.7	135	Tabular cross-stratification
			Guandacay	1102.3	114	Tabular cross-stratification
			Guandacay	1102.3	123	Tabular cross-stratification
			Guandacay	1106.0	142	Tabular cross-stratification

Section	Latitude (°S)	Longitude (°W)	Formation	Stratigraphic Position (mabs)[1]	Trend (°, already rotated for bedding dip)	Sedimentary Structure
			Guandacay	1106.0	90	Tabular cross-stratification
			Guandacay	1106.0	97	Tabular cross-stratification
			Guandacay	1106.0	114	Tabular cross-stratification
			Guandacay	1106.0	138	Axis trough cross-stratification
			Guandacay	1106.0	112	Tabular cross-stratification
			Guandacay	1106.0	109	Tabular cross-stratification
			Guandacay	1106.0	55	Tabular cross-stratification
			Guandacay	1106.0	75	Tabular cross-stratification
			Guandacay	1106.0	115	Tabular cross-stratification
			Guandacay	1106.0	107	Tabular cross-stratification
			Guandacay	1106.0	121	Tabular cross-stratification
			Guandacay	1106.5	123	Tabular cross-stratification
			Guandacay	1108.0	135	Tabular cross-stratification
			Guandacay	1111.4	121	Tabular cross-stratification
			Guandacay	1111.4	100	Tabular cross-stratification
			Guandacay	1111.4	120	Tabular cross-stratification
			Guandacay	1111.4	125	Tabular cross-stratification
			Guandacay	1111.4	131	Tabular cross-stratification
			Guandacay	1111.4	120	Tabular cross-stratification
			Guandacay	1111.4	100	Tabular cross-stratification
			Guandacay	1111.4	120	Tabular cross-stratification
			Guandacay	1111.4	140	Tabular cross-stratification
			Guandacay	1166.3	268	Axis trough cross-stratification
			Guandacay	1234.4	205	Tabular cross-stratification
			Guandacay	1234.4	115	Tabular cross-stratification
			Guandacay	1234.4	133	Tabular cross-stratification
			Guandacay	1234.4	158	Tabular cross-stratification
			Guandacay	1234.4	114	Tabular cross-stratification
			Guandacay	1234.4	104	Tabular cross-stratification
			Guandacay	1234.4	110	Tabular cross-stratification
			Guandacay	1234.4	121	Tabular cross-stratification
			Guandacay	1305.8	23	Tabular cross-stratification
			Guandacay	1305.8	233	Tabular cross-stratification
			Guandacay	1305.8	213	Tabular cross-stratification
			Guandacay	1305.8	214	Tabular cross-stratification
			Guandacay	1307.9	236	Tabular cross-stratification
			Guandacay	1307.9	242	Tabular cross-stratification
			Guandacay	1307.9	264	Tabular cross-stratification
			Guandacay	1307.9	317	Tabular cross-stratification
			Guandacay	1307.9	259	Tabular cross-stratification
			Guandacay	1309.5	275	Tabular cross-stratification
			Guandacay	1309.5	132	Tabular cross-stratification
			Guandacay	1309.5	214	Tabular cross-stratification
			Guandacay	1309.5	230	Tabular cross-stratification
			Guandacay	1309.5	226	Tabular cross-stratification
			Guandacay	1326.1	221	Tabular cross-stratification
			Guandacay	1326.1	228	Tabular cross-stratification
			Guandacay	1326.1	222	Tabular cross-stratification
			Guandacay	1326.1	153	Tabular cross-stratification
			Guandacay	1326.1	199	Tabular cross-stratification
			Guandacay	1326.1	207	Tabular cross-stratification

Section	Latitude (°S)	Longitude (°W)	Formation	Stratigraphic Position (mabs)[1]	Trend (°, already rotated for bedding dip)	Sedimentary Structure
Emborozu	22.33	64.5	Tariquia	976.0	68	Scour Axis
			Guandacay	1708.0	45	Clast imbrication
			Guandacay	1798.0	275	Clast imbrication
			Guandacay	1832.0	201	Clast imbrication
			Guandacay	1857.0	40	Clast imbrication
			Guandacay	2158.0	120	Scour Axis
			Guandacay	2158.0	67	Scour Axis
			Guandacay	2188.0	17	Clast imbrication
			Guandacay	2215.0	186	Clast imbrication
			Guandacay	2295.0	28	Clast imbrication
			Guandacay	2325.0	183	Clast imbrication
			Guandacay	2337.0	10	Clast imbrication
			Guandacay	2345.0	10	Clast imbrication
			Guandacay	2416.0	62	Clast imbrication
			Guandacay	2445.0	205	Clast imbrication
			Guandacay	2457.0	26	Clast imbrication
			Guandacay	2501.0	5	Clast imbrication
			Guandacay	2691.0	181	Clast imbrication
			Guandacay	2778.0	357	Clast imbrication

[1]mabs = meters above base section.
*Data already rotated 90° in direction of paleocurrent.

Appendix 6

Categories for sandstone point count analyses for 45 samples from the western sub-Andean basin

Symbol	Grain Categories	Recalculated parameters
Qm	Monocrystalline quartz	**Q-F-L**
Qp	Polycrystalline quartz	*Q = Qm + Qp + Qpt + C*
Qpt	Polycrystalline quartz with tectonic fabric	*F = P + K*
K	Potassium feldspar	*L = Lv + Ls + Lm*
P	Plagioclase feldspar	*Lv = Lvf + Lvm + Lvg*
Lvf	Felsitic lithic fragment	*Ls = Lmu + Lzls*
Lvm	Microlitic lithic fragment	*Lm = Lmzls + Lmm + Lmqf*
Lvg	Vitric lithic fragment	
Lmu	Mudrock lithic fragment	**Qm-F-Lt**
Lzls	Siltstone lithic fragment	*Qm = Qm*
C	Chert sedimentary lithic fragment	*F = P + K*
Lmzls	Metasiltstone lithic fragment	*Lt = Lv + Ls + Lm + Qp + Qpt + C*
Lmm	Mica-dominated lithic fragment	
Lmqf	Quartz-foliated lithic fragment	**Lm-Lv-Ls**
A	Accesory minerals (heavy minerals and micas)	*Lm = Lmzls + Lmm + Lmqf*
		Lv = Lvf + Lvm + Lvg
		Ls = Lmu + Lzls + C
		Qm-P-K
		Qm = Qm
		P = P
		K = K

Appendix 7

Recalculated modal point-count data for 45 samples from the western sub-Andean basin

				QFL (%)			*QmFLt (%)*			*QmPK (%)*			*LmLvLs (%)*		
Section	*Formation*	*Sample*	*Level (mabs*)*	*Q*	*F*	*L*	*Qm*	*F*	*Lt*	*Qm*	*P*	*K*	*Lm*	*Lv*	*Ls*
El Rosal	Petaca	VLC18PG	6.0	89.3	5.3	5.3	87.6	5.3	7.0	94.3	4.2	1.5	58.3	20.8	20.8
	Petaca	VLC04	30.0	93.1	2.3	4.6	91.1	2.3	6.6	97.6	0.0	2.4	52.2	17.4	30.4
	Petaca	MK02	65.0	92.3	3.1	4.6	91.2	3.1	5.7	96.7	2.4	0.9	75.0	5.0	20.0
	Petaca	MK01DZ	102.0	94.0	4.0	2.0	93.0	4.0	3.0	95.9	0.0	4.1	27.3	27.3	45.5
	Tariquia	MK06	245.0	86.2	0.8	13.0	85.9	0.8	13.3	99.0	0.3	0.7	73.9	21.7	4.3
	Tariquia	MK08	280.0	87.6	2.8	9.6	87.0	2.8	10.2	96.9	0.6	2.5	75.0	16.7	8.3
	Tariquia	MK09	480.0	86.1	2.5	11.3	85.8	2.5	11.6	97.1	1.9	1.0	73.2	9.8	17.1
	Tariquia	MK10	610.0	76.4	5.7	17.9	76.1	5.7	18.2	93.1	6.6	0.3	65.1	12.7	22.2
	Tariquia	MK11	900.0	81.7	1.7	16.6	81.1	1.7	17.1	97.9	1.4	0.7	65.5	29.3	5.2
	Tariquia	MK12	935.0	79.4	2.8	17.8	79.4	2.8	17.8	96.6	2.1	1.4	76.2	4.8	19.0
	Tariquia	MK13	1100.0	78.4	6.3	15.3	78.1	6.3	15.6	92.5	3.8	3.8	85.2	5.6	9.3
	Tariquia	MK14	1220.0	88.6	1.7	9.7	88.3	1.7	10.0	98.1	1.6	0.3	67.6	29.4	2.9
	Tariquia	RA01	1500.0	87.2	1.7	11.1	86.3	1.7	12.0	98.1	0.0	1.9	50.0	40.0	10.0
	Tariquia	RA04	1600.0	86.3	7.1	6.6	86.3	7.1	6.6	92.4	0.3	7.3	52.2	26.1	21.7
Entre Rios	Petaca	RSA10	7.5	84.6	10.3	5.1	84.3	10.3	5.4	89.1	6.0	4.8	100.0	0.0	0.0
	Tariquia	ERS01	47.6	70.6	5.4	24.0	70.0	5.4	24.6	92.8	1.9	5.3	32.9	1.2	65.9
	Tariquia	ERS02	113.0	80.8	6.3	12.9	80.5	6.3	13.2	92.7	0.8	6.5	90.0	2.5	7.5
	Tariquia	ERS03	317.0	68.9	9.7	21.4	68.9	9.7	21.4	87.6	2.5	9.8	68.0	0.0	32.0
	Tariquia	ERS06	515.8	68.9	6.3	24.9	68.9	6.3	24.9	91.6	3.4	4.9	73.6	0.0	26.4
	Tariquia	ERS10	748.3	75.7	6.0	18.3	75.4	6.0	18.6	92.6	1.1	6.3	52.3	0.0	47.7
	Guandacay	ERS11	911.0	66.2	8.5	25.4	65.6	8.5	25.9	88.6	2.7	8.7	50.0	2.2	47.8
	Guandacay	ERS15	1040.1	64.6	7.4	28.0	64.3	7.4	28.3	89.7	8.7	1.6	78.0	2.0	20.0
	Guandacay	ERS16	1113.9	74.6	6.8	18.5	74.4	6.8	18.8	91.6	0.4	8.1	44.6	6.2	49.2
	Guandacay	ERS19	1255.7	71.5	5.1	23.4	71.2	5.1	23.6	93.3	1.5	5.2	60.2	3.6	36.1
	Guandacay	ERS20	1340.8	76.3	4.2	19.5	75.5	4.2	20.3	94.8	0.0	5.2	61.6	1.4	37.0
	Guandacay	ERS22	1397.3	72.1	8.0	19.9	70.9	8.0	21.1	89.9	0.0	10.1	80.3	4.2	15.5
Rio Azero	Petaca	BT-01PF	9.0	90.9	9.1	0.0	85.1	9.1	5.8	90.3	2.1	7.6	50.0	0.0	50.0
	Petaca	BT-02PF	21.8	75.9	24.1	0.0	75.9	24.1	0.0	75.9	13.6	10.5	0.0	0.0	0.0
	Petaca	BT-03PF	44.8	83.6	16.4	0.0	82.2	16.4	1.4	83.3	5.1	11.6	0.0	0.0	0.0
	Tariquia	BT-05PF	194.7	73.8	9.3	16.9	72.0	9.3	18.7	88.5	1.6	9.8	34.2	65.8	0.0
	Tariquia	BT-06PF	263.0	87.6	5.2	7.1	87.1	5.2	7.6	94.3	0.5	5.2	33.3	66.7	0.0
	Tariquia	BT-08PF	380.0	87.9	2.6	9.4	84.9	2.6	12.5	97.0	0.0	3.0	22.2	70.4	7.4
	Tariquia	BT-02	437.0	81.9	4.4	13.7	78.6	4.4	16.9	94.7	0.5	4.9	23.7	65.8	10.5
	Tariquia	BT-04	567.0	90.7	4.8	4.5	86.2	4.8	9.0	94.7	0.8	4.5	38.9	33.3	27.8
	Tariquia	BT-12PF	491.4	93.0	3.7	3.4	90.6	3.7	5.7	96.1	0.0	3.9	0.0	9.1	90.9
	Tariquia	BT-17PF	1037.3	88.3	4.3	7.4	86.3	4.3	9.4	95.3	1.3	3.4	0.0	5.3	94.7
	Tariquia	BT-19PF	1198.7	89.7	8.0	2.3	84.0	8.0	8.0	91.3	0.8	7.9	0.0	25.0	75.0
	Tariquia	BT-21PF	1444.4	94.3	3.8	1.9	88.2	3.8	8.0	95.9	0.0	4.1	0.0	25.0	75.0
	Tariquia	BT-22PF	1595.0	97.2	2.5	0.4	95.1	2.5	2.5	97.5	0.0	2.5	0.0	0.0	100.0
	Guandacay	BT-24PF	1710.5	96.4	1.1	2.5	93.9	1.1	5.0	98.9	0.0	1.1	0.0	28.6	71.4
	Guandacay	BT-25PF	1875.0	91.7	6.7	1.6	88.6	6.7	4.7	93.0	0.0	7.0	0.0	25.0	75.0
	Guandacay	BT-26PF	2060.1	77.0	15.8	7.3	70.3	15.8	13.9	81.7	0.4	17.9	45.8	4.2	50.0
	Guandacay	BT-27PF	2315.0	90.9	6.2	2.9	88.4	6.2	5.5	93.5	0.0	6.5	0.0	100.0	0.0
	Guandacay	BT-28PF	2564.9	86.6	3.6	9.7	85.6	3.6	10.8	96.0	0.0	4.0	60.6	21.2	18.2
	Guandacay	BT-29PF	2636.9	92.5	5.3	2.1	90.4	5.3	4.3	94.4	0.8	4.7	10.0	70.0	20.0

Section	Formation	Sample	Level (mabs*)	QFL (%)			QmFLt (%)			QmPK (%)			LmLvLs (%)		
				Q	F	L	Qm	F	Lt	Qm	P	K	Lm	Lv	Ls
Petaca	*Average*			88.0	9.3	2.7	86.3	9.3	4.4	90.4	4.2	5.4	60.5	11.7	27.8
	Standard deviation			5.8	7.1	2.3	5.3	7.1	2.4	7.1	4.1	3.8	32.7	10.5	18.9
Tariquia	*Average*			83.3	4.8	11.9	81.9	4.8	13.4	94.4	1.4	4.2	46.0	21.9	32.1
	Standard deviation			7.8	2.3	6.8	7.0	2.3	5.9	2.9	1.5	2.7	29.9	22.8	32.2
Guandacay	*Average*			80.6	6.2	13.2	78.9	6.2	14.9	92.6	1.1	6.3	41.6	23.7	34.6
	Standard deviation			10.3	3.5	9.3	9.8	3.5	8.3	4.3	2.3	4.3	28.1	29.3	22.3

*mabs = meters above base section.

Appendix 8

Clast compositional data and bedrock age assignation

Provenance clast compositional data on 24 stations from the Rio Azero, San Juan del Piray, and Entre Rios sections. Lithologic identification and bedrock age assignment was constrained by (1) brown yellow, brown gray, olive gray, and light gray quartzites from Ordovician rocks; (2) greenish brown, greenish gray, yellowish brown, and light yellow lithic sandstones derived from Silurian rocks (mainly Tarabuco Formation); (3) micaceous, olive gray, very fine to fine-grained, fair sorted with scarce lithic fragments, and silica cement sandstones, with planar and cross-lamination sourced from Devonian Formations (Huamampampa, Los Monos, and Iquiri Formations); (4) medium red, pale red, brown red, dark purple, medium- to fine-grained, moderately to poorly sorted with silica cement sandstones, medium gray, brown red, poorly sorted diamictites, purple very fine-grained, with disorganized mica chips and lithics, and silica cement sandstones, and pale red granule conglomerates sourced from Carboniferous units (Tupambi, Escarpment, Chorro, and Tarija Formations, and minor Saipuru Formation); (5) black and pale yellow chert and light gray, laminated carbonate mudstones derived from Permian Formation (Vitiacua and perhaps Copacabana Formations); (6) purple basalt derived from Triassic volcanic unit (Entre Rios Basalt); (7) red medium-grained sandstone with honey -colored quartz, with calcite cement; white medium-grained, moderately to well-sorted sandstone, smocky chert, white, rounded to well-rounded semi-spherical quartz from Mesozoic units (Tapecua, Ichoa, and Castellon Formations).

REFERENCES

Allmendinger, R. W., V. A. Ramos, T. E. Jordan, M. Palma, and B. L. Isacks, 1983, Paleogeography and Andean structural geometry, northwest Argentina: Tectonics, v. 2, no. 1, p. 1–16, DOI: 10.1029/TC002i001p00001.

Allmendinger, R. W., and T. Gubbels, 1996, Pure and simple shear plateau uplift, Altiplano-Puna, Argentina and Bolivia: Tectonophysics, v. 259, p. 1–13, DOI: 10.1016/0040-1951(96)00024-8.

Allmendinger, R. W., T. E. Jordan, S. M. Kay, and B. L. Isacks, 1997, The evolution of the Altiplano-Puna plateau of the central Andes: Annual Review of Earth and Planetary Sciences, v. 25, p. 139–174, DOI: 10.1146/annurev.earth.25.1.139.

Amidon, W. H., L. V. Luna, G. B. Fisher, D. W. Burbank, A. R. Kylander-Clark, and R. Alonso, 2015, Provenance and tectonic implications of Orán Group foreland basin sediments, Río Iruya canyon, NW Argentina (23°S): Basin Research, p. 1–17, DOI: 10.1111/bre.12139.

Anderson, R. B., S. P. Long, B. K. Horton, A. Z. Calle, and D. F. Stockli, 2014, New apatite and zircon (U-Th)/He constraints on the timing of thrust-related exhumation in the southern Bolivian (21°S) Andes: American Geophysical Union 95, no. 59.

Anderson, R. B., S. P. Long, B. K. Horton, A. Z. Calle, and V. Ramirez, 2017, Shortening and structural architecture of the Andean fold-thrust belt of southern Bolivia (21°S): Implications for kinematic development and crustal thickening of the central Andes: Geosphere, v. 13, no. 2, p. 1–21, DOI: 10.1130/GES01433.1.

Augustsson, C., T. Rüsing, H. Niemeyer, E. Kooijman, J. Berndt, H. Bahlburg, and U. Zimmermann, 2015, 0.3 byr of drainage stability along the Palaeozoic palaeo-Pacific

Gondwana margin: A detrital zircon study: Journal of the Geological Society of London, v. 172, no. 2, p. 186–200, doi: 10.1144/jgs2014-065.

Ayaviri, A., 1964, Geología del área de Tarija entre los Rios Pilaya-Pilcomayo y Rio Bermejo: Informe interno Yacimientos Petroliferos Fiscales Bolivianos, 77 p.

Ayaviri, A., 1971, El Terciario Subandino: Informe interno Yacimientos Petrolíferos Fiscales Bolivianos, 6 p.

Baby, P., G. Hérail, R. Salinas, and T. Sempere, 1992, Geometry and kinematic evolution of passive roof duplexes deduced from cross section balancing: examples from the foreland thrust system of the southern Bolivian Subandean zone: Tectonics, v. 11, no. 3, p. 523–536, DOI: 10.1029/91TC03090.

Baby, P., P. Rochat, G. Mascle, and G. Hérail, 1997, Neogene shortening contribution to crustal thickening in the back arc of the central Andes: Geology, v. 25, no. 10, p. 883–886, DOI: 10.1130/0091-7613(1997)025<0883.

Barnes, J. B., and J. Pelletier, 2006, Latitudinal variation of denudation in the evolution of the Bolivian Andes: American Journal of Science, v. 306, p. 1–31, DOI: 10.2475/ajs.306.1.1.

Barnes, J. B., T. A. Ehlers, N. McQuarrie, P. B. O'sullivan, and S. Tawackoli, 2008, Thermochronometer record of central Andean Plateau growth, Bolivia (19.5°S): Tectonics, v. 27, no. 3, DOI: 10.1029/2007TC002174.

Barnes, J. B., and T. A. Ehlers, 2009, End member models for Andean Plateau uplift: Earth-Science Reviews, v. 97, no. 1–4, p. 105–132, DOI: 10.1016/j.earscirev.2009.08.003.

Barnes, J. B., and W. A. Heins, 2009, Plio-Quaternary sediment budget between thrust belt erosion and foreland deposition in the central Andes, southern Bolivia: Basin Research, v. 21, no. 1, p. 91–109, DOI: 10.1111/j.1365-2117.2008.00372.x.

Barnes, J. B., T. A., Ehlers, N. Insel, N., McQuarrie, and C. J., Poulsen, 2012, Linking orography, climate, and exhumation across the central Andes: Geology, v. 40, no. 12, p. 1135–1138, DOI: 10.1130/G33229.1.

Bookhagen, B., and M. R., Strecker, 2008, Orographic barriers, high-resolution TRMM rainfall, and relief variations along the eastern Andes: Geophysical Research Letters, v. 35, no. 6, DOI: 10.1029/2007GL032011.

Bridge, J. S., and I. A. Lunt, 2006, Depositional models of braided rivers, *in* G. H. Sambrook Smith, J. L. Best, C. S. Bristow, and G. E. Petts, eds., Braided rivers: Processes, deposits, ecology and management: IAS Special Publication 36, p. 11–50.

Brusset, S., P. Rochat, P. Baby, and J. Flinch, 2002, Thrust kinematics and foreland basin dynamics of the southern Subandean zone in Bolivia: New insight from apatite fission track analysis: ISAG International Symposium on Andean Geodynamics, p. 101–104.

Cabrera-Vildoso, A., 1965, Informe geológico zonas Andina y Subandina relevamiento geológico de itinerarios Rio Azero, Parapeti y Pilcomayo: Informe interno Yacimientos Petroliferos Fiscales Bolivianos, 60 p.

Calle, A. Z., 2013, Neogene sedimentation and provenance record of the Subandean Zone and Chaco foreland basin, southern Bolivia, Master's Thesis, University of Texas at Austin, Austin, Texas, 138 p.

Canavan, R., B. Carrapa, M. Clementz, J. Quade, P. G. DeCelles, and L. Schoenbohm, 2014, Early Cenozoic uplift of the Puna plateau, central Andes, based on stable isotope paleoaltimetry of hydrated volcanic glass: Geology, v. 42, no. 5, p. 447–450, DOI: 10.1130/G35239.1.

Canile, F. M., M. Babinski, and A. C. Rocha-Campos, 2016, Evolution of the Carboniferous-Early Cretaceous units of Parana Basin from provenance studies based on U-Pb, Hf and O isotopes from detrital zircons: Gondwana Research, v. 40, p. 142–169, DOI: 10.1016/j.gr.2016.08.008.

Carrapa, B., J. D. Trimble, and D. F. Stockli, 2011, Patterns and timing of exhumation and deformation in the Eastern Cordillera of NW Argentina revealed by (U-Th)/He thermochronology: Tectonics, v. 30, TC3003, DOI: 10.1029/2010TC002707.

Carrapa, B., S. Reyes-Bywater, R. Safipour, E. R. Sobel, L. M. Schoenbohm, P. G. DeCelles, P. W. Reiners, and D. Stockli, 2014, The effect of inherited paleotopography on exhumation of the central Andes of NW Argentina: Geological Society of America Bulletin, v. 126, no. 1–2, p. 66–77, DOI: 10.1130/B30844.1.

Carrapa, B., and P. G. DeCelles, 2015, Regional exhumation and kinematic history of the central Andes in response to cyclical orogenic processes, *in* P. G. DeCelles, M. N. Ducea, B. Carrapa, and P. A. Kapp, eds., Geodynamics of a cordilleran orogenic system: The central Andes of Argentina and northern Chile: GSA Memoir 212, p. 201–213.

Choque, N., and O. Almendras, 2012, Servicio Nacional de Geologia y Tecnico de Minas: Mapa geologico de Bolivia, scale 1:1,000,000, 1 sheet.

Collinson, J. D., 1996, Alluvial sediments, *in* H. G. Reading, ed., Sedimentary environments: Processes, facies and stratigraphy, Blackwell Science, Oxford, p. 37–82.

Constantini, L. A., A. Rodríguez, C. Fontana, R. M. Hernández, and M. L. Rodriguez-Schelotto, 2002a, Los reservorios del Conglomerado Galarza y la Serie Abigarrada, *in* M. Schiuma, G. Hinterwimmer, and G. Vergani, eds., Rocas Reservorio de las cuencas productivas del NW Argentino: V Simposio de Exploración y Desarrollo de Hidrocarburos, p. 753–766.

Constantini, L. A., A. Rodríguez, C. Fontana, M. L. Rodriguez-Schelotto, and R. M. Hernández, 2002b, Los reservorios de la Formación Tranquitas y Terciario Subandino, *in* M. Schiuma, G. Hinterwimmer, and G. Vergani, eds., Rocas Reservorio de las cuencas productivas del NW Argentino: V Simposio de Exploración y Desarrollo de Hidrocarburos, p. 767–786.

Coutand, I., P. R. Cobbold, M. de Urreiztieta, P. Gautier, A. Chauvin, D. Gapais, E. A. Rossello, and O. López-Gamundi, 2001, Style and history of Andean deformation, Puna plateau, northwestern Argentina: Tectonics, v. 20, p. 210–234, DOI: 10.1029/2000TC900031.

DeCelles, P. G., 2012, Foreland basin systems revisited: Variations in response to tectonic settings, *in* C. Busby and A. Azor Perez, Tectonics of sedimentary basins: Recent advances: Oxford, UK, Wiley-Blackwell, p. 405–426.

DeCelles, P. G., and K. A. Giles, 1996, Foreland basin systems: Basin Research, v. 8, no. 2, p. 105–123, DOI: 10.1046/j.1365-2117.1996.01491.x.

DeCelles, P. G., and B. K. Horton, 2003, Early to middle Tertiary foreland basin development and the history of Andean crustal shortening in Bolivia: Geological Society of America Bulletin, v. 115, no. 1, p. 58–77, DOI: 10.1130/0016-7606(2003)115<0058:ETMTFB>2.0.CO;2.

DeCelles, P. G., B. Carrapa, B. K. Horton, and G. E. Gehrels, 2011, Cenozoic foreland basin system in the central Andes of northwestern Argentina: Implications for Andean geodynamics and modes of deformation: Tectonics, v. 30, TC6013, DOI: 10.1029/2011TC002948.

Del Papa, C., F. Hongn, J. Powell, P. Payrola, M. Do Campo, M. R. Strecker, I. Petrinovic, A. K. Schmitt, and R. Pereyra, 2013, Middle Eocene-Oligocene broken-foreland evolution in the Andean Calchaqui Valley, NW Argentina: Insights from stratigraphic, structural and provenance studies: Basin Research, v. 25, p. 574–593, DOI: 10.1111/bre.12018.

Dickinson, W. R., 1985, Interpreting provenance relation from detrital modes of sandstones, *in* G. G. Zuffa, ed., Provenance of Arenites: Dordrecht, Reidel Publishing Company, p. 333–363.

Dickinson, W. R., and C. A. Suczek, 1979, Plate tectonics and sandstone compositions: AAPG Bulletin, v. 63, p. 2164–2182, DOI: 10.1306/2F9188FB-16CE-11D7-8645000102C1865D.

Dickinson, W. R., and G. E. Gehrels, 2009, Use of U-Pb ages of detrital zircons to infer maximum depositional ages of strata: A test against a Colorado Plateau Mesozoic database: Earth and Planetary Science Letters, v. 288, no. 1–2, p. 115–125, DOI: 10.1016/j.epsl.2009.09.013.

Dunn, J. F., K. G. Hartshorn, and P. W. Hartshorn, 1995, Structural styles and hydrocarbon potential of the Subandean belt of southern Bolivia, *in* A. J. Tankard, S. R. Suárez, and H. J. Welsink, eds., Petroleum basins of South America: AAPG Memoir 62, p. 523–543.

Echavarría, L., R. Hernández, R. Allmendinger, and J. Reynolds, 2003, Subandean thrust and fold belt of northwestern Argentina: Geometry and timing of the Andean evolution: AAPG Bulletin, v. 87, no. 6, p. 965–985, DOI: 10.1306/01200300196.

Ege, H., 2004, Exhumations- und Hebungsgeschichte der zentralen Anden in Südbolivien (21°S) durch Spaltspur-Thermochronologie an Apatit, Ph.D. Dissertation, Freie Universitat, Berlin, 182 p.

Ege, H., E. R. Sobel, E. Scheuber, and V. Jacobshagen, 2007, Exhumation history of the southern Altiplano plateau (southern Bolivia) constrained by apatite fission track thermochronology: Tectonics, v. 26, p. 1–24, DOI: 10.1029/2005TC001869.

Eichelberger, N., N. McQuarrie, T. A. Ehlers, E. Enkelmann, J. B. Barnes, and R. O. Lease, 2013, New constraints on the chronology, magnitude, and distribution of deformation within the central Andean orocline: Tectonics, v. 32, p. 1432–1453, DOI: 10.1002/tect.20073.

Erikson, J. P., and S. A. Kelley, 1995, Late Oligocene initiation of foreland-basin formation in Bolivia based on newly dated volcanic ash: Proceedings of the IX Congreso Latinoamericano de Geología, Caracas, Venezuela, 13 p.

Escayola, M. P., C. R. Van Staal, and W. J. Davis, 2011, The age and tectonic setting of the Puncoviscana Formation in northwestern Argentina: An accretionary complex related to Early Cambrian closure of the Puncoviscana Ocean and accretion of the Arequipa-Antofalla block: Journal of South American Earth Sciences, v. 32, no. 4, p. 438–459, DOI: 10.1016/j.jsames.2011.04.013.

Folk, R. L., 1980, Petrology of sedimentary rocks: Austin, Hemphill Publishing Company, 190 p.

Galli, C. I., B. L. Coira, R. N. Alonso, M. P. Iglesia Llanos, C. B. Prezzi, and S. M. Kay, 2016, Tectonostratigraphic history of the Neogene Maimará basin, Northwest Argentina: Journal of South American Earth Sciences, v. 72, p. 137–158, DOI: 10.1016/j.jsames.2016.09.007.

Galloway, W. E., and D. K., Hobday, 1996, Fluvial systems, *in* W. E. Galloway and D. K. Hobday, eds., Terrigenous Clastic depositional Systems, applications to fossil fuel and groundwater resources: Berlin, Heidelberg, Springer, p. 60–90.

Garzione, C. N., P. Molnar, J. C. Libarkin, and B. J. MacFadden, 2006, Rapid late Miocene rise of the Bolivian Altiplano: Evidence for removal of mantle lithosphere: Earth and Planetary Science Letters, v. 241, no. 3–4, p. 543–556, DOI: 10.1016/j.epsl.2005.11.026.

Garzione, C. N., G. D. Hoke, J. C. Libarkin, S. Withers, B. MacFadden, J. Eiler, P. Ghosh, and A. Mulch, 2008, Rise of the Andes: Science, v. 320, p. 1304–1307.

Gillis, R. J., B. K. Horton, and M. Grove, 2006, Thermochronology, geochronology, and upper crustal structure of the Cordillera Real: Implications for Cenozoic exhumation of the central Andean plateau: Tectonics, v. 25, TC6007, DOI: 10.1029/2005TC001887.

Grader, G., V. Davydov, J. Tait, and P. Isaacson, 2007, Late Paleozoic stratigraphic framework in Bolivia: Constraints from the warm water Cuevo megasequence, *in* E. Díaz-Martínez, and I. Rábano, eds., 4th European Meeting on the Paleontology and Stratigraphy of Latin America: Cuadernos del Museo Geominero 8, p. 181–188.

Grier, M. E., J. A. Salfity, and R. W. Allmendinger, 1991, Andean reactivation of the Cretaceous Salta rift, northwestern Argentina: Journal of South American Earth Sciences, v. 4, p. 351–372.

Gubbels, T. L., B. L. Isacks, and E. Farrar, 1993, High-level surfaces, plateau uplift, and foreland development, Bolivian central Andes: Geology, v. 21, p. 695–698.

Hampton, B. A., and B. K. Horton, 2007, Sheetflow fluvial processes in a rapidly subsiding basin, Altiplano plateau, Bolivia: Sedimentology, v. 54, no. 5, p. 1121–1148, DOI: 10.1111/j.1365-3091.2007.00875.x.

Hartley, A. J., G. S. Weissmann, G. J. Nichols, and G. L. Warwick, 2010, Large distributive fluvial systems: Characteristics, distribution, and controls on development: Journal of Sedimentary Research, v. 80, no. 2, p. 167–183, DOI: 10.2110/jsr.2010.016.

Hernández, R. M., J. H. Reynolds, and A. Disalvo, 1996, Análisis tectosedimentario y ubicación geocronológica del Grupo Oran en el Rio Iruya: Boletín de Informaciones Petroleras, p. 80–93.

Hernández, R. M., T. E. Jordan, A. D. Farjat, L. Echavarría, B. D. Idleman, and J. H. Reynolds, 2005, Age, distribution, tectonics, and eustatic controls of the Paranense and Caribbean marine transgressions in southern Bolivia and Argentina: Journal of South American Earth Sciences, v. 19, no. 4, p. 495–512, DOI: 10.1016/j.jsames.2005.06.007.

Hernández, R., and L. Echavarría, 2009, Faja plegada y corrida Subandina del noroeste Argentino: Estratigrafia, geometria y cronologia de la deformacion: Revista de la Asociacion Geologica Argentina, v. 65, no. 1, p. 68–80.

Hongn, F., R. Mon, I. Petrinovic, C. Del Papa, and J. Powell, 2010, Inversión y reactivación tectónicas cretácico-cenozoicas en el noroeste Argentino: Influencia de las heterogeneidades del basamento Neoproterozoico-Paleozoico inferior: Revista de la Asociacion Geologica Argentina, v. 66, no. 1, p. 38–53.

Horton, B. K., 1998, Sediment accumulation on top of the Andean orogenic wedge: Oligocene to late Miocene basins of the Eastern Cordillera, southern Bolivia: Geological Society of America Bulletin, v.110, p. 1174–1192, DOI: 10.1130/0016-7606(1998)110<1174:SAOTOT>2.3.CO;2.

Horton, B. K., 1999, Erosional control on the geometry and kinematics of thrust belt development in the central Andes: Tectonics, v. 18, p. 1292–1304, DOI: 10.1029/1999TC900051.

Horton, B. K., 2005, Revised deformation history of the central Andes: Inferences from Cenozoic foredeep and intermontane basins of the Eastern Cordillera, Bolivia: Tectonics, v. 24, TC3011, DOI: 10.1029/2003TC001619.

Horton, B. K., 2012, Cenozoic evolution of hinterland basins in the Andes and Tibet, *in* C. Busby and A. Azor Perez, eds., Tectonics of sedimentary basins: Recent advances: Oxford, UK, Wiley-Blackwell, p. 427–444.

Horton, B. K., and P. G. DeCelles, 1997, The modern foreland basin system adjacent to the central Andes: Geology, v. 25, no. 10, p. 895–898, DOI: 10.1130/0091-7613(1997)025<0895:TMFBSA>2.3.CO;2.

Horton, B. K., and P. G. DeCelles, 2001, Modern and ancient fluvial megafans in the foreland basin system of the central Andes, southern Bolivia: Implications for drainage network evolution in fold-thrust belts: Basin Research, v. 13, no. 1, p. 43–63, DOI: 10.1046/j.1365-2117.2001.00137.x.

Horton, B. K., B. A. Hampton, and G. Waanders, 2001, Paleogene synorogenic sedimentation in the Altiplano plateau and implications for initial mountain building in the central Andes: Geological Society of America Bulletin, v. 113, p. 1387–1400, DOI: 10.1130/0016-7606(2001)113<1387:PSSITA>2.0.CO;2.

Horton, B. K., B. A. Hampton, B. N. LaReau, and E. Baldellón, 2002, Tertiary provenance history of the northern and central Altiplano (central Andes, Bolivia): A detrital record of plateau-margin tectonics: Journal of Sedimentary Research, v. 72, p. 711–726, doi: 10.1306/020702720711.

Horton, B. K., F. Fuentes, A. Boll, D. Starck, S. G. Ramirez, and D. F. Stockli, 2016, Andean stratigraphic record of the transition from backarc extension to orogenic shortening: A case study from the northern Neuquén basin, Argentina: Journal of South American Earth Sciences, v. 71, p. 17–40, DOI:10.1016/j.jsames.2016.06.003.

Hulka, C., 2005, Sedimentary and tectonic evolution of the Cenozoic Chaco foreland basin, southern Bolivia, Ph.D. Dissertation, Freie Universitat, Berlin, 100 p.

Hulka, C., K. U. Gräfe, B. Sames, C. E. Uba, and C. Heubeck, 2006, Depositional setting of the middle to late Miocene Yecua Formation of the Chaco Foreland Basin, southern Bolivia: Journal of South American Earth Sciences, v. 21, no. 1, p. 135–150, DOI: 10.1016/j.jsames.2005.08.003.

Hulka, C., and C., Heubeck, 2010, Composition and provenance history of Late Cenozoic sediments in southeastern Bolivia: Implications for Chaco foreland basin evolution and Andean uplift: Journal of Sedimentary Research, v. 80, no. 3, p. 288–299, DOI: 10.2110/jsr.2010.029.

Insel, N., M. Grove, M. Haschke, J. B. Barnes, A. K. Schmitt, and M. R. Strecker, 2012, Paleozoic to early Cenozoic cooling and exhumation of the basement underlying the eastern Puna plateau margin prior to plateau growth: Tectonics, v. 31, no. 6, DOI: 10.1029/2012TC003168.

Isacks, B. L., 1988, Uplift of the central Andean plateau and bending of the Bolivian orocline: Journal of Geophysical Research: Solid Earth, v. 93, p. 3211–3231, DOI: 10.1029/JB093iB04p03211.

Jacques, J., 2003, A tectonostratigraphic synthesis of the Subandean basins: Implications for the geotectonic segmentation of the Andean Belt: Journal of the Geological Society of London, v. 160, no. 5, p. 687–701, DOI: 10.1144/0016-764902-088.

Jordan, T. E., 1981, Thrust loads and foreland basin evolution, Cretaceous, western United States: AAPG Bulletin, v. 65, p. 2506–2520; DOI 10.1306/03B599F4-16D1-11D7-8645000102C1865D.

Jordan, T. E., 1995, Retroarc foreland and related basins, *in* C. J. Busby and R. V. Ingersoll, eds., Tectonics of sedimentary basins: Cambridge, MA, Blackwell Science, p. 331–362.

Jordan, T. E., J. H. Reynolds, and J. P. Erikson, 1997, Variability in age of initial shortening and uplift in the central Andes, 16–33°30´S, *in* W. F. Ruddiman, ed., Tectonic uplift and climate change: New York, Plenum Press, p. 41–61.

Kennan, L., S. Lamb, and C. Rundle, 1995, K-Ar dates from the Altiplano and Cordillera Oriental of Bolivia: Implications for Cenozoic stratigraphy and tectonics: Journal of South American Earth Sciences, v. 8, p. 163–186, DOI: 10.1016/0895-9811(95)00003-X.

Kley, J., 1993, Der Übergang vom Subandin zur Ostkordillere in Südbolivien: Geologische Struktur und Kinematik. Berliner Geowissenschaftliche Abhandlungen, Reihe A, Band 156, 88 p.

Kley, J., 1996, Transition from basement-involved to thin-skinned thrusting in the Cordillera Oriental of southern Bolivia: Tectonics, v. 15, no. 4, p. 763–775, DOI: 10.1029/95TC03868.

Kley, J., A. H. Gangui, and D. Krüger, 1996, Basement-involved blind thrusting in the eastern Cordillera Oriental, southern Bolivia: Evidence from cross-sectional

balancing, gravimetric and magnetotelluric data: Tectonophysics, v. 259, no. 1–3, p. 171–184, DOI: 10.1016/0040-1951(95)00067-4.

Kley, J., J. Müller, S. Tawackoli, V. Jacobshagen, and E. Manutsoglu, 1997, Preandean and Andean-age deformation in the Eastern Cordillera of southern Bolivia: Journal of South American Earth Sciences, v. 10, p. 1–19, DOI: 10.1016/S0895-9811(97)00001-1.

Kley, J., and C. R. Monaldi, 1998, Tectonic shortening and crustal thickness in the central Andes: How good is the correlation?: Geology, v. 26, no. 8, p. 723–726, DOI: 10.1130/0091-7613(1998)026<0723:TSACTI>2.3.CO;2.

Kley, J., and C. R. Monaldi, 2002, Tectonic inversion in the Santa Barbara System of the central Andean foreland thrust belt, northwestern Argentina: Tectonics, v. 21, no. 6, p. 11-1-11–18, DOI:10.1029/2002TC902003.

Kley, J., C. R. Monaldi, and J. A. Salfity, 1999, Along-strike segmentation of the Andean foreland: Causes and consequences: Tectonophysics, v. 301, no. 1–2, p. 75–94, DOI: 10.1016/S0040-1951(98)90223-2.

Kley, J., E. A. Rossello, C. R. Monaldi, and B. Habighorst, 2005, Seismic and field evidence for selective inversion of Cretaceous normal faults, Salta rift, northwest Argentina: Tectonophysics, v. 399, p. 155–172, DOI: 10.1016/j.tecto.2004.12.020.

Kraus, M., 1999, Paleosols in clastic sedimentary rocks: Their geologic applications: Earth Science Reviews, v. 47, p. 41–70.

Lamb, S., 2011, Did shortening in thick crust cause rapid Late Cenozoic uplift in the northern Bolivian Andes? Journal of the Geological Society of London, v. 168, p. 1079–1092, DOI: 10.1144/0016-76492011-008.

Lamb, S., 2016, Cenozoic uplift of the central Andes in northern Chile and Bolivia—Reconciling paleoaltimetry with the geological evolution: Canadian Journal of Earth Sciences, v. 53, p. 1227–1245, DOI: 10.1139/cjes-2015-0071.

Lamb, S., and L. Hoke, 1997, Origin of the high plateau in the central Andes, Bolivia: Tectonics, v. 16, no. 4, p. 623–649.

Lease, R. O., T. A. Ehlers, and E. Enkelmann, 2016, Large along-strike variations in the onset of Subandean exhumation: Implications for central Andean orogenic growth: Earth and Planetary Science Letters, v. 451, p. 62–76, DOI: 10.1016/j.epsl.2016.07.004.

Leier, A. L., P. G. DeCelles, and J. D. Pelletier, 2005, Mountains, monsoons, and megafans: Geology, v. 33, no. 4, p. 289–292, DOI: 10.1130/G21228.1.

Levina, M., B. K. Horton, F. Fuentes, and D. F. Stockli, 2014, Cenozoic sedimentation and exhumation of the foreland basin system preserved in the Precordillera thrust belt (31–32°S), southern central Andes, Argentina: Tectonics, v. 33, p. 1659–1680, DOI: 10.1002/2013TC003424.

Marshall, L. G., and T. Sempere, 1991, The Eocene to Pleistocene vertebrates of Bolivia and their stratigraphic context: A review: Revista Técnica de Yacimientos Petrolíferos Fiscales Bolivianos, v. 12, no. 3–4, p. 631–652.

Marshall, L. G., T. Sempere, and M. Gayet, 1993, The Petaca (Upper Oligocene–Middle Miocene) and Yecua (Upper Miocene) Formations of the Subandean–Chaco basin, Bolivia, and their tectonic significance: Documents des Laboratoires de Ge Lyon, v. 125, p. 291–301.

Mascle, G., and D. Zubieta-Rossetti, 2005, Erosion in the Andes and sedimentation in the foreland basin of eastern Bolivia: 6th International Symposium on Andean Geodynamics, Extended Abstracts, p. 497–498.

Masek, J. G., B. L. Isacks, T. L. Gubbels, and E. J. Fielding, 1994, Erosion and tectonics at the margins of continental plateaus: Journal of Geophysical Research, v. 99, p. 13941–13956, DOI: 10.1029/94JB00461.

McCarthy, P. J., and I. P. Martini, 1997, Anatomy and evolution of a Lower Cretaceous alluvial plain: Sedimentology and palaeosols in the upper Blairmore Group, south-western Alberta, Canada: Sedimentology, v. 44, p. 197–220, DOI: 10.1111/j.1365-3091.1997.tb01521.x.

McGroder, M. F., R. O. Lease, and D. M. Pearson, 2015, Along-strike variation in structural styles and hydrocarbon occurrences, Subandean fold-and-thrust belt and inner foreland, Colombia to Argentina, *in* P. G. DeCelles, M. N. Ducea, B. Carrapa, and P. A. Kapp, eds., Geodynamics of a cordilleran orogenic system: The central Andes of Argentina and northern Chile: GSA Memoir 212, p. 79–113.

McQuarrie, N., 2002a, Initial plate geometry, shortening variations, and evolution of the Bolivian orocline: Geology, v. 30, p. 867–870, DOI: 10.1130/0091-7613(2002)030<0867:IPGSVA>2.0.CO;2.

McQuarrie, N., 2002b, The kinematic history of the central Andean fold-thrust belt, Bolivia: Implications for building a high plateau: Geological Society of America Bulletin, v. 114, no. 8, p. 950–963, DOI: 10.1130/0016-7606(2002)114<0950:TKHOTC>2.0.CO;2.

McQuarrie, N., B. K. Horton, G. Zandt, S. Beck, and P. G. DeCelles, 2005, Lithospheric evolution of the Andean fold-thrust belt, Bolivia and the origin of the central Andean plateau: Tectonophysics, v. 399, p. 15–37, DOI: 10.1016/j.tecto.2004.12.013.

Miall, A. D., 1992, Alluvial deposits, *in* R. G. Walker and N. P. James, eds., Facies models response to sea level changes: Canada, Geological Association of Canada, p. 119–142.

Miall, A. D., 1996, The geology of fluvial deposits: Berlin, Springer-Verlag, 581 p.

Miall, A. D., 2010, Alluvial deposits, *in* N. P. James and R. W. Dalrymple, eds., Facies models 4: Canada, Geological Association of Canada, p. 105–137.

Montgomery, D. R., G. Balco, and S. D. Willett, 2001, Climate, tectonics, and the morphology of the Andes: Geology, v. 29, no. 7, p. 579–582, DOI: 10.1130/0091-7613(2001)029<0579:CTATMO>2.0.CO;2.

Moretti, I., P. Baby, E. Mendez, and D. Zubieta, 1996, Hydrocarbon generation in relation to thrusting in the Sub Andean zone from 18 to 22°S, Bolivia: Petroleum Geoscience, v. 2, no. 1, p. 17–28, DOI: 10.1144/petgeo.2.1.17.

Mosolf, J. G., B. K. Horton, M. T. Heizler, and R. Matos, 2011, Unroofing the core of the central Andean fold-thrust belt during focused late Miocene exhumation: Evidence from the Tipuani-Mapiri wedge-top basin, Bolivia: Basin Research, v. 23, p. 346–360, DOI:10.1111/j.1365-2117.2010.00491.x.

Mulch, A., C. E. Uba, M. R. Strecker, R. Schoenberg, and C. P. Chamberlain, 2010, Late Miocene climate variability and surface elevation in the central Andes: Earth and Planetary Science Letters, v. 290, no. 1–2, p. 173–182, DOI: 10.1016/j.epsl.2009.12.019.

Müller, J. P., J. Kley, and V. Jacobshagen, 2002, Structure and Cenozoic kinematics of the Eastern Cordillera, southern Bolivia (21°S): Tectonics, v. 21, p. 1–23, DOI: 10.1029/2001TC001340.

Nardin, T., H. R. Feldman, and B. J. Carter, 2013, Stratigraphic architecture of a large-scale point-bar complex in the McMurray Formation: Syncrude's Mildred Lake Mine, Alberta, Canada, *in* F. J. Hein, D. Leckie, S, Larter, and J. R. Suter, eds., Heavy-oil and oil-sand petroleum systems in Alberta and beyond: AAPG Studies in Geology 64, p. 273–311.

Nash, D. J., S. J. Mclaren, and J. A. Webb, 2004, Petrology, geochemistry and environmental significance of silcrete-calcrete intergrade duricrusts at Kang Pan and Tswaane, central Kalahari, Botswana: Earth Surface Processes and Landforms, v. 29, p. 1559–1586, DOI: 10.1002/esp.1138.

Nemec, W., and R. J. Steel, 1984, Alluvial and coastal conglomerates: Their significant features and some comments on gravelly mass-flow deposits, *in* E. H. Koster and R. J. Steel, eds., Sedimentology of gravels and conglomerates: CSPG Memoir 10, p. 1–31.

Oncken, O., D. Hindle, J. Kley, K. Elger, P. Victor, and K. Schemann, 2006, Deformation of the central Andean upper plate system—Facts, fiction, and constraints for plateau models, *in* O. Oncken, G. Chong, G. Franz, P. Glese, H. J. Götze, V. Ramos, M. Strecker, and P. Wigger, eds., The Andes: Active subduction orogeny: Berlin, Springer, p. 3–27.

Pearson, D. M., P. Kapp, P. G. DeCelles, P. W. Reiners, G. E. Gehrels, M. N. Ducea, and A. Pullen, 2013, Influence of pre-Andean crustal structure on Cenozoic thrust belt kinematics and shortening magnitude: Northwestern Argentina: Geosphere, v. 9, no. 6, p. 1766–1782, DOI: 10.1130/GES00923.1.

Peri, V. G., M. Naipauer, M. Pimentel, and H. Barcelona, 2016, Eolian deposits of the southwestern margin of the Botucatu paleoerg: Reconstruction of the Gondwana landscape in central northern Argentina: Sedimentary Geology, v. 339, p. 234–257, DOI: 10.1016/j.sedgeo.2016.03.019.

Pingel, H., M. R. Strecker, R. N. Alonso, and A. K. Schmitt, 2013, Neotectonic basin and landscape evolution in the Eastern Cordillera of NW Argentina, Humahuaca Basin (~24°S): Basin Research, v. 25, p. 554–573, DOI: 10.1111/bre.12016.

Plink-Björklund, P., 2015, Morphodynamics of rivers strongly affected by monsoon precipitation: Review of depositional style and forcing factors: Sedimentary Geology, v. 323, p. 110–147, DOI: 10.1016/j.sedgeo.2015.04.004.

Poire, P. G., D. Tineo, G. Gonzalez-Rigas, P. Bona, N. Toledo, M. Requero, A. Scarano, G. D. Vergani, and L. M. Perez, 2013, Hallazgos de vertebrados continentals de la formacion Petaca (Oligoceno tardio), Cuenca del Chaco, Bolivia: Ameguiniana, v. 50, p. R65.

Prezzi, C.B., C. E. Uba, and H.-J. Götze, 2009, Flexural isostasy in the Bolivian Andes: Chaco foreland basin development: Tectonophysics, v. 474, p. 526–543, DOI:10.1016/j.tecto.2009.04.037.

Quade, J., M. P. Dettinger, B. Carrapa, P. G. DeCelles, K. E. Murray, K. W. Huntington, A. Cartwright, R. R. Canavan, G. Gehrels, and M. Clementz, 2015, The growth of the central Andes, 22°S–26°S, *in* P. G. DeCelles, M. N. Ducea, B. Carrapa, and P. A. Kapp, eds., Geodynamics of a cordilleran orogenic system: The central Andes of Argentina and Northern Chile: GSA Memoir 212, p. 277–308.

Reiners, P. W., et al., 2015, Low-temperature thermochronologic trends across the central Andes, 21°S–28°S, *in* P. G. DeCelles, M. N. Ducea, B. Carrapa, and P. A. Kapp, eds., Geodynamics of a cordilleran orogenic system: The central Andes of Argentina and northern Chile: GSA Memoir 212, p. 215–249.

Retallack, G. J., 1988, Field recognition of paleosols, *in* J. Reinhardt and W. R. Sigleo, eds., Paleosols and weathering through geologic time: Principles and applications: GSA Special Papers 216, p. 1–20, DOI: 10.1130/SPE216-p1.

Reynolds, J. H., R. M. Hernández, C. I. Galli, and B. D. Idleman, 2001, Magnetostratigraphy of the Quebrada La Porcelana section, Sierra de Ramos, Salta Province, Argentina: Age limits for the Neogene Oran Group and uplift of the southern Sierras Subandinas: Journal of South American Earth Sciences, v. 14, p. 681–692, DOI: 10.1016/S0895-9811(01)00069-4.

Riba, O., 1976, Syntectonic unconformities of the Alto Cardener, Spanish Pyrenees: A genetic interpretation: Sedimentary Geology, v. 15, no. 3, p. 213–233, DOI: 10.1016/0037-0738(76)90017-8.

Saylor, J. E., and K. E. Sundell, 2016, Quantifying comparison of large detrital geochronology data sets: Geosphere, v. 12, no. 1, p. 203–220, DOI: 10.1130/GES01237.1.

Scherer, C. M., and K. Goldberg, 2007, Palaeowind patterns during the latest Jurassic–earliest Cretaceous in Gondwana: Evidence from aeolian cross-strata of the Botucatu Formation, Brazil: Palaeogeography, Palaeoclimatology, Palaeoecology, v. 250, no. 1, p. 89–100, DOI: 10.1016/j.palaeo.2007.02.018.

Sempere, T., 1994, Kimmeridgian? to Paleocene tectonic evolution of Bolivia, *in* J. A. Salfity, ed., Cretaceous tectonics of the Andes: SpringerVieweg Verlag, Wiesbaden, p. 168–212.

Siks, B. C., and B. K. Horton, 2011, Growth and fragmentation of the Andean foreland basin during eastward advance of fold-thrust deformation, Puna plateau and Eastern Cordillera, northern Argentina: Tectonics, v. 30, TC6017, DOI: 10.1029/2011TC002944.

Sobel, E. R., G. E. Hilley, M. R. Strecker, 2003, Formation of internally drained contractional basins by aridity-limited bedrock incision: Journal of Geophysical Research, v. 108, no. B7, p. 2344, DOI: 10.1029/2002JB001883.

Starck, D., 2011, Cuenca Cretacica-Paleogena del Noroeste Argentino: VIII Congreso de Exploración y Desarrollo de Hidrocarburos Simposio Cuencas Argentinas: Visión Actual, Instituto Argentino del Petróleo y el Gas, p. 407–453.

Starck, D., and A. Schulz, 1996, La configuración estructural del límite entre Cordillera Oriental y Sierras Subandinas en el extremo norte de la República Argentina: Boletín de Informaciones Petroleras, Tercera Epoca, v. 52, p. 39–46.

Steel, R. J., and D. B. Thompson, 1983, Structures and textures in Triassic braided stream conglomerates ("Bunter"pebble beds) in the Sherwood Sandstone Group, North Staffordshire, England: Sedimentology, v. 30, no. 3, p. 341–367, DOI: 10.1111/j.1365-3091.1983.tb00677.x.

Steidtmann, J. R., and J. G. Schmitt, 1988, Provenance and dispersal of tectogenic sediments in thin-skinned, thrusted terrains, *in* K. L. Kleinspehn and C. Paola, eds., New perspectives in basin analysis: New York, Springer-Verlag, p. 353–366.

Strecker, M. R., R. N. Alonso, B. Bookhagen, B. Carrapa, G. E. Hilley, E. R. Sobel, and M. H. Trauth, 2007, Tectonics and climate of the southern central Andes: Annual Review of Earth and Planetary Sciences, v. 35, p. 747–787, DOI: 10.1146/annurev.earth.35.031306.140158.

Strecker, M. R., R. Alonso, B. Bookhagen, B. Carrapa, I. Coutand, M. P. Hain, G. E. Hilley, E. Mortimer, L. Schoenbohm, and E. R. Sobel, 2009, Does the topographic distribution of the central Andean Puna plateau result from climatic or geodynamic processes? Geology, v. 37, no. 7, p. 643–646, DOI: 10.1130/G25545A.1.

Streit, R. L., D. W. Burbank, M. R. Strecker, R. N. Alonso, J. M. Cottle, and A. R. C. Kylander-Clark, 2015, Controls on intermontane basin filling, isolation and incision on the margin of the Puna plateau, NW Argentina (~23°S): Basin Research, v. 29, DOI: 10.1111/bre.12141.

Thiry, M., and B. Maréchal, 2001, Development of tightly cemented sandstone lenses in uncemented sand: Example of the Fontainebleau Sand (Oligocene) in the Paris Basin: Journal of Sedimentary Research, v. 71, no. 3, p. 473–483, DOI: 10.1306/2dc40956-0e47-11d7-8643000102c1865d.

Uba, C. E., C. Heubeck, and C. Hulka, 2005, Facies analysis and basin architecture of the Neogene Subandean synorogenic wedge, southern Bolivia: Sedimentary Geology, v. 180, no. 3, p. 91–123, DOI: 10.1016/j.sedgeo.2005.06.013.

Uba, C. E., C. Heubeck, and C. Hulka, 2006, Evolution of the late Cenozoic Chaco foreland basin, southern Bolivia: Basin Research, v. 18, no. 2, p. 145–170, DOI: 10.1111/j.1365-2117.2006.00291.x.

Uba, C. E., M. R. Strecker, and A. K. Schmitt, 2007, Increased sediment accumulation rates and climatic forcing in the central Andes during the late Miocene: Geology, v. 35, no. 11, p. 979–982, DOI: 10.1130/G224025A.1.

Uba, C. E., J. Kley, M. R. Strecker, and A. K. Schmitt, 2009, Unsteady evolution of the Bolivian Subandean thrust belt: The role of enhanced erosion and clastic wedge progradation: Earth and Planetary Science Letters, v. 281, no. 3–4, p. 134–146, DOI: 10.1016/j.epsl.2009.02.010.

Vermeesch, P., 2013, Multi-sample comparison of detrital age distributions: Chemical Geology, v. 341, p. 140–146, DOI: 10.1016/j.chemgeo.2013.01.010.

Viramonte, J. G., S. M. Kay, R. Becchio, M. Escayola, and I. Novitski, 1999, Cretaceous rift related magmatism in central-western South America: Journal of South American Earth Sciences, v. 12, no. 2, p. 109–121, doi: 10.1016/S0895-9811(99)00009-7.